Università degli Studi di Catania

Dottorato di Ricerca in Scienza dei Materiali
XXIV Ciclo

Valentina Spampinato

Physico-chemical characterization of ultra thin films of functional supramolecular systems on surfaces

Tutor: Prof. A. Licciardello
Coordinatore: Prof. A. Licciardello

Tesi di Dottorato di Ricerca

Ottobre 2011

Riassunto

Lo scopo del presente lavoro di dottorato è stato lo sviluppo di nuove metodologie per l'ancoraggio su superficie di sistemi molecolari e supramolecolari adatti per applicazioni nell'elettronica e nella fotonica molecolare e nella realizzazione di dispositivi per il riconoscimento molecolare. I sistemi preparati sono costituiti, come di consueto, da sistemi ibridi, composti da una parte molecolare e da un supporto solido. La parte molecolare espleta la funzione desiderata, mentre il supporto solido (un metallo o un semiconduttore su cui la parte molecolare è legata) permette di coniugare le proprietà che lo caratterizzano con quelle che caratterizzano il sistema molecolare, ed inoltre di mantenere le molecole in un ordine predeterminato.
Tali sistemi sono stati poi caratterizzati dal punto di vista composizionale e strutturale, tramite tecniche di indagine superficiale come la spettrometria di massa di ioni secondari con analizzatore a tempo di volo (ToF-SIMS), e la spettroscopia di fotoelettroni a raggi-X (XPS).
Parte cruciale del lavoro di ricerca è stata quindi la funzionalizzazione di superfici. Varie tipologie di superfici sono state utilizzate a questo scopo, in particolare di ossido di silicio (come sistema modello), di ossidi semiconduttori trasparenti (come l'ossido di indio drogato con stagno, ITO), e superfici metalliche (oro in particolare).
Le superfici di tali materiali sono state funzionalizzate impiegando un approccio "bottom up", e in particolare il processo di formazione di *self-assembled monolayers* (SAM, monostrati auto-assemblati), sfruttando il chemisorbimento - sulle superfici considerate - di molecole caratterizzate da opportuni gruppi funzionali.
Nel caso di superfici di ossidi sono state scelte molecole che fossero caratterizzate da un gruppo fosfonico come gruppo attivo alla superficie, capace di legarsi al substrato, opportunamente funzionalizzato, sfruttando la chimica zirconio fosfato-fosfonato (ZP). Nel caso di superfici di oro invece, sono state utilizzate molecole caratterizzate da un gruppo tiolico come gruppo responsabile del chemisorbimento alla superficie.
Nella maggior parte dei casi studiati, le molecole adoperate per la realizzazione di tali sistemi presentano come gruppo di coda funzionalità terpiridiniche. Questa tipologia di gruppo di coda è stata scelta in quanto

i leganti contenenti la 2,2':6',2"-terpiridina (Tpy) come sito chelante sono tra i composti eterociclici azotati più utilizzati per la loro alta affinità nei confronti degli ioni metallici bivalenti, e per la loro capacità di formare complessi stereospecifici, achirali e di simmetria spesso ottaedrica.
L'approccio generale è stato quello di ottenere, direttamente mediante reazioni di coordinazione *alla* superficie, complessi terpiridinici di ioni metallici. Utilizzando leganti ditopici è stato possibile utilizzare tale approccio per ottenere, mediante processi iterativi "passo dopo passo", sistemi multistrato che possono anche essere riguardati come assemblaggi di fili molecolari. Nello specifico sono state sfruttate le proprietà di leganti polifenilici coniugati recanti unità terpiridiniche alle due estremità.
Un approccio simile è stato utilizzato anche per l'ottenimento di sistemi utili alla realizzazione di dispositivi per il riconoscimento molecolare. A tale scopo l'attenzione è stata focalizzata sulla funzionalizzazione di superfici di oro per ottenere, in un caso, l'ancoraggio non covalente (mediante la tecnica ZP prima accennata) e spazialmente controllato di sequenze oligonucleotidiche e, nell'altro, la formazione, direttamente alla superficie mediante interazione host-guest, di "pseudo-rotaxani". Nel caso delle catene oligonucleotidiche si è dimostrata l'effettiva capacità dei sistemi ancorati di ibridizzare selettivamente le sequenze complementari. L'assemblaggio degli pseudo-rotaxani, d'altra parte, ha permesso di fare un passo avanti sullo studio di tali sistemi, dimostrando la possibilità di ottenere, controllando opportunamente l'ancoraggio dell'host (una catena lineare recante un gruppo funzionale amminico) la complessazione del guest calixarenico direttamente alla superficie.

Alle persone importanti
della mia vita

Table of contents

1 Introduction

1.1 Outline

Molecular and supramolecular layers on solid surfaces attract an increasing interest in many technological fields, due to the virtually infinite possibilities that they offer for tailoring a number of surface properties.
A typical example is given by the trends in electronic devices, where the use of molecular systems as active elements is spreading fast, making a reality the concept of molecular electronics. The possibility to create electronics devices that employ single molecules as building-blocks has motivated researchers for years, parallel with the tendency to miniaturization. Historically, semiconductor devices are made-up by the "top-down" approach that uses lithographic and etching techniques for patterning a substrate. The difficulty of applying such an approach becomes evident as the size of the elements and devices decreases towards the nanometre scale. In fact, at nanometre scale, there is a real complication in controlling electronic properties of semiconductor structures prepared by conventional lithographic processes. In order to avoid this problem, the elements of a electronic device can be synthesized by means of the "bottom-up" approach. This approach allows to build small structures from the atomic, molecular, or single device level and, in principle, allows a very precise positioning of atoms or molecules with specific functionalities. Moreover, a proper chemical engineering of organic molecules allows a fine tailoring of physical and electronic properties, and thus the preparation of materials with new characteristics that do not exist in inorganic electronics materials. Finally, by chemical synthesis it is possible to obtain large quantities of systems with nanometre size at significantly less cost, compared to other batch-fabrication processes. At the present stage of technology, a key point is the interfacing and integration of these molecular systems in a solid state device, and this very often implies their preparation in form of a thin or ultra-thin layer anchored on the surface of another material, either organic or inorganic.
The role of organic thin films, of course, is not limited to the above mentioned electronic applications; organic layers are of wide interest in many other different areas of technology, again because of the possibility

of tuning properties by modifying specific functional groups and leaving the rest unchanged.

From the point of view of the control and engineering of the materials properties, an important role is played by the surface. From microelectronic industry up to biomedical or aerospace applications, the surfaces constitute the essential part of the material. For example, in many technological applications, interfacing two or more materials (sometimes chemically very different) is essential, so it is necessary to know – and to be able to control and engineer - physico-chemical properties of surfaces and interfaces such as adsorption, wettability, adhesion, chemical reactivity, catalytic activity, presence of impurities, optical and electrical properties, etc…

During the last decades, many methods for the design and control of the materials surfaces have been developed, with the aim of tailoring the surface properties. Some of such methods imply the modification of the existing surface layers of the original material, while other methods add a new surface layer to the material by depositing on it (ultra-)thin films. According to the wide variety of molecular properties, there are different routes for the preparation of organic thin films. For example, spin-coating is a very popular preparation method[1] for thin polymer films. For the preparation of ordered films of relatively small molecules, formation of Langmuir films is one of the most common methods. Langmuir films consist of amphiphilic molecules solution spreads on a liquid subphase like water[2] and Langmuir-Blodgett (LB) films are prepared by transferring Langmuir films onto a solid substrate. Another common method for films preparation is the self-assembly process with the formation of a SAM (self-assembled monolayer) grown from solution or from the gas phase.

In this context, the development of reproducible methods for the preparation and modification of molecular surfaces is intimately connected with the development and availability of analytical techniques allowing the characterisation and control of the engineered surfaces from the point of view of elemental and molecular composition, structure, morphology etc…

Ideally, a technique for studying molecular surface should have some important characteristics: it should be non destructive, supply molecular information and not only elemental, be extremely sensitive. Moreover, because of the tendency to the miniaturization, the ideal technique should

also have a very high spatial resolution. Probably, among the techniques for surface chemical characterization, static secondary ions mass spectrometry - best performed with time-of-flight instrumentation (ToF-SIMS)- is the one that closer approaches the ideal technique. In fact, it is *quasi* non-destructive, it allows the detection of all of the elements including hydrogen, it is characterized by high sensitivity and good lateral resolution, and it provides molecular information about the uppermost monolayers of the materials.

The aim of this thesis is the preparation and the characterization of functional ultrathin films on surfaces. During this work some new molecular film preparation methods have been developed and problems concerning physico-chemical characterization of molecular films have been faced. In particular, self-assembled mono and multilayers were prepared by bottom-up methods, by means of direct reaction at the surface of a properly functionalized substrate. The functional films have been studied by surface-sensitive techniques such as time-of-flight secondary ion mass spectrometry (ToF-SIMS), atomic force microscopy (AFM) and X-ray photoelectron spectroscopy (XPS).

The thesis is divided into three main sections. The introduction (chapter 1) contains some background informations about the molecular systems used and on the method for their anchoring on surfaces. The second section (chapter 2) contains the description and discussion of the obtained results and the third section (chapter 3) is dedicated to the conclusions. In order to simplify the presentation and discussion of the experimental results, many details on the characterization techniques have been concentrated in a final appendix (chapter 4).

1.2 Methods for surface anchoring

The high interest towards nanotechnology and nanoscience, has led scientists to learn how to manipulate and characterize individual atoms and small groups of atoms and how to control the properties and structure of materials at the nanoscale. For this reason, new tools and approaches are needed for assembling atoms and molecules into nanoscale systems and for the further assembly of small systems into more-complex objects with unique capabilities.
Bottom-up approaches to nanofabrication use chemical or physical forces operating at the nanoscale level in order to assemble basic units ("molecular building blocks") into larger structures. As component size decreases in nanofabrication, bottom-up approaches provide an increasingly important complement to top-down techniques, allowing the synthesis of molecules in solution and the next anchoring at the surfaces, or allowing the synthesis directly at the surfaces by tuning the reaction conditions in order to adapt them to the surface chemistry.
Synthetic approaches such as self-assembly and preparation of Langmuir films, or patterning techniques like lithography and contact printing, are very useful tools for the aims of this kind of research.

1.2.1 Self-assembled monolayers

Self-assembled monolayers, SAMs, are formed when surfactant molecules spontaneously adsorb on surfaces to form a monomolecular layer, organizing spontaneously (and sometimes epitaxially) into crystalline (or semicrystalline) structures. They provide a convenient, flexible, and simple method for tailoring surface and interfacial properties of metals, metal oxides, and semiconductors. The molecules that form SAMs are "surface active" molecules that have a chemical functionality, "head group", with a specific affinity for a substrate; in many cases, the affinity for the surfaces is so high that can lead to the displacing of adsorbed adventitious organic materials from the surface. The molecules used to form SAMs are characterized by two other important functionalities. One is the "tail group", which is conveniently

chosen to give a new functionality to the surface. The other one is the "backbone" (or "spacer"), which connects tail and head groups and helps the correct assembly of SAM on surface. See Figure 1.

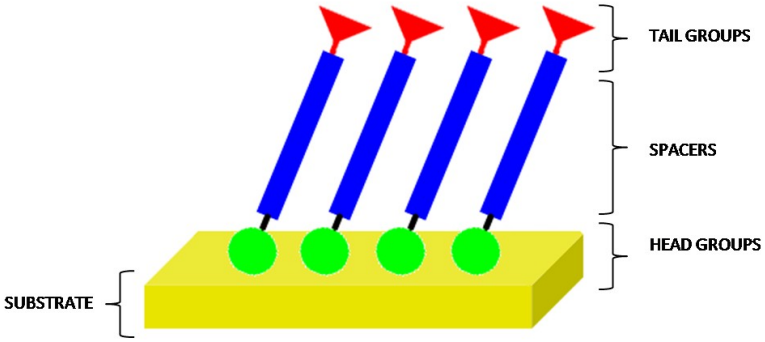

Figure 1. Schematic diagram of an ideal SAM on a substrate.

SAMs are very useful for combining physical properties that allow fundamental studies of interfacial chemistry, solvent-molecule interactions and self-organization. They can be considered as ideal model systems in many fields[3] because of their well-ordered arrays and ease of functionalization.. In fact they are very easy to prepare, they do not require ultrahigh vacuum or other specialized equipment in their preparation and they can form nanometre-scale objects (for example, thin films, nanowires, colloids, and other nanostructures). Moreover, by modifying the "tail group" of the surfactant, surface properties can be easily tuned. For the above reasons, SAMs can be used for coupling the external environment to the electronic (current-voltage responses, electrochemistry) and optical (local refractive index, surface plasmon frequency) properties of metallic structures; and they link molecular-level structures to macroscopic interfacial phenomena, such as wetting, adhesion, and friction.

The most extensively studied class of SAMs is derived from the adsorption of alkanethiols on gold[4], silver and other metals. The high affinity of thiols for the surfaces of noble and coinage metals makes it possible to generate well-defined organic surfaces (Figure 2) with useful chemical functionalities at the exposed interface.[5]

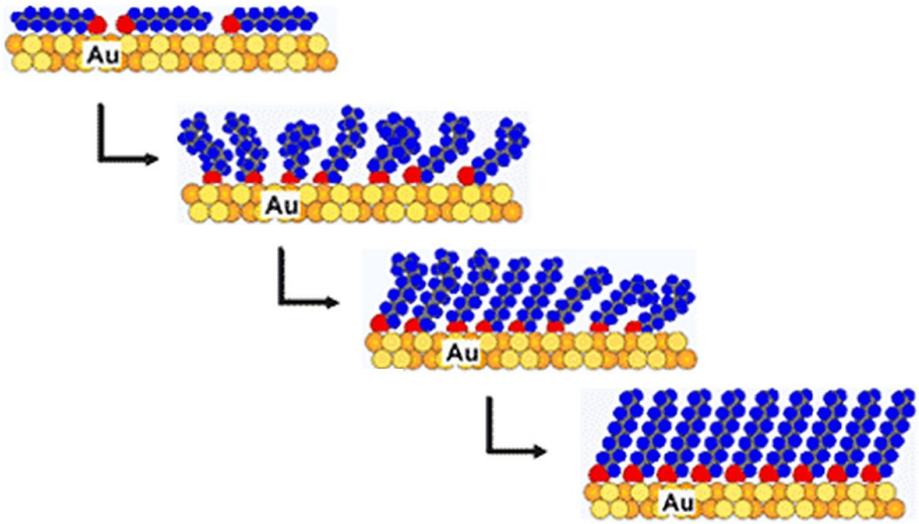

Figure 2. Formation of well-defined SAM film on gold surface. (from Nuzzo, R. G.; Allara, D. L. J. Am. Chem. Soc. 1983, 105, 4481)

The experiments on alkanethiol SAMs on gold[6] established many of the basic structural characteristics of these systems (surface structure, chain organization, orientation), practical protocols for preparing SAMs (concentrations, time for immersion, solvents, temperature), and some details of the thermodynamics and kinetics the assembly process. In fact gold is a reasonably inert metal easy to obtain as a thin film; it binds thiols with a high affinity;[7] it is easy to pattern by a combination of lithographic tools and chemical etchants, it is a convenient substrate for characterization, as thin films of gold are common substrates used for a number of existing spectroscopies and analytical techniques. Moreover gold is compatible with cells and SAMs formed from thiols on gold are stable for periods of days to weeks when in contact with the complex liquid media required for cell studies.

The most common protocol for preparing SAMs on gold, and other materials is immersion of a freshly prepared or clean substrate into a dilute (~1-10 mM) ethanolic solution of thiols for ~12-18 h at room temperature. This procedure resulted from a combination of studies planned to optimize the reproducibility of the SAMs.[8] It is possible to obtain dense coverage of adsorbates quickly (milliseconds to minutes)

from millimolar solutions, but, in order to maximize the density of molecules and minimize the defects in the SAM, a slow reorganization process is required (hours). A very wide number of experimental factors can affect the structure of the resulting SAM and the rate of formation, like solvent, temperature, concentration of adsorbate, immersion time, purity of the adsorbate, concentration of oxygen in solution, cleanliness of the substrate, and structure of the adsorbate.[9]
The first gold-alkylthiolate monolayer was produced by Allara and Nuzzo at Bell laboratories in 1983.[10] They realized the utility of combining a relatively inert gold surface with a bifunctional organic molecule in well-ordered, regularly oriented array.

Thiolic monolayers comprising a well-defined mixture of molecular structures are called "mixed" SAMs. There are three easy methods for synthesizing mixed SAMs: coadsorption from solutions containing mixtures of thiols, adsorption of asymmetric disulfides, and adsorption of asymmetric dialkylsulfides. Mixed SAMs provide a useful methodology for incorporating into a SAM a molecular species that for some reason (steric hindrance, presence of charges) cannot form directly a well-organized assembly.
The upper limit on the density of molecules on the surface is determined by the geometric arrangement of the thiols on the surface and the nearest-neighbour distances between the metal atoms at the surface. In order to minimize the free energy of the organic layer, the molecules adopt conformations that allow high degrees of van der Waals interactions[11] (and in some cases hydrogen bonds[12]) with the neighbouring molecules. If a simple single-chain model is considered, two parameters describe the variations in the orientation of the organic molecules in the SAM: the angle of tilt for the linear backbone of the molecule away from the surface normal (α) and the angle of rotation about the long axis of the molecule (β). As defined in Figure 3, α can assume both positive and negative values; values of β range from 0° to 90°. For alkanethiols SAMs on gold, the alkane chains adopt a quasi-crystalline structure if the chains are fully extended in a nearly all-trans conformation. The tilts of these chains for gold are near 30 and the average β for gold is near 50. These data are consistent with space-filling models involving chain tilts lying along the direction of the next-nearest neighbour, that is, an ordered structure involving a hexagonal arrangement of the sulphur atoms. These

assumptions have been largely confirmed by the results of diffraction studies.[13]

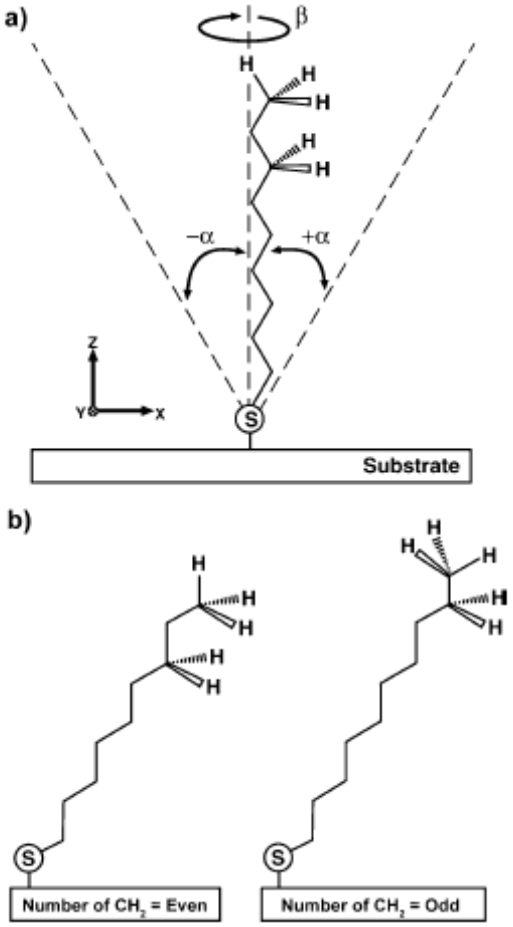

Figure 3. Representation of simple chain-model for alkanethiolates SAM on gold surface (from Chemical Reviews, 2005, Vol. 105, No. 4 1111).

SAMs can be fabricated into patterns having 10-100-nm-scale dimensions in the plane of a surface by using microcontact printing (μCP),[14] scanning probes,[15] and beams of photons,[16] electrons,[17] or atoms.[18] The techniques developed to generate patterns of SAMs on surfaces belong to a general class of techniques termed "soft

lithography"[19] that can replicate patterns of organic (or organometallic) molecules and other materials on substrates. One of the patterning strategies employed the physical transfer of the molecular components of a SAM to the substrate in an imposed pattern. Microcontact printing and scanning probe lithography are examples of methods that use this principle.
In microcontact printing the pattern is resulting from the direct contact between a stamp "inked" with an ethanolic solution of a thiol and the gold surface for few seconds. "Stamps" with patterned reliefs are formed from elastomers, for example poly(dimethylsiloxane), PDMS, that have been poured over a master, cured and then peeled. See Figure 4.

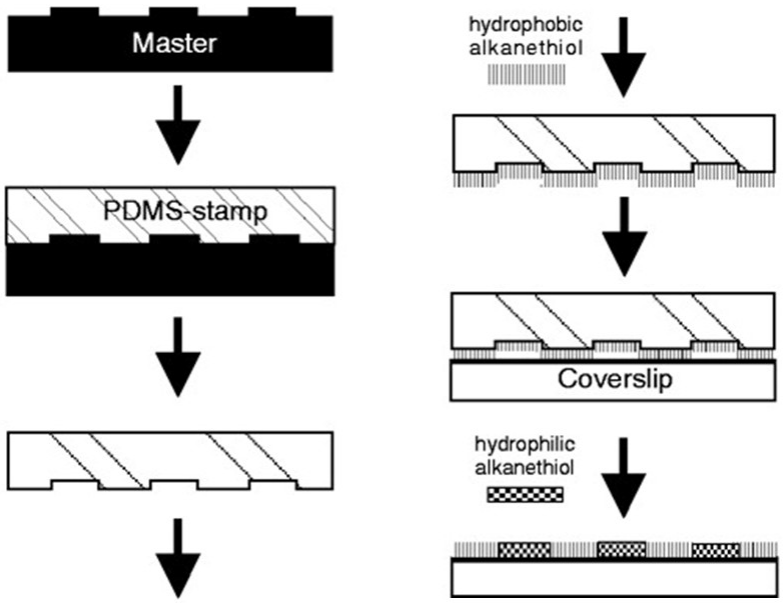

Figure 4. PDMS stamp preparation and micro-contact printing of alkanethiols on subrate (from Lehnert et al., *J Cell Sci , 2004 117, 41-52*).

Another strategy for generating in-plane patterns of SAMs relies on damage to a preformed SAM; an energetic beam of photons, electrons, or

atoms, or mechanical scratching can cause either chemical or physical damage to the SAM.

1.2.2 Multilayers by SAM and LB

In the 1930s, Irving Langmuir and Katherine Blodgett introduced a new method, the Langmuir-Blodgett (LB) technique, for fabricating mono- and multilayers of surfactants,[20] and obtain a wide variety of organized thin films.[21] Typically, LB films are fabricated by vertically dipping a solid support through a surfactant monolayer at the air–water interface and by the subsequent drawing of the substrate from the subphase. Further dipping and drawing can then lead to multilayers of the surfactant. (Figure 5)

.

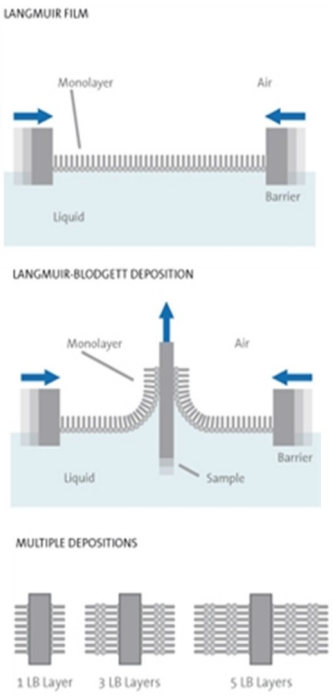

Figure 5. Schematic description of LB deposition.

In recent years, there has been a steady shift away from the LB technique towards self-assembly methods for the fabrication of monolayer and multilayer arrays. Two are the reasons for this shift: the greater robustness of self-assembled materials relative to most LB films, and also their ease of preparation. In contrast to the LB method, which requires a film balance and careful control over surface pressures during dipping and transfer, self-assembly is carried out by simple immersion of a suitable support into a solution and the next chemisorptions of molecules at the surface. The formation of multilayer arrays *via* self-assembly is also possible. For example, a surface can be dipped into a solution containing a molecule bringing particular chemical functionality, and next dipped into a second solution that contains transition metal ion.[22] (Figure 6).

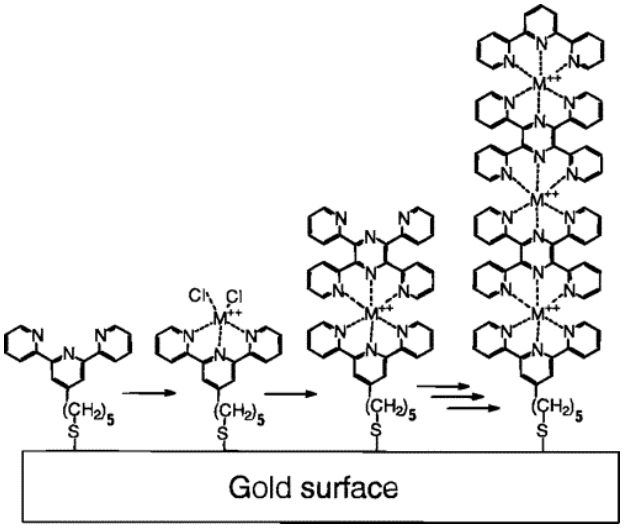

Figure 6. Schematic representation of a possible bottom up approach. (From Maskus, M.; Abruna, H., Langmuir 1996, 12, 4455).

In this way one can use ligands and ions as building blocks for multilayers growth by the repetition of such dipping in a layer-by-layer manner, with the possibility of controlling surface structure at the molecular level.

1.3 Supramolecular chemistry and weak interactions

Supramolecular chemistry refers to the area of chemistry that focuses on the non-covalent bonding interactions of molecules. While traditional chemistry deals with covalent bonding, supramolecular chemistry examines the weaker and reversible non-covalent interactions between molecules. So the aim is the study of complex molecular systems formed from several discrete chemical components. The driving force of these multicomponent entities is a set of reversible interactions, so they may dissociate and reform in response to particular chemical or environmental *stimuli*. The aggregation of these components gives rise to new entities with different properties that can behave in new and unexpected ways. (Figure 7).

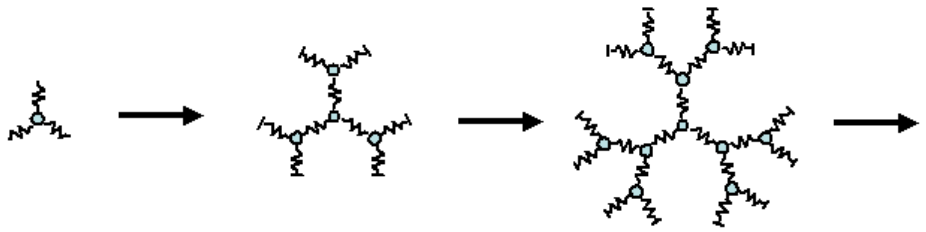

Figure 7. Example of synthetic scheme of a supramolecular complex.

The field of "weak interactions" includes hydrogen bonding, electrostatic effects, van der Waals force, hydrophobic effect and π-π stacking leading to new structural motifs like molecular self-assembly, mechanically interlocked molecular architectures, folding, molecular recognition, host-guest complexes, etc. The role of weak interaction in biology is very important, too. For example, the co-operative weak non-covalent forces decisively dominate the structure of DNA double helix or globular protein forms. The concept of complex intermolecular interactions being described as 'supramolecular' – literally 'beyond, or transcending, the molecule' – is associated with Jean-Marie Lehn's definition from the late 1970s: "Just as there is a field of *molecular chemistry* based on the covalent bond, there is a field of *supramolecular chemistry*, the chemistry of molecular assemblies and of the intermolecular bond."[23] As

Lehn acknowledges, the application of this terminology to chemical species has much to do with Wolf's earlier description of the *übermolecül* - a definition originally designed to cover the self-association of carboxylic acids to form a 'supermolecule' through hydrogen bonding-.[24] Indeed, Lehn also used this simpler definition to describe chemical organization in terms of: "an assembly of two or more molecules, a *supermolecule*."

Central to supramolecular chemistry is Fischer's 'lock and key' analogy of enzyme catalysis.[25] The molecular recognition can be regarded in many ways as the most fundamental kind of supramolecular chemistry, based on how to recognize molecules, how to influence molecules, and how to express specific functions due to molecular interactions. These interactions can be briefly overviewed.

Electrostatic interactions occur between charged molecules. An attractive force is observed between oppositely charged molecules, and a repulsive force between molecules with the same type of charge (both negative or both positive).

Dipole–dipole and dipole–ion interactions play important roles in neutral species instead of electrostatic interactions.

Hydrogen bonding sometimes plays a crucial role during recognition, although a hydrogen bonding interaction is weaker than an electrostatic interaction. It only occurs when the functional groups that are interacting are properly oriented. This is the reason why hydrogen bonding is the key interaction during recognition in many cases. The importance of hydrogen bonding to molecular recognition is evident in the base-pairing that occurs in DNA strands, where nucleobases recognize their correct partners in a highly specific way.

Coordinate bonding is another type of direction-specific interaction. This type of interaction occurs between metal ions and electron-rich atoms and it is of moderate strength.

The Van der Waals interaction is weaker and less specific than those described above, but it is important because this interaction is very common to all kinds of molecules. It is driven by the interactions of dipoles created by instantaneous unbalanced electronic distributions in neutral substances. Although individual interactions are insignificant, the combined cooperative contributions from numerous Van der Waals interactions make a significant contribution to molecular recognition. When the interacting molecules have surfaces with complementary

shapes, as in the “lock and key” concept, the Van der Waals interaction becomes more efficient. π–π interactions occur between aromatic rings, and these sometimes provide important contributions to molecular recognition. When the aromatic rings face each other, the overlap of π-electron orbitals results in an energetic increase. For example, the double-strand structure of DNA is partially stabilized through π–π interactions between neighbouring base-pairs.
Usually, in molecular recognition systems, selective and effective recognition is achieved through various combinations of the above-mentioned molecular interactions. When several types of molecular interaction work together, a cooperative improvement in molecular association is often observed. Finding an appropriate combination of molecular interactions is the key to designing efficient molecular recognition systems.

Many efforts of scientific world are oriented to imitate nature’s supramolecular design motifs to generate robust nano-structured materials in a facile manner. The potential applications for these materials range from new catalysts to biocompatible structures for tissue and bone replacement therapy. Another aim is that of fabricating , new synthetic materials from nanoscale and microscale ordering, using functional small-molecule building blocks.. The need for improved miniaturization and device performance in the microelectronics industry has inspired many investigations into supramolecular chemistry. It is conceivable that ‘‘bottom up’’ materials fabrication approaches based on supramolecular chemistry will provide a solution to the size limitations of ‘‘top down’’ approaches, such as photolithography, thereby providing the means to fabricate ultrasmall electronic components. Perhaps more likely is that hybrid devices will become increasingly important. These devices integrate the outstanding electronic and photonic properties of non-molecular hard materials, such as silicon, to the excellent bio recognition, chemical sensing, and related properties of soft molecular materials to yield structures capable of performing disease diagnosis, environmental monitoring, controlled drug delivery, and so on.
Macromolecular organic building blocks include phase-separated block copolymers and more recently dendrimers. These have been used to generate sophisticated ordered composites and to allow nanopatterning on surfaces. Self-assembling coordination compounds featuring ligand-

functionalized porphyrins and related components have been a mainstay of inorganic supramolecular chemistry.[26] More recently, semiconductor or metal nanoparticles have been used as ‘‘macromolecular’’ inorganic components for supramolecular arrays with interesting electronic properties. In summary, principles of supramolecular chemistry can be applied to the synthesis of new structured assemblies featuring long-range order and displaying useful functional behaviour. Further work on supramolecular materials fabrication will yield many additional examples of functional, self-organized assemblies, including assemblies displaying useful photonic and electronic properties.

1.4 Polypyridine based metal complexes

Polypyridines are multidentate ligands with characteristic properties; for example they are stable to heat, light and electricity. Polypyridine complexes are compounds in which a polypyridine coordinates to a metal ion. Polypyridine-based metal complexes have very interesting physical and chemical properties, like optical, electrochemical, and magnetic properties. Among many polypyridine-derivates, 2,2'-bipyridines derivatives and 2,2'; 6,2"-terpyridine derivatives have become an ever-expanding synthetic and structural frontier because 2,2'-bipyridine metal complexes, 2,2'; 6,2'-terpyridine metal complexes (Figure 8) and mixed bipyridine-terpyridine metal complexes have special redox properties suitable for various applications.

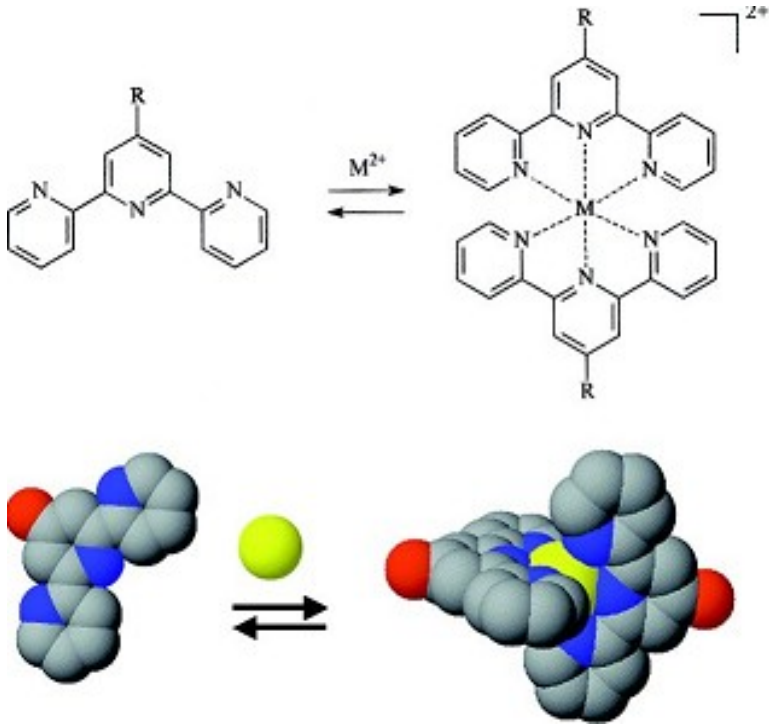

Figure 8. Example of terpyridine-based metal complex.

In fact, these complexes can be used in several branches of nanothecnologies such as molecular electronics and photonics, light harvesting, sensor devices, biotechnologies, etc. Unlike the bipyridine-based ones, terpyridine-based complexes do not suffer of problems related to the presence of various possible isomeric conformations, thus they have been used in many research field, for example in the conversion of solar energy to electricity. Some complexes exhibit a strong absorption band in the visible light region, which is called metal-to-ligand charge transfer (MLCT) or ligand-to-metal charge transfer (LMCT). The properties of the complexes can be tuned easily by introducing, for example, substituents performing electron donation or electron withdrawal, and/or π-conjugating groups to the polypyridine moiety. The MLCT absorption band can be shifted, the emission wavelength can be changed, and the emission lifetime can be extended.
Up to nowadays several studies have been performed to investigate the properties of terpyridine-based metal complexes. After the advent of supramolecular chemistry, the synthesis and the study of aggregates based on coordinative bonds increased exponentially. In particular, terpyridine moieties have been used to build macromolecule, multilayers and biochemical aggregates.
Generally, metallo-supramolecular homopolymers result from the complexation of metal ions and ditopic chelating ligands As shown in Figure 9, the chelating macro-monomer is connected by a (transition) metal ion *via* coordinative bonds resulting in a metallo-supramolecular polymer. This concept requires that the chelating monomer is a telechelic system capable of a continuous chain extension in the presence of a metal ion by following the well-known polycondensation-like mechanism.

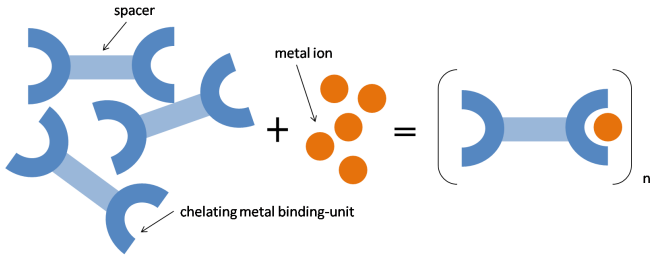

Figure 9. Schematic representation of the metallo-supramolecular polymerization process.

The aim of synthesizing metallo-supramolecular structures is to create novel materials that can reveal specific and multifunctional properties (Figure 10). The building blocks should therefore be carefully selected in order to create new materials with tailored properties. Beside the use of low molar mass ditopic "organic" ligands, telechelic polymers bearing suitable ligands at their extremity are extremely valuable candidates for the formation of metallo-supramolecular polymers. In this way, the properties of the designed materials can be manipulated not only by the careful choice of the metal ions, but also by the polymer backbone (Figure 10). This allows the formation of materials combining the characteristic features of the metal ligand complexes (special electrochemical, optical, magnetic properties) to the ones of polymers (processability, mechanical properties, solubility, *etc.*.).

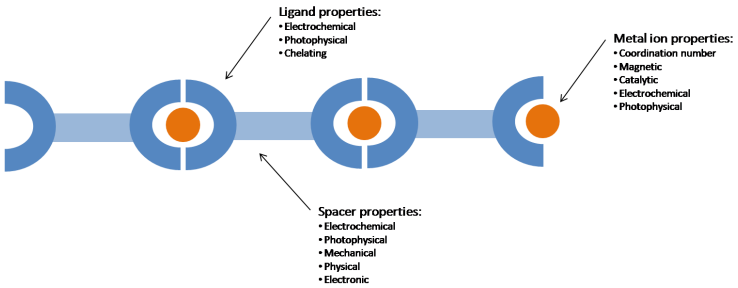

Figure 10. Schematic overview of the properties of metallo-supramolecular polymers.

A well-known example of a polypyridine complex is ruthenium-tris(bipyridine), $Ru[(bpy)_3]^{2+}$, which exhibits intense luminescence at room temperature in aqueous solution. Another example is a platinum-bipyridine-dithiolate complex, Pt(bpy)(bdt), in which bdt denotes a 1,2-benzenedithiolate anion. This complex also exhibits photoluminescence at room temperature, and its wavelength and lifetime can be tuned by substitution of either bipyridine or dithiolate moieties. Structural control is easier than for ruthenium complexes due to the square planar structure of the platinum complex.

1.5 Applications

Supermolecules involved in electron conduction (molecular electronic devices), supermolecules that react to light and control photonic information (molecular photonic devices), supermolecules that can be used for information processing and calculations (molecular computer), and supermolecules that are able to move and rotate (molecular machines) are examples of molecular devices. (Figure 11).

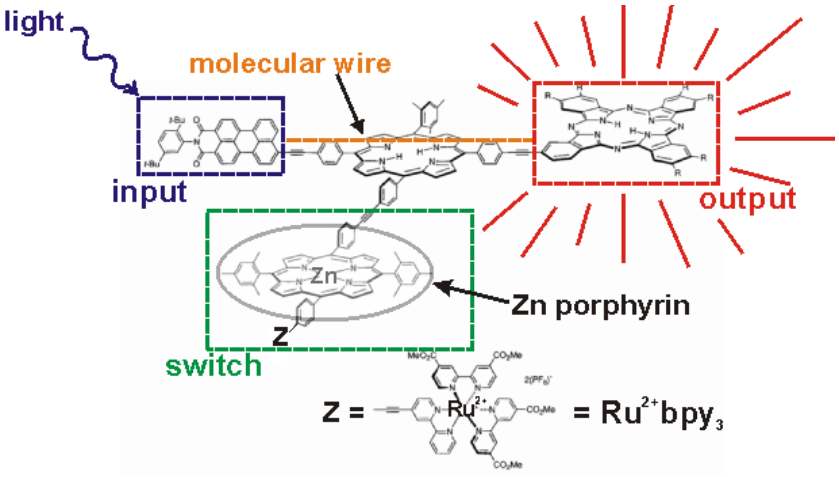

Figure 11. A molecular electronic device called an optoelectronic switch. Energy is allowed to flow from the "input" to the "output" through the "molecular wire" when the "switch" is turned "on". The "on/off" state of the switch depends on the oxidation state of the molecular components in the switch. [From *Chem. Mater.* 13, 1023-1034 (2001).]

All these examples explain why supramolecular chemistry can be an important tool in the development of nanotechnology which will probably revolutionize our life style in the near future.
In these molecular devices molecules replace functional units. Molecular devices are expected to provide the key to the development of nanotechnology, and the possibility to fabricate complicated functional systems through the supramolecular assembly of relatively simple

components, with the additional advantage of combining functional parts with great freedom . Molecular devices are generally interfaced with external devices that can store signals from the device and convert them in other signals easier to understand and interpret. Therefore, it is important to understand the methods used to evaluate molecular device state.

The first step is to develop molecular sized electronic parts and then find a way to combine them into molecular electronic devices. Molecules with conjugated linkages are very interesting candidates for electron-conductive "molecular wires" for molecular electronics. Especially when used in supramolecular systems, a regulated conjugation length is sometimes advantageous.

In the near future, the number of devices utilizing photonics (the optical equivalent of electronics) is expected to increase dramatically.

Light can be seen as a mixture of visible wavelengths that all travel at the same (fast) speed. Therefore, photonic systems can be used to transmit huge amounts of information within an extraordinarily short period of time. Recently, photonic technology has been applied to various devices, like compact discs, photocopiers and barcode readers, or to the possibility to rapidly communicate large amounts of data between different parts of the world, for example made possible through fiber optic cables. From these considerations, it is clear that supramolecular chemistry is therefore expected to play an important role in the all-days technology, in particular in the development of photonic devices with huge information densities.

2 Results and discussions

2.1 Introduction

The work described in this thesis was aimed to the anchoring and characterize different types of functional molecular and supramolecular layers on inorganic surfaces, namely oxide or noble metal surfaces. In some of the cases discussed, the possibility of anchoring the layers in a spatially resolved way (patterning) has been demonstrated.
In particular, section 2.2 is dedicated to the description of the results on the development of a methodology for modification of oxide surfaces, useful for anchoring organic layers on top of them, by exploiting the reactivity of zirconium (IV) with phosphates and phosphonates. Such a strategy (henceforth called ZP strategy) can represent an alternative to more common methods based, for example, on silane chemistry. The ZP strategy has been employed here for the anchoring, on two different oxide surfaces, of a SAM containing a terpyridine ligand which, in turn allows the growth - directly at the surface – of metal-complex-based multilayers by stepwise self-assembly (section 2.3). Sections 2.4 and 2.5 are dedicated to experiments performed on more conventional gold substrates. In particular, in section 2.4 we used an approach similar to that exploited on oxide surfaces (i.e. involving the formation of metal ion complexes *at* a surface functionalised with a terpyridine-containing SAM) for anchoring oligonucleotide sequences on gold surfaces. At variance of the case of oxides, the anchoring of the terpyridine-based SAM on gold involves the use of ligands with a thiol head group. In section 2.5 thiol-based SAMs were used for anchoring, on gold surfaces, monolayers based on pseudo-rotaxanes. In both cases (sections 2.4 and 2.5) the prepared layers were exploited for studying, directly at surface, molecular recognition interactions.
The characterization of the surface layers has been performed by different techniques, including ToF-SIMS, XPS, UV-Visible spectroscopy, QCM-D analysis (see appendix in chap. 4 for details on these techniques).

2.2 Oxide surfaces modification methodology

Self-assembled monolayers of molecules containing polypyridinic functional groups are very interesting systems for preparing, at the surface, opto- and electroactive metal complexes that could be used in several application fields, such as molecular electronics and photonics or sensing devices.[27] Anchoring transition metal complexes with particular properties onto oxide surfaces could be very useful in order to have a conjunction between electrical and redox properties of molecules and substrates. Several transparent semiconductor oxides (such as TiO_2, WO_3, ITO, etc.) are widely used for organic photovoltaic[28] and organic electronics and optoelectronics.[29] Several anchoring strategies have been proposed. For instance, carboxylic and dicarboxylic acid[30] or phosphonic groups[31] are often used, since they provide a simple route to surface adsorption; or silanes are used to provide robust surface anchoring via the formation of covalent bonds.

Carboxylic acids have been used successfully to bind to different metal oxides, but usually through a variety of binding moieties, including as an uncoordinated anion, a monodentate ligand, a bidentate chelate or a bridging bidentate. Despite the fact that high–coverage monolayers can be prepared utilizing carboxylic acids, the combination of binding modes and their relative weakness leads to the formation of monolayers that often are weakly bound to the surface and that can be easily removed, sometimes by simple rinsing in solvents.[32] Furthermore, the presence of additional polar sites in the carboxylic acid molecules can result in competition for surface sites, thus preventing well–organized, high coverage monolayers.[33]

Silanes have been and still are a widely used functionality that binds to metal oxides, in particular silicon dioxide. There are many types of silanes that are commercially available. They have been used to form very dense monolayers for a variety of applications and on a variety of surfaces *via* a covalent bond to the surface and among other silanes.[34] The use of silanes (typically molecules bringing a chloro- amino- or alkoxy-silane head-group) is based on the silanization reaction of M-OH groups present at the surface of an oxide substrate such as glass or quartz.[35,36] In appropriate condition, this process can lead to the formation

of a monolayer, covalently bound to the surface by siloxane groups. It is reported that, for this kind of anchoring methodology, the formation of M-O-Si bond is accompanied by the formation of Si-O-Si "horizontal" bonds between adjacent molecules.[37]

However, the formation of robust monolayers based on silanes can be difficult, as it depends heavily on the hydrolysis of the silane,[38] which is dependent on the water content, pH, and temperature. If the modification conditions are such that the amount of hydrolysis is not sufficient (such as when not enough water is present) then an incomplete monolayer will be formed.[39] By contrast, when an excess of water is present, the rate and extent of hydrolysis will be too high and self–condensation will occur and multilayers can be formed on the surface. Only when the conditions can be carefully monitored and controlled, robust well–formed monolayers can be obtained by using silanes. Another drawback to silanes is that to ensure their long–term integrity, which implies the need of storage in anhydrous conditions as they may self–condense over time.[40]

A few methods have been proposed in order to overcome the aforesaid problems. For instance, it is possible to use molecules bringing a phosphonic acid group instead of a silane. Phosphonic acids are thought to bind to a metal oxide surface by first coordination of the phosphoryl oxygen to Lewis acid sites on the surface, followed by condensation of the P–OH groups with surface hydroxyl groups or other surface oxygen species.[41] One important difference between phosphonic acids and silanes is that the homocondensation of P–OH and P–O- bonds does not occur at mild conditions and/or in aqueous conditions. Thus, multilayers should not form *via* this mechanism on the surface. The fact that the quality of modification is independent of the amount of water present means that less stringent conditions need to be followed when using phosphonic acids with respect to silanes. One other advantage of phosphonic acids is their stability. Assuming any additional organic groups on the compound are inert, they are almost always white crystalline solids which are stable in ambient conditions over long periods of time.

A problem arising with the use of phosphonic acids is connected with the fact that the strength of the obtained bond is largely dependent on the nature of the oxide so that, in many cases (for example on silicon oxide) the bond is quite weak, and the formation of a stable ordered monolayer undergoes problems similar to those mentioned above in the case of

carboxylic acids. This problem, however, can be overcome using a methodology in which the phosphonate moiety interact with a zirconium ion, as this interaction is well known to be quite strong.[42] A method for doing this is that of using a surface priming method based on the direct phosphorilation of a suitably hydroxylated oxide surface and its successive reaction with a zirconium salt.[43] Such primed surface, in turn, will be able to bind organic molecules bringing a phosphonic acid functionality. Such a method is referred as ZP strategy.
In the present work our aim was that of anchoring, by means of the ZP strategy, molecules containing, in addition to the phosphonic moiety, a terpyridinic function to be used as a ligand for the formation of metal complexes directly at the surface. However, the presence of two functionalities (terpyridinic and phosphonic acid) poses a critical problem related to the fact that surface anchoring of such molecule on a zirconium-containing layer in principle can occur *via* both the functionalities. Our results show that, in fact, bifunctional molecules adsorb preferentially by means of the terpyridine moiety so that, in order to obtain the desired upward orientation of terpyridine, it is necessary to protect such functionality before the surface anchoring and hence force the molecule to adsorb *via* the phosphonate group. For this aim, a labile complex with Zn has been exploited for protecting the terpyridine functionality. After the deprotection of terpyridine function by dissociation of the Zn complex, the desired metal complexes can be formed directly on such functionalized oxide surface.

2.2.1 Zirconium-phosphate-phosphonate chemistry

As outlined in the previous chapter, self-assembled mono- and multilayer structures (SAMs) have received a great attention in the materials community for many reasons. An incredible amount has been learned about interfacial monolayers and the associated measurement technology using the alkanethiol/gold system.[44] While studies of this system have led to important advances in understanding of organic-modified interfaces, thiol/gold monolayers suffer from long-term chemical stability limitations[45] These limitations have been a driving force for research to identify alternative layer growth strategies, with, for instance, silane[46] and

zirconium-phosphate-phosphonate (ZP) chemistry.[47] The interest in SAMs based on ZP chemistry arises from their ease of assembly, the soft conditions used in the formation of these layers, and their structural and thermal stability, once formed.

Mallouk and co-workers were the first who developed a strategy for surface anchoring of organic molecules on oxides, based on the chemistry of zirconium phosphonate and the high affinity of many transition metal ions for the phosphonate or phosphate.[48]

In solid-state chemistry, the metal-phosphorus interaction leads to a wide variety of layered and crystalline materials, including the prototypical α-zirconium phosphate, with high solvent resistance, intercalation ability, and the potential for catalytic activity.

The Mallouk group first demonstrated that such materials could be grown on substrates by the deposition of individual layers of metal ions and phosphate compound. With very few exceptions, metal phosphonate salts form layered structures in which the metal ions and phosphonate oxygen atoms lie in puckered sheets. The bonding requirements of the metal determine the atomic arrangement within these layers, which is rather insensitive to the nature of the organic group (Figure 12).

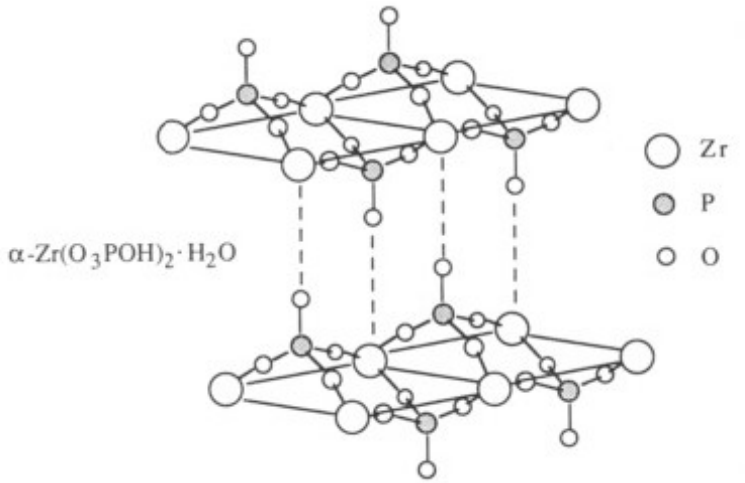

Figure 12. Idealized structure of a-zirconium phosphate, showing the pseudohexagonal unit cell.

Building up a metal phosphonate film on a surface requires first, either by adsorption or by covalent binding to the substrate, anchoring of molecules bearing the phosphonate functionality. Then the substrate has to react with transition metal ions solution, in this case Zr^{4+}. Multilayer films are then prepared by alternately adsorbing metal ions Zr^{4+}, and α,ω - bis-phosphonic acids from aqueous solution (see Figure 13).

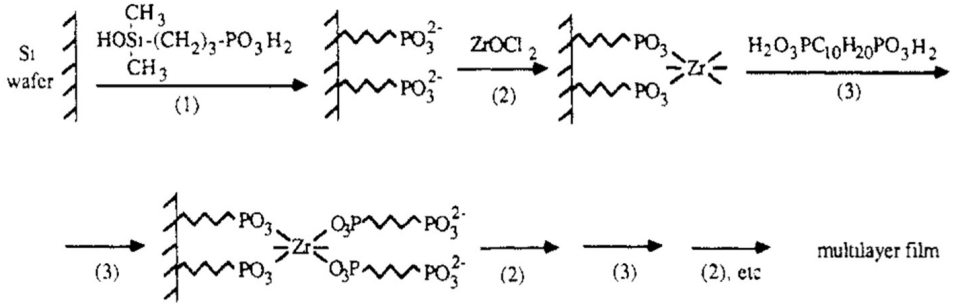

Figure 13. Reaction scheme for Mallouk's group proposed strategy.

Metal phosphonates are an ideal choice for this kind of synthesis because, as bulk phases, their morphology is similar to LB multilayers. The structural analogy is shown in Figure 14.

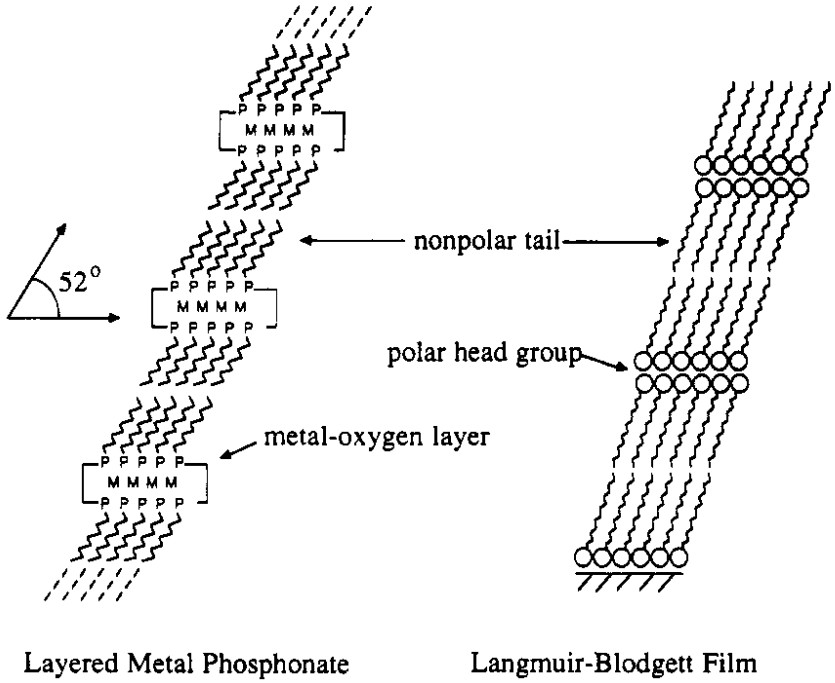

Figure 14. Structural analogy between metal phosphonate salts and Y-type Langmuir-Blodgett films. The tilt angle in the former is inferred from powder X-ray diffraction data.

Katz and co-workers,[49] by using a modification of Mallouk's method, assembled zirconium phosphate phosphonate non-centrosymmetric multilayers containing different azoic push-pull dyes.[50] These molecules were characterized by a phosphonate group in one end and, a hydroxyl at the other, linked by a conjugated system.

The key of the sequential deposition technique used by Katz has been to design a three-step adsorption sequence involving molecules (see Figure 15). The three steps are: chemisorption of the phosphonate end of the molecule on the Zr^{4+} phosphate layer, phosphorylation of the exposed hydroxyl group with $POCl_3$ to regenerate a phosphoryl-terminated surface thus allowing the reaction with zirconium ions.

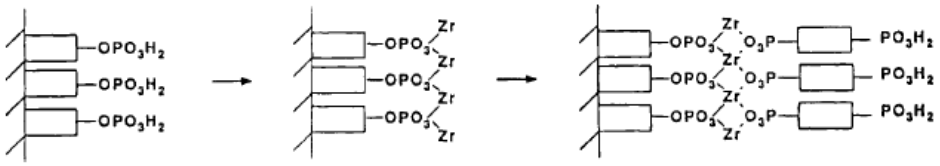

Figure 15. Reaction scheme for Katz's group proposed strategy.

The reiteration of this sequence led to multilayered hybrid organic/inorganic films[51] that showed second-order non-linear optic coefficients of the same order of magnitude of $LiNbO_3$ together with very high chemical, mechanical and thermal stabilities, which are prerequisites for their integration in optoelectronic devices.
Kohli e Blanchard[52] developed a priming methodology for oxide substrates that allows the phosphorylation directly at the surface. This strategy (see Figure 16) is characterized by three steps: the first step is the substrate cleaning by its immersion in oxidising ("piranha") solution (3:1 H_2SO_4:H_2O_2) in order to increase the amount of hydroxyl groups on the surface; the second step is the phosphorylation of hydroxyl groups by $POCl_3$ and collidine in anhydrous acetonitrile; the third step is the reaction of phosphoryl groups with a zirconium salt aqueous solution.

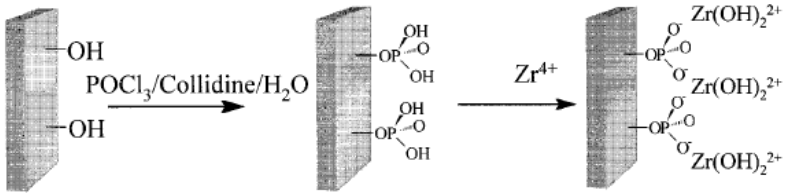

Figure 16. Reaction scheme for Kohli and Blancard proposed strategy.

The priming strategy used in the present work, and described in the next section, is essentially a modification of Blanchard's method. The zirconium-terminated surface will be used as "platform" for anchoring of a terpyridyl-benzenephosphonic acid on a model oxide (SiO_2).

2.2.2 Surface priming

As model substrates, we used 500 nm thick thermally grown SiO_2 on silicon or quartz slides, while as a substrate of technological interest and the choice was on Indium Tin Oxide (ITO) sputtered on glass slides. When the priming process is performed on ITO substrate it is necessary to avoid aggressive treatments which could etch the ITO film on glass slides. Therefore a slightly different approach from SiO_2 and quartz substrates was employed, as detailed later.
As preliminary treatment, all the "as-received" substrates were consecutively cleaned with chloroform, acetone and ethanol. After this cleaning step, in order to enrich the surface with OH groups, silicon dioxide substrates were immersed for 15 minutes in a H_2SO_4:H_2O_2 (3:1) while ITO substrates were treated for 15 minutes in UV-O_3. Immediately after these treatments, both kind of samples were rinsed in pure water. Subsequently, in order to transform the surface hydroxyl groups in phosphate groups, specimens were immersed in neat $POCl_3$ (18 hours in the case of SiO_2 and 1 hour for ITO films), then rinsed with water, and finally immersed in a $ZrCl_2O$ solution (10^{-4} M, water) for 15 minutes and again rinsed with water, that completes the priming procedure (see Figure 17). For a discussion of the zirconium phosphate/phosphonate chemistry see reference[53]. The results reported in the following, for the sake of simplicity, refer to SiO_2 substrates.

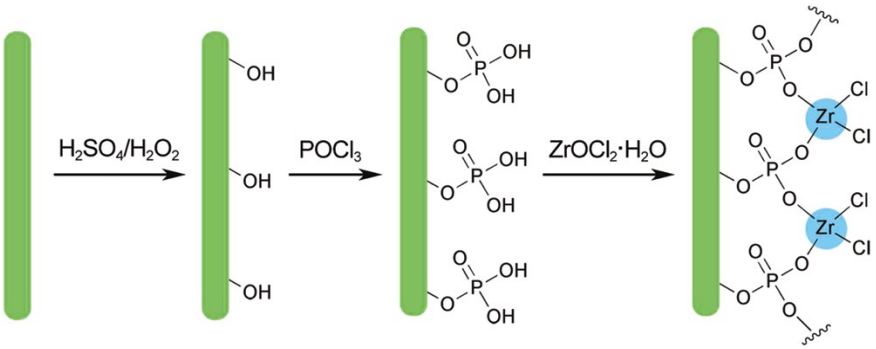

Figure 17. Reaction scheme for oxide surface priming and formation of a ZP layer.

2.2.3 Anchoring of a terpyridine-containing SAM on zirconium-primed surfaces

A phosphonate-functionalized terpyridine ligand, i.e., the 4-(2,2':6',2''-terpyridine-4-yl)benzenephosphonic acid (Figure 18, henceforth PPTP) was synthesized in order to develop a suitable procedure for its surface anchoring on zirconium-phosphonate surface. The synthesis of PPTP ligand was performed on purpose by Dr Quici's group at CNR-ISTM in Milan, Italy.

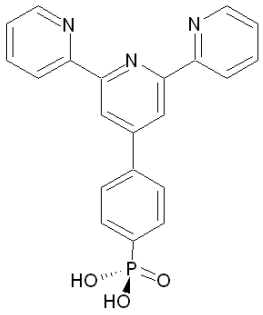

Figure 18. Molecular structure of PPTP ligand.

Surface anchoring of PPTP was performed using two different approaches (Figure 19). In the first case ("direct" reaction, approach A) substrates were immersed for 24 hours in a PPTP solution (10^{-4} M in a 1:1 DMF:H_2O mixture) and then rinsed in water. In the second case, a protection/deprotection procedure (approach B), was used: PPTP was reacted with the stoichiometric amount of Zinc trifluoromethanesulfonate at room temperature, so obtaining the $Zn(PPTP)_2$ complex (10^{-4} M). Substrates were then incubated in the above solution for 24 hours and then rinsed in water. Afterwards, specimens were dipped in HCl solution (0.1 M, water) for 15 minutes in order to restore terpyridine function.

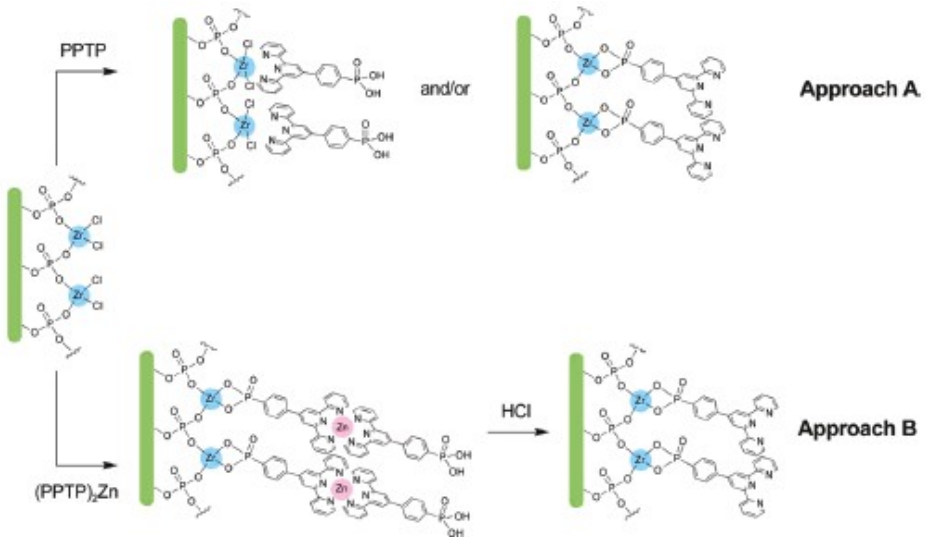

Figure 19. Reaction scheme for the two different approach for anchoring PPTP.

In order to check the availability of the terpyridine function for further coordination reactions, substrates prepared with both the approaches were treated with solutions of iron(II) sulfate heptahydrate (10^{-4} M, 1:1 ethanol/water) for 1 minute, washed with a water/ethanol mixture and then treated with a terpyridine solution (~10^{-4} M, ethanol) for 1 hour in order to form the PPTP-Fe(II)-tpy heteroleptic complex. Samples were finally rinsed in ethanol and dried under nitrogen flux.
While the first anchoring mechanism would imply the availability of the terpyridine ligand for further coordination steps, the second anchoring geometry would block further coordination reactions. See Figure 20.

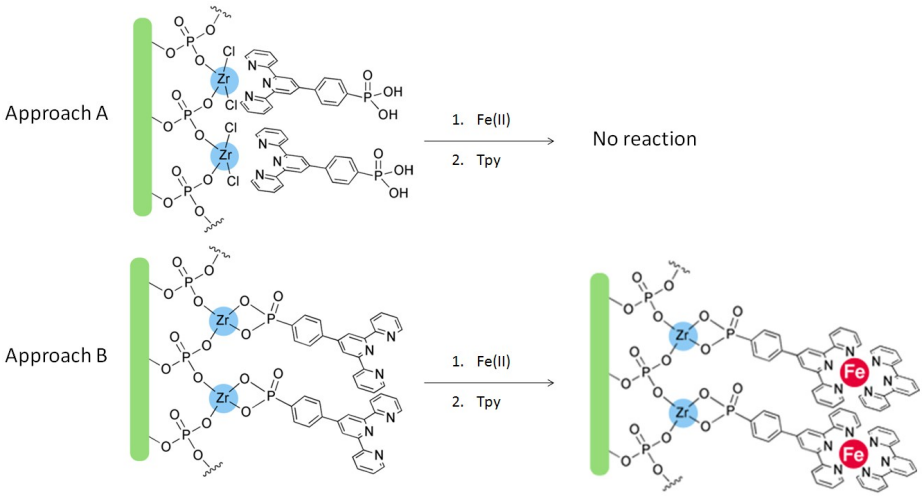

Figure 20. Reaction scheme for reaction of the two different approach products with iron and terpyridine ligand.

2.2.4 ToF-SIMS characterization

Samples prepared by means of the two adsorption approaches were characterized by time-of-flight secondary ion mass spectrometry (ToF-SIMS). ToF-SIMS spectra were acquired with a reflector-type TOFSIMS IV spectrometer (ION-TOF GmbH, Muenster, Germany) using 25 keV Bismuth primary ions. Spectra were acquired in static mode (Bi^+ primary ion fluence < 10^{12} ions·cm^{-2}) in order to preserve the molecular information.
This technique provides high level of molecular information from the uppermost surface layers with very high sensitivity[54] and it is well suited for studying SAMs[55] and for verifying the potential formation of complexes at the surface.[56] Figure 21 shows a portion of the typical ToF-SIMS spectra of PPTP layers prepared by approaches A and B respectively. The same spectral region obtained after priming but before functionalization with PPTP is reported for comparison. The spectra, from the surfaces functionalised with approaches A and B are very similar to each other, and both contain the same characteristic fragments. In particular, the presence of molecular fragments bringing a Zr atom are

a signature of the successful anchoring of PPTP on the surface. In particular, the $[C_{21}H_{13}N_3PO_3Zr]^+$ peak (m/z 476) corresponds to the entire PPTP molecular ion plus a zirconium atom, as demonstrated by the mass and the isotopic pattern. Hence, no difference among the surfaces prepared via the two methods can be inferred from these spectra.

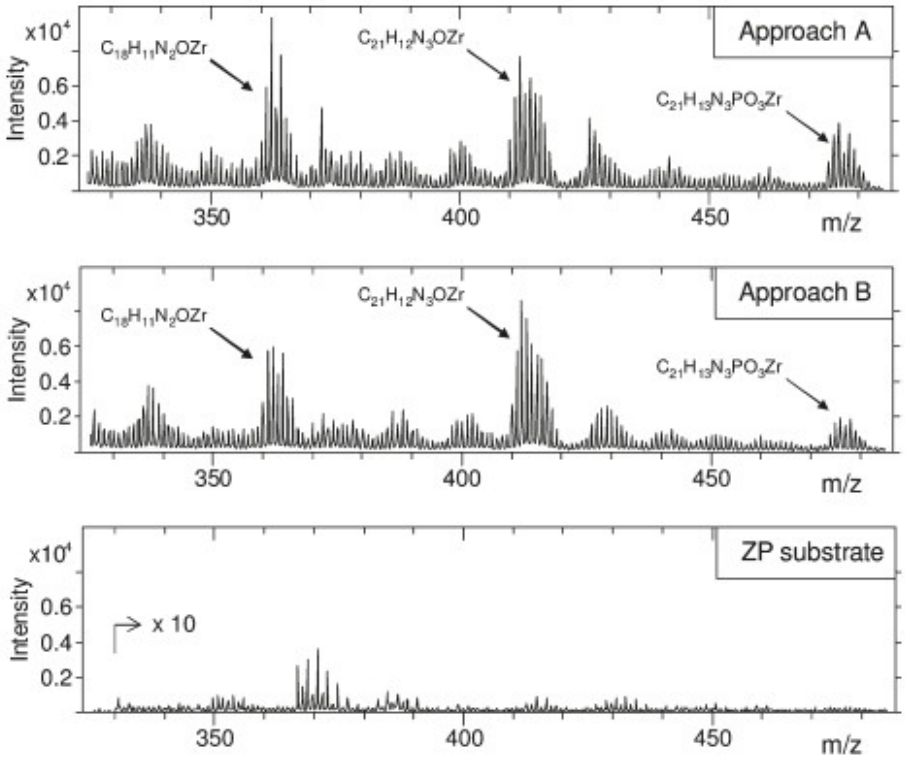

Figure 21. Portion of the positive ToF-SIMS spectra of PPTP anchored samples via two different approaches, showing some relevant PPTP-Zr fragment ions. The spectrum of SiO_2/ZP substrate is reported for comparison.

By contrast, after immersion in the Fe(II) solution, the ToF-SIMS spectra of samples prepared by means of the two approaches show significant differences. In particular, it was found (see Figure 22) that the iron complex is formed only on surfaces prepared by approach B, as clearly indicated by the presence, on those surfaces, of relevant complex-related

fragment ions such as that at m/z 597, assigned at the entire complex missing only of the phosponate group, and those at 595 m/z and 613 m/z (597 - H_2 and 597 + O, respectively).

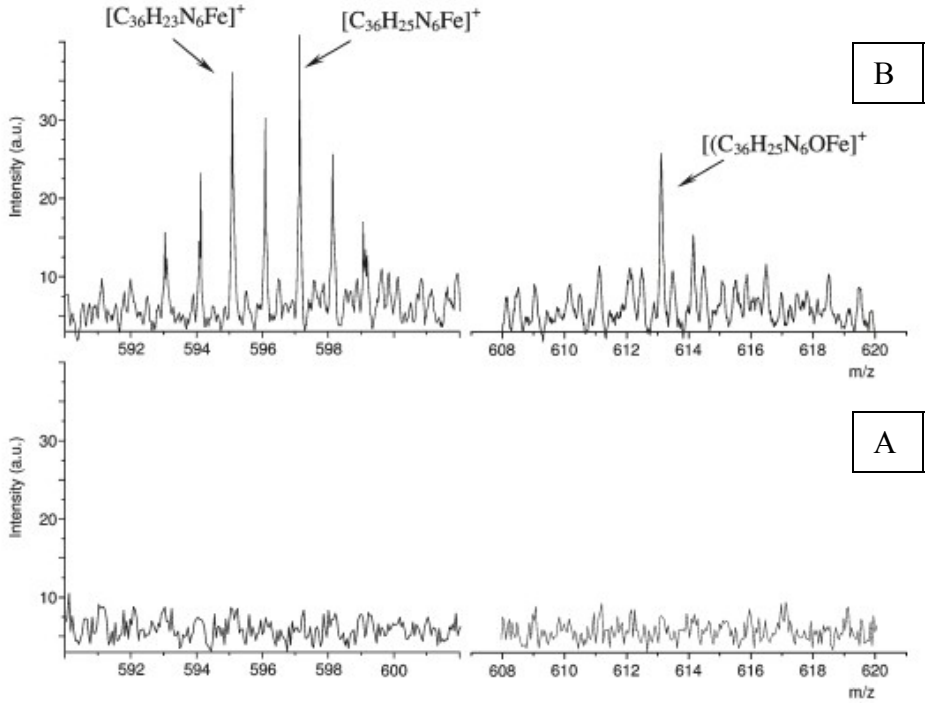

Figure 22. Portion of the positive ToF-SIMS spectra of PPTP anchored samples via two different approaches, and reacted with iron and terpyridine ligand (bottom spectrum approach A, upper spectrum approach B).

2.2.5 XPS characterization

Each stage of the priming procedure was monitored by means of X-ray photoelectron spectroscopy (XPS). XPS measurements were performed with a ESCALAB IIB spectrometer (VG Scientific Ltd., UK), using the Mg $K\alpha_{1,2}$ line at 1253.6 eV. Pass energy was 50 eV for wide scans and 10 eV for high resolution scans. All the B.E. values are referenced to the

aromatic C 1s band at 284.7 eV. Integration of the XPS bands was carried out using the XPSPEAK freeware software. The XPS data, among others, allowed us to obtain information on the success of each step, and to achieve a better understanding the orientation of PPTP anchored by means of the two different approaches (A and B).

Figure 23 shows the region of XPS spectra where the main photoelectrons lines (Si 2p, Zr 3d, P 2s and P 2p), obtained for specimens after treatment with (a) piranha solution, (b) $POCl_3$, and (c) zirconyl chloride.

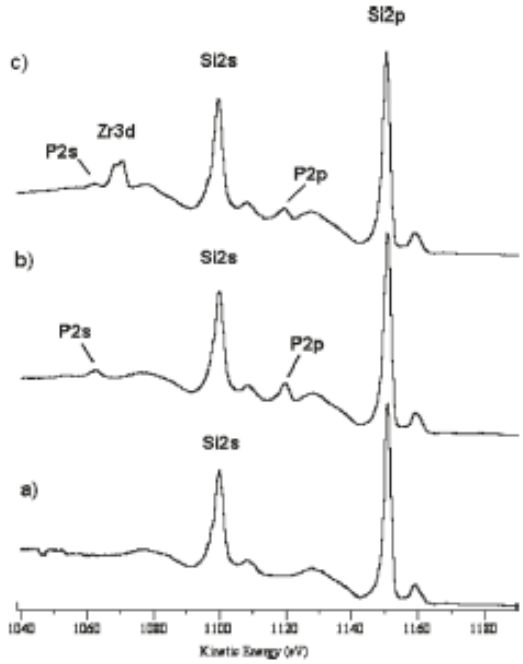

Figure 23. XPS spectral region with phosphorus, zirconium and silicon main peaks, measured at different stages of SiO_2 surface treatment: a) piranha treatment; b) phosphorilation; c) treatment with $ZrOCl_2$.

The sequential appearance of phosphorus (Figure 23b) and zirconium (Figure 23c) peaks is a first clue of the success of the priming process. More detailed information on the surface composition can be obtained

from the analysis of the quantitative data extracted from the XPS intensities, and reported in Table 1.

treatment stage	P/Zr	C/N	Si/P	Si/Zr
SiO_2+$POCl_3$			14	
+ PPTP (approach A)	2.0	10	16	32
+ PPTP (approach B)	1.7	7.2	17	30

Table 1. Atomic ratios from XPS intensities.

In particular, as to the phosphorilation step, the value of about 14 for Si/P atomic ratio after the treatment with $POCl_3$ is compatible with the formation of a complete phosphate monolayer at the oxide surface. Indeed, a calculation of the coverage degree R of the phosphate overlayer formed onto the SiO_2 surface can be evaluated by the formula[57] reported below:

$$1 / (1 + R) = \alpha [1 - \exp(-x)]$$

were $R=(I_{Si}E_P\sigma_P N_P)/(I_P E_{Si}\sigma_{Si}N_{Si})$ and $x = d_P/(\lambda_P \cos\theta)$, I_{Si} and I_P are the peak areas, σ_{Si} and σ_P are the photoionization cross sections,[58] E_{Si} and E_P are the photoelectron kinetic energies, N_{Si} and N_P are the estimated atomic densities of Si and P in SiO_2 and H_3PO_4, respectively; d_P is the thickness of a phosphate group bound to a SiO_2 surface and, according to *ab initio* calculation, has the value d_P = 2.2 Å; λ_P is the effective attenuation length of photoelectrons travelling through the phosphate, which, according to the relationship proposed in ref[59] has a calculated value of λ_P = 24 Å; finally, θ (45° in this case) is the angle between the direction of detected photoelectrons and the normal to the surface. The calculation performed by using the measured experimental intensities gives the value of 1, expected for the formation of a homogeneous monolayer. In the third step, i.e., after the treatment with zirconyl chloride, the measured P/Zr atomic ratio is 1.5, indicating the average bonding of 2 Zr atoms per 3 phosphate groups. In summary, XPS data suggest that the priming process is able to produce a full, homogeneous layer of a nonstoichiometric Zr phosphate.

From Table 1 one notes also that the carbon-to-nitrogen atomic ratio, obtained from the intensities of C 1s and N 1s peaks, is markedly different for the monolayers prepared following the two approaches, namely about 10 for approach A and about 7 for approach B. It turns out that the value obtained for approach B coincides with the one theoretically expected from the atomic composition of the PPTP molecule. On the other hand, the higher value found in the case of approach A suggests a PPTP orientation at surface that yields an attenuated nitrogen signal with respect to the carbon one. This can be easily demonstrated by means of a model in which, for the sake of simplicity, we hypothesize that PPTP molecules can lay on the ZP surface in two alternative orientations. In particular, in the case of approach A, a monolayer is proposed to be formed via a coordinative bond of terpyridine moiety with the zirconium atoms, the phosphonic group being directed upward. At variance of this, in samples prepared with approach B, the bond to surface is obtained only via the phosphonic group, with an outward orientation of the terpyridine moiety, due to its protection by means of the $[Zn(PPTP)_2]^{2+}$ complex. This simplified hypothesis (that, for example, does not take into account the possibility of mixed situations) is represented in the left hand side of Figure 24. The right hand side of the figure reports he C 1s and N 1s XPS peaks recorded on the surfaces obtained with the two different approaches. The carbon band is fitted by means of four components, assigned,[60] respectively, to aromatic carbon at 284.7 eV of binding energy (BE), to carbon atoms bound to nitrogen at 286.5 eV of BE, to carboxylic moiety at 289.0 eV of BE, and to a shake-up satellite at 291.7 eV of BE.[61] It should be noted that the two additional small components on the low BE side of the band (between 265 and 280 eV) are in fact due to the $K\alpha_{3,4}$ satellite lines of the unmonochromatized Mg $K\alpha_{1,2}$ radiation. The N 1s region shows a single band peaked at about 399.1 eV in the sample obtained with the approach B, while in the sample obtained with approach A this band lays at 399.6 eV. All the above BE values, together with the ones obtained for Zr 3d, P 2p, and Si 2p peaks, are reported in Table 2.

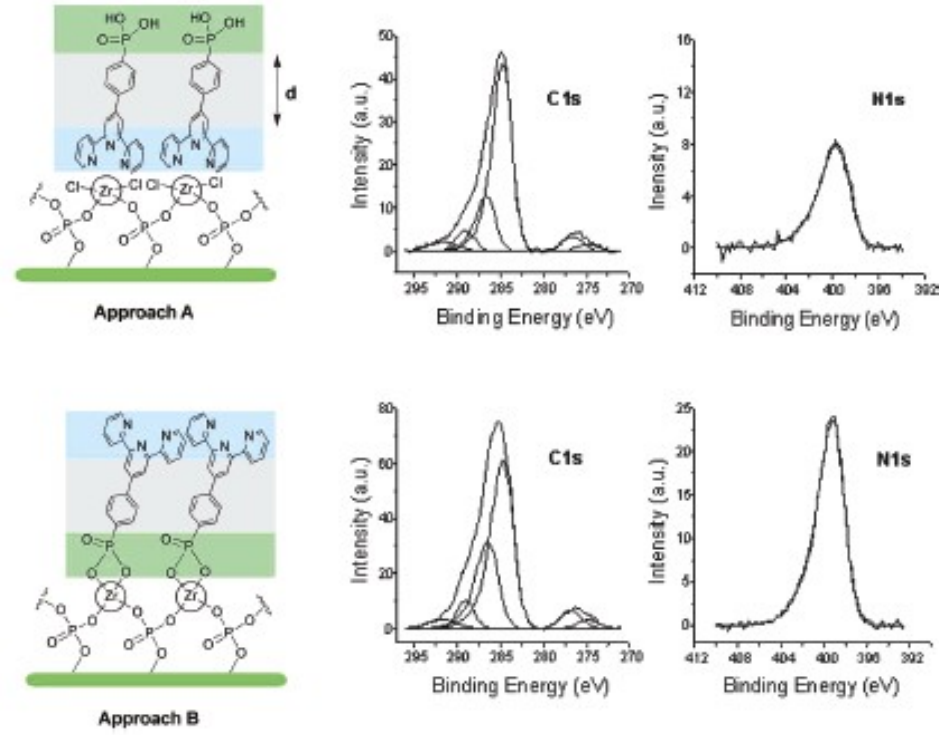

Figure 24. C 1s and N 1s XPS spectra obtained from the samples prepared by approaches A and B. The corresponding orientations of PPTP are sketched in the left side of the picture.

In the framework of layer scheme outlined in Figure 24 in case A, the N 1s photoelectrons are attenuated by a layer (of thickness d) of aromatic carbon atoms and by the outer P-containing layer that attenuates also the C 1s electrons of the C-based layer. In case B, there is no attenuation of N 1s photoelectrons, as the N-containing layer is the uppermost one. Since comparison between the two cases involves the carbon-to-nitrogen intensity ratios, the attenuation due to the outermost P-containing layer in approach A is cancelled as it affects in the same way the photoelectrons of the N- and C-containing layers. Such attenuation effects can be expressed by the following analytical equation:

$$R = R_0 \times e^{-d/\lambda (\cos \theta)}$$

where R is the N/C ratio in the case of approach A (i.e., with the attenuation due to the C-containing overlayer of thickness d), R_0 is the N/C ratio without attenuation, i.e. the one measured in the case of approach B, λ is the attenuation length of N 1s photoelectrons in the C-containing overlayer (evaluated to be 21 Å), and θ (45° in this case) is the angle of detected photoelectrons with respect to the surface normal. The obtained value of d is 6.0 Å, in agreement with the value estimated from the structure of PPTP. Further support to the model of different surface bonding of PPTP following the two preparation approaches, is given by the evaluation of P/Zr atomic ratios (see Table 1). Indeed, we find that the value of 1.5, characteristic of the SiO_2 surface after the ZP treatment, increases to 2.0 or 1.7 after anchoring of PPTP via approach A or B respectively. This can be explained by considering that in case A the phosphonic group of the PPTP molecule protrudes outward, so that the corresponding phosphorus signal is not significantly attenuated, while in case B it is attenuated by the overlaying phenylterpyridine moiety.
All above is finally confirmed also by the comparison of BE values of N 1s in the XPS spectra of the surfaces prepared by the two approaches. In particular, the N 1s BE is 0.5 eV higher in case A, with respect to case B. This is consistent with the presence, in the sample A, of a coordination interaction between the pyridinic nitrogens and the zirconium ions, which is expected to cause a decrease of the electron density on nitrogen atoms.
The different surface orientation of PPTP the two cases is in complete agreement with the ToF-SIMS data, that clearly show that iron complex is formed in the case of approach B (upward orientation of terpyridine moiety) and not in approach A (downward orientation).

	C1s (main)	C1s (C-N)	C1s (ox)	N1s	Zr3d3/2	Zr3d5/2	P2p	Si2p
Approach A	284.7	286.7	289.1	399.6	185.2	182.8	133.8	102.8
Approach B	284.7	286.5	289.1	399.1	185.0	182.6	133.5	102.8

Table 2. Binding energies (eV) from the monolayers prepared via approaches A and B. Uncertainty of reported BE is ±0.1 eV.

2.2.6 Surface patterning by micro-contact printing and ZP strategy

Part of the thesis work was dedicated to a preliminary exploration of the possibility of using the ZP anchoring method in conjunction with patterning techniques, in order to obtain laterally resolved structures of the deposited layer. Apart the possible technological implications, the capability of patterned deposition is useful also in the characterization of the layers, as it allows, in conjunction with scanning probe techniques, the estimation of thickness and tilting angle of SAMs anchored by the methodology under study.. For this purpose a micro-contact printing technique was used.[62] As model molecule, we used octadecilphosphonic acid (ODPA), that was micro-contact printed in form of submicrometre-sized lines on SiO_2 substrates primed with the ZP method.
A solution of ODPA was prepared in 2-propanol ($5 \cdot 10^{-4}$ M), and it was filtered through 0.2 μm filter. A poly(dimethylsiloxane) stamp, prepared by using a silicon grating as a master, was used to print the ODPA pattern on the oxide surface. The stamp was dipped in the ODPA solution for 30 seconds, then dried under nitrogen flux. The "inked" stamp was the placed in contact with the ZP substrate for 60 seconds. After printing, the substrate was rinsed in 2-propanol and dried under N_2 flux. ToF-SIMS measurements were performed in order check the effective deposition of ODPA on surface. A series of peaks related to phosphonic group bonded to zirconium ion are present in the spectra, evidencing the formation of the SAM on the surface.
AFM measurements were performed in order to gain information about the patterning on the surface, and to estimate thickness and tilt angle of the SAM. Figure 25 shows the AFM height and phase images, a cross-section as well as the histogram analysis, the latter providing an average value of the height difference between SAM lines and uncovered substrate areas.

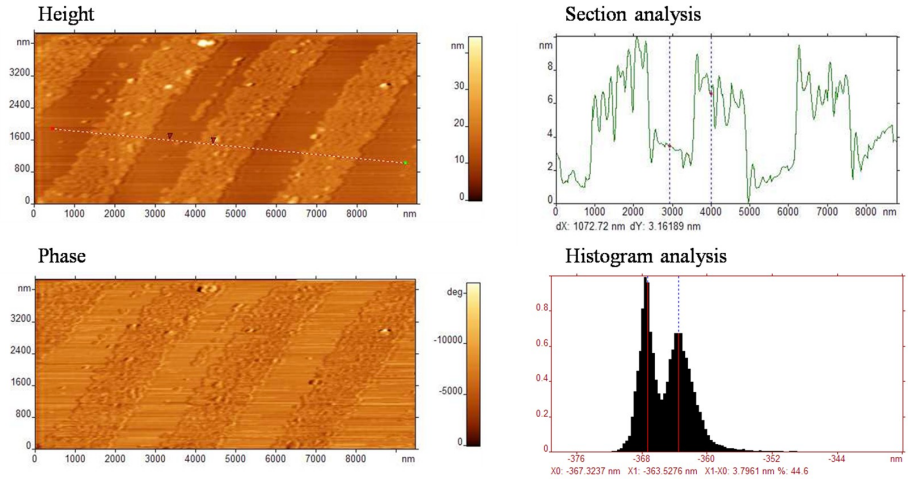

Figure 25. AFM analysis of ZP SiO_2 surface patterned with ODPA.

From histogram analysis, and according to section analysis, thickness value for ODPA printed on SiO_2 is about 3.8 nm. This value is higher than the one (about 2.5 nm) expected for ODPA even in the hypothesis of vertical orientation in all-trans configuration, so suggesting that a bilayer is formed on the surface. According to literature data on similar systems,[63] two possible molecular arrangements are proposed for the formation of ODPA bilayer: one vertically aligned, the other tilted, as shown in Figure 26.

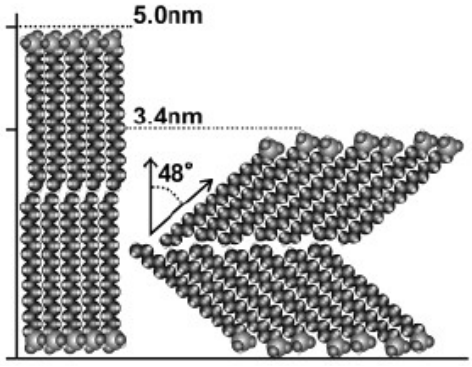

Figure 26. ODPA bilayer models showing possible molecular arrangements.

Considering that the measured thickness value is smaller than the one that we should expect for the vertically aligned arrangement, and in the hypothesis that a tilted structure is prevailing, it is possible to extract the average tilt angle to surface normal, which turns to be about 40.5°.
Although the data reported above are quite preliminary and have been obtained with a model alkyl-phosphonate molecule, they show that the ZP method can be used in conjunction with patterning techniques, and this is of a certain interest for example for obtaining patterned functional multilayers such as those discussed in the next sections.

2.2.7 Conclusions

A general method for anchoring, onto oxide surfaces, a terpyridine functionalized monolayer has been described. The surface anchoring was obtained by exploiting the reaction of a phosphonic acid functionalized terpyridine ligand (PPTP) with a zirconium phosphate monolayer. XPS and ToF-SIMS data showed that the adsorption of PPTP can also occur *via* interaction of the terpyridine moiety with the zirconium phosphate layer, thus preventing further terpyridine reactions, that are necessary in view of the "construction" of multy-layers made out of multi-centre metal complexes. An alternative anchoring method was developed, involving a protection step of the terpyridine group that allowed stable anchoring of the molecule through the phosphonic group. The upward orientation of terpyridine was demonstrated by XPS measurements as well as by the chemical availability of the group for further coordination reactions, which were indeed observed by ToF-SIMS measurements. Finally, the applicability of the zirconium-phosphate-phosphonate (ZP) method in conjunction with soft patterning techniques onto oxide surfaces was explored. It was shoun that micro-contact printing on ZP primed oxide surface is a valid method for priming SiO_2 and that, in the case of a model alkylphosphonic molecule, it leads to the formation of a tilted bilayer on the surface.
The successful formation of a stable terpyridine-containing layer on oxides opens the way to the design of multilayers of functional molecules, based on coordination reactions and exhibiting interesting electrical and photophysical properties of large technological interest.

The results, shown in this work for SiO_2 surfaces, can be in principle extended to any oxide surface capable to be hydroxylated. Similar results were obtained for quartz and ITO substrates. In particular, applying this anchoring methodology to transparent conducting and/or semiconducting oxides can be very attractive for applications in sensors, optical waveguides, photovoltaics, and antenna systems, as well as molecular electronic devices.

2.3 Stepwise formation of Fe and Ru complexes on oxide surfaces

The continuous quest for minimizing the size of electronic devices is motivating researchers to investigate the role of single molecules that could perform a function in electronic devices. Unlike conventional electronics, molecular electronics is based on the chemical engineering of molecules, whose physico-chemical properties can be tailored by synthetic methods, bringing a new dimension in design flexibility that does not exist in typical inorganic electronic materials. It is well known that electronic devices are fabricated with a ''top-down'' approach that employs a variety of sophisticated lithographic and etching techniques to pattern a substrate. In contrast, molecules and supramolecular aggregates are synthesized by the ''bottom-up'' approach that builds small structures from the molecular level. In principle, this allows a very precise positioning of molecules with specific functionalities. In particular, the application of principles of supramolecular chemistry to the direct assembly of functional layers at surfaces added a new and highly diverse class of materials to modern material science. Indeed, the application of the basic principles of supramolecular chemistry to surface modification is highly promising for the construction of two-dimensional (2D) and three-dimensional (3D) supramolecular systems on surfaces.[64] Among functional p-systems, perylene bisimides have attracted considerable attention on account of their intense luminescence, light fastness, and n-type semiconductor properties.[65] Upon functionalization with suitable supramolecular receptor groups, these dyes can be self-assembled into a variety of architectures including p-stacks, hydrogenbonded networks and metallosupramolecular cycles and polymers.[66] Well-defined self-assembled monolayers have been achieved on a variety of surfaces and multilayer assemblies were obtained on quartz substrates by the layer-by-layer approach.[67] In this section, attention will be focused on the bottom-up preparation of supramolecular self-assembled multilayers (SAMLs) of terpyridine-functionalized perylene bisimide metal complexes by successive, stepwise coordination reactions performed at the surface of a self-assembled monolayer. SAMLs were prepared by means of direct reaction at the surface of a properly functionalized conductive substrate.

2.3.1 Molecular building blocks

Perylene tetracarboxylic acid bisimide, in short perylene bisimide, based dyes have received considerable attention in academic as well as industrial dye and pigment research.[68] Several members of the perylene bisimide family found high grade industrial applications as pigments (especially in automotive finishes) due to the favourable combination of insolubility and migrational stability, light- and weather-fastness, thermal stability and chemical inertness.[69] More recent applications of perylene bisimide pigments are in the field of electronic materials, among which perylene bisimides are among the best n-type semiconductors available.[70] This n-type semiconductivity is related to the high electron affinity of perylene bisimide dyes,[71] which makes them promising for application in organic field effect transistors.[72] In addition, based on their unique combination of optical, redox, and stability properties perylene bisimide dyes have already been investigated for more than a decade in photovoltaics.[73]

Perylene bisimides bearing four aryloxy substituents in the 1,6,7,12 positions (so called bay area) and two receptor units at the imide nitrogens are most useful fluorescent building blocks for the realization of a broad variety of supramolecular architectures. This versatility is not only due to the outstanding fluorescence properties of these dyes with quantum yields close to unity, but also a consequence of pronounced twisting of the π-system with an inversion barrier of around 60 kJ/mol (leading to atropisomerism) and conformational flexibility of aryloxy units. The latter two properties endow these dyes with high solubility even in least polar aliphatic solvents and enable the dyes to maintain a distance of ≥4 Å in their supramolecular assemblies. This feature particularly reduces the, otherwise often observed, fluorescence quenching in dye aggregates. Thus, bright luminescent cyclic and polymeric supramolecular architectures have become available from these dyes by hydrogen-bond and metal-ion directed self-assembly. In those cases where additional π−π-stacking interactions come into play, luminescent organogels and liquid crystals are obtained.

Fluorophores are widely applied functional dyes that are characterized by a radiative depopulation of an excited singlet state. Owing to other competing processes, such as intersystem crossing to the triplet state and internal conversion to the ground state, only few fluorophores exhibit high fluorescence quantum yields (>95 %) in a broad range of solvents as observed for many perylene bisimide derivatives (Figure 27).

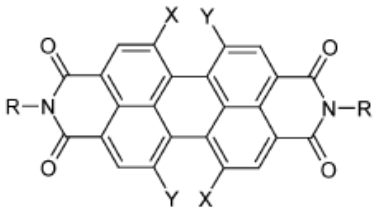

1a: X = Y = H: λ_{fl} = 531 nm, Φ = 1.00
1b: X = Y = F: λ_{fl} = 512 nm, Φ = 0.93
1c: X = Y = Cl: λ_{fl} = 548 nm, Φ = 0.93
1d: X = H, Y = Br: λ_{fl} = 547 nm, Φ = 0.76
1e: X = H, Y = OPh: λ_{fl} = 575 nm
1f: X = Y = OPh: λ_{fl} = 608 nm, Φ = 0.96

Figure 27. Perylene bisimide fluorophores and their fluorescence maxima and quantum yields (for R =2,6-diisopropylphenyl) in dichloromethane or chloroform.

By this means, the energy of π–π-stacking is strongly reduced. Thus, an originally insoluble pigment chromophore (with high lattice energy) is liberated as a soluble dye that can be equipped with receptor groups to realize desired luminescent supramolecular architectures.
When equipped with supramolecular receptor units for metal-ion or hydrogen-bond directed self-assembly processes, a broad variety of dye assemblies can be made available upon addition of a complementary binding partner. With binding partners containing a second functional π-conjugated system, novel photophysical functionalities are achievable on the nanoscale. Numerous perylene bisimide dyes have been synthesized for their applicaton as fluorescent standards, in fluorescent light collectors, or as laser dyes.[74] For such applications it has been proven to be very advantageous that the imide substituent has a negligible influence on the absorption and emission properties of perylene bisimides because of the nodes of the HOMO and LUMO orbitals at the imide nitrogens.
Therefore, perylene bisimides can be regarded as a closed chromophoric system with an S_0–S_1 transition (polarized along the extended molecular axis) whose intensity and position remain unaltered by the respective imide substituents.[75]

Perylene bisimides are fairly electron deficient dyes, which are easy to reduce and rather difficult to oxidize. The electron-deficient character of perylene bisimide dyes is also a prerequisite for the high photochemical stability of these dyes because photooxidation is disfavored. On the other hand, the majority of these dyes are strong reductants in their photoexcited state.

The parent perylene bisimides exhibit flat p-systems as confirmed by X-ray diffraction of several single crystals.[76] According to the bond lengths observed in these crystals, perylene bisimides can be regarded as being composed of two naphthalene half units (marked in red in Figure 28), each of which is attached to an imide unit and connected to the other naphthalene unit by two C sp^2–C sp^2 single bonds.

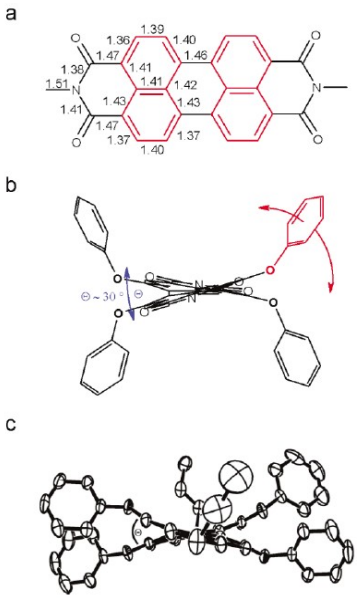

Figure 28. a) Bond lengths of R=CH_3 perylene bisimide in the crystal; b) preferred conformation of the phenoxy substituents in bay-substituted perylene bisimides in the gas phase; and c) in the solid state according to a single crystal X-ray analysis.

Photoluminescent polymers have received significant interest in the last decade especially in the fields of organic light emitting diodes[77] and plastic solar cells.[78] Introduction of metal ions into conjugated polymers has been investigated with regard to higher electroluminescence quantum yields by harvesting triplet state emission.[79] However the purification and processing of such polymers is a difficult task. Therefore new concepts such as supramolecular polymerization[80] of photoactive building blocks might be of interest. Studies have been reported on the metal-directed polymerization of highly fluorescent perylene bisimide dyes provided with terpyridine receptor units and a dimeric assembly which proved to be useful to elucidate the impact of the metal ion on the photophysical properties of the perylene dye.
The complexation of monotopic tpy-functionalized perylene bisimide ligand with an octahedrally coordinating metal ion yields a dimeric complex which can be seen as a model reaction for the formation of the coordination polymer.

2.3.2 Synthetic strategy for preparation of SAMLs polypyridine-based metal complexes

In order to obtain terpyridine-based self assembled mono- and multilayers on oxide surfaces, a stepwise method based on a bottom up approach has been used. Something similar has been previously made on gold surfaces[81,85] and the obtained films showed outstanding properties.[82] This work, therefore, can be seen as contribution to the possibility of applying these kinds of materials to the modern technology, in view of the fact that the "construction" of these multilayers onto transparent oxides allows a better exploitation of their optical properties, perhaps in conjunction with their electrical properties if transparent (semi)conducting oxide (TCO) substrates are used.
The method relies on the preparation of a SAM "platform'' of 4-(2,2':6',2''-terpyridine-4-yl)benzenephosphonic acid (PPTP) assembled on oxide surfaces by means of the ZP method described in section 2.2). Substrates are either quartz (choosen as a model) or indium tin oxide (ITO).

The preparation of the complex-based layer exploits the coordination between terpyridine functions of PPTP first with the metal ion of choice (in our case we used either ruthenium or iron) and then with the proper terpyrydinic ligand. By using a ditopic ligand the procedure can be iteratively repeated giving rise to a layer-by-layer deposition of a self assembled multilayers of the desired thickness. Different mono- or ditopic terpiridyne ligands have been used, differing each other for the aromatic moiety connected to the terpyridine units (see Figure). In particular, we used a commercially available 4',4''''-(1,4 phenylene)bis(2,2':6'2''terpyridine) (henceforth DT), as well as some on-purpose synthesized molecules where the aromatic group attached to terpyridine is a perilene bisimide dye. The molecular structures of ligands used are reported in Figures 29-30.

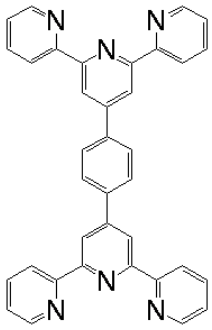

Figure 29. Molecular structure of 4',4''''-(1,4 phenylene)bis(2,2':6'2''terpyridine).

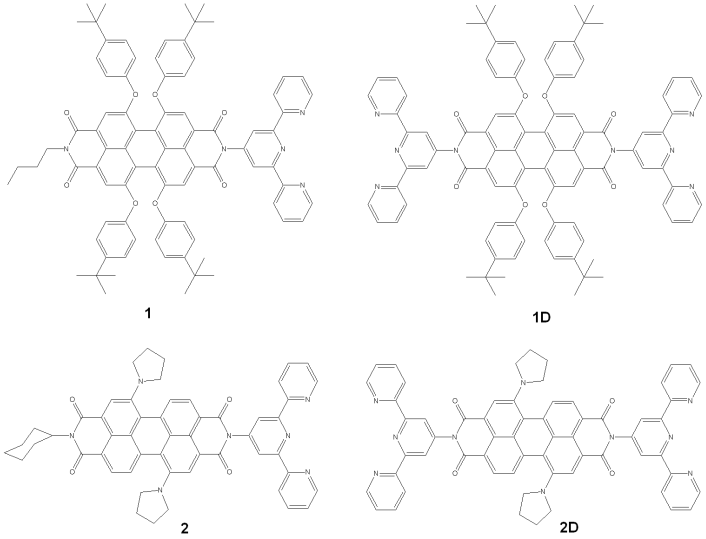

Figure 30. Molecular structures of perilene bisimide based ligands 1, 2, 1D, 2D (see text).

Having a ZP primed surface, characterized by resistance to hard working condition, like high temperatures and/or long reflux times, it is possible to imagine to anchor on such surfaces very interesting complexes, like ruthenium(II) ones. 2,2':6',2''-terpyridine-ruthenium(II) complexes are very attractive because of their photochemical and electrochemical properties.[83] Homo- and heteroleptic Ru complexes can be prepared starting from [Ru(terpy)Cl_3] precursors,[84] but drastic conditions are required. The in-situ reduction of Ru(III) to Ru(II) requires in fact, forcing reaction conditions to provide the electrons for the metal reduction.[85] These conditions strongly limit the possibility to perform such reactions on a thiol-based platform on gold, due to the scarce thermal stability of such layers,[86]. Milder conditions are requested to prepare a mono-terpy ruthenium(II) complexes from Ru(II)-based precursors bearing labile ligands, like [Ru^{II}-(terpy)(DMSO)Cl_2] compound, widely used in the preparation of Ru-bis(terpyridine) types of complexes.[87]

With all above in mind, a primed quartz substrate bearing the PPTP platform was dipped in ethanolic Ru(III) solution [Ru(terpy)Cl_3] for 24 hours (reflux, 78°C), in order to explore the possibility of obtaining the

anchored PPTP-Ru-Terpy complex in reasonable times compared with the prohibitive ones necessary for a similar preparation on a thiol-based platform on gold.[89].
By contrast, in order to have the possibility of growing multilayers on the surface, the functionalized quartz substrate was dipped in ethanolic Ru(II) solution, using $[Ru(DMSO)_6]^{2+}(O_3SCF_3)^{2-}$ as precursor. In this way, the PPTP-Ru(II) complex is available to interact with a ditopic ligand such as the DT. For this purpose, two different anchoring methodologies were used. In the first, a monolayer of DT molecules was deposited on Ru(II)-functionalised surface by horizontal Langmuir-Blodgett technique. In the second method, PPTP-Ru(II)-DT complex formation was performed by immersing the Ru(II)-functionalised surface in a DT solution (chloroform, 62°C) for 3 hours.

A faster and easier coordinative reaction to the terpyridine ligand is performed by Fe(II) metal ion, that can be used to grow Fe(II)-metal-complex-based multilayers, in very mild working conditions.
For this purpose the aforementioned a stepwise, layer-by-layer approach can be applied. The method, in principle, allows to tailor the assembled multilayer in terms of number of layers, thickness, kind of metal or ligand and their sequence. Moreover, since this method is based on self-assembly, the prepared film reaches a spontaneous thermodynamic stability during the preparation process.
Self-assembled multilayers were prepared by a stepwise procedure according to Figure 31.

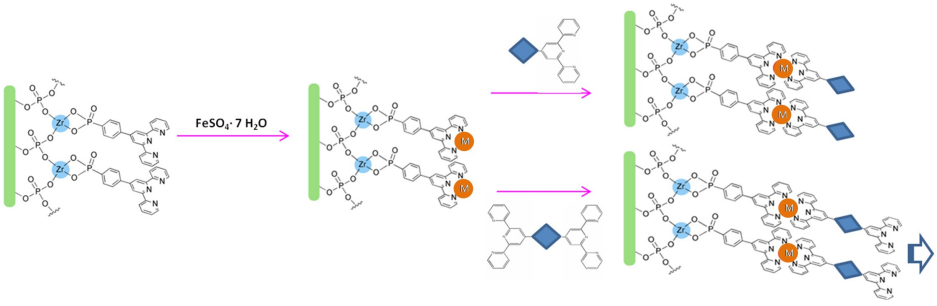

Figure 31. Scheme for stepwise procedure of self-assembled multilaters preparation.

Multilayers were prepared by successive reaction steps: the substrates (quartz and ITO), already covered with the ‘‘platform’’ SAM, were dipped for 90 seconds in $FeSO_4 \cdot 7H_2O$ solution (0.5 mM, 1:1 water/ethanol) and then rinsed with water, ethanol and chloroform; then they were immersed in DT solution (10^{-5} M, CH_2Cl_2) for 15 minutes and rinsed with warm chloroform. The two steps were repeated iteratively up to the desired number of layers. Same procedure was applied for ITO substrates. The functional SAMLs have been studied by time-of-flight secondary ion mass spectrometry (ToF-SIMS) and UV-Vis.

Other types of terpyridine-based ligands were used in order to obtain mono- and multilayers on primed oxide (quartz and ITO) surfaces, as previously described: perylene bisimide dye-based ligands.
In a preliminary step, a perylene bisimide ligand bearing only one terpyridine function were used, in order to obtain iron-based monolayers onto the oxide surfaces.
Monotopic ligands can be also used as terminal stopper in polypyridine-based complexes molecular wires in order to investigate energy- and electron- transfer properties of these particular supramolecular architectures. In fact, if the chromophore is anchored at the end of the molecular wire, it can act as a “bridge” between substrate and chromophore, and it can be possible to observe as optical and electrical properties of this system change by varying the thickness of the molecular “bridge”.
For this purpose two different monotopic ligands were used:
bis-imide N-butyl-N’-(4’-(2,2’:6’,2”-terpyridil))-1,6,7,12-tetra(4-tert-butylphenoxy)perylene-3,4:9,10-tetracarboxylic acid, a red ligand, henceforth 1 and bis-imide N-cyclohexyl-N’-(4’-(2,2’:6’,2”-terpyridil))-1,7-dipirrolydinilperylene-3,4:9,10-tetracarboxylic acid, a green ligand, henceforth 2.
In order to grow on the surface perylene bisimide-based multilayers two different ditopic ligands were used: bis-immide N,N’-(4’-(2,2’:6’,2”-terpyridil))-1,6,7,12-tetra(4-tert-butilphenoxy)perylene-3,4:9,10-tetracarboxylic acid, red ligand, henceforth 1D and bis-imide N,N’-(4’-(2,2’:6’,2”-terpyridil))-1,7-dipirrolydinilperilene-3,4:9,10-tetracarboxylic acid, green ligand, henceforth 2D.

The synthesis of 1, 2, 1D and 2D ligands was performed on purpose by Prof. Würthner's group at University of Würzburg, Germany.
The metal center of choice was Fe(II). Chomophores 1 and 2 were anchored either on quartz or ITO substrates functionalised with the PPTP platform as described in section 2.2. For this purpose, substrates were dipped for 90 seconds in $FeSO_4 \cdot 7H_2O$ solution (0.5 mM, 1:1 water/ethanol), then sequentially rinsed with water, ethanol and CH_2Cl_2; t immersed in the ligand solution (10^{-5} M, CH_2Cl_2) and finally rinsed with warm dichloromethane, ethanol and water. In this way a monolayer of the heteroleptic PPTP-iron-chromophore was obtained
Multilayers were prepared in a similar way, by iterating the procedure: after the preparation of the first iron-containing layer by dipping the PPTP functionalised substrates for 90 seconds in Fe(II) solution, and the subsequent cycle of rinsing, then they were immersed in the ligand solution of the ditopic ligand (10^{-5} M, CH_2Cl_2) for 15 minutes and rinsed with warm dichloromethane, ethanol and water. The surface obtained in this way contains again free terpyridine groups so that the procedure can be repeated iteratively up to the desired number of layers.
The functional SAMLs prepared in the above decribed ways were studied by time-of-flight secondary ion mass spectrometry (ToF-SIMS) and UV-Vis absorbtion spectroscopy.

2.3.3 ToF-SIMS characterization

The stepwise approach to the mono- and multilayer growth requires a strict control of each of the several synthetic steps. For this purpose we made use of ToF-SIMS, a very powerful technique that provides information on the molecular composition of the uppermost surface layers,[88] in order to confirm the formation of the terpyridine-functionalized perylene bisimide metal complexes at the surface and detect the formation of undesired species or the adsorbtion of impurities. The experimental conditions used are the same described in section 2.2.4. For analysis of multilayers on quartz, an insulating substrate, in order to obtain surface charge compensation it was necessary to flood the surface with electrons (~20 eV).

Figure 32 shows the spectrum of a sample containing the complex PPTP-Ru-Terpy, obtained from Ru(III) precursor. It is possible to observe the presence of the metal ion $[Ru]^+$ (m/z 102) and of peaks assigned to ruthenium coordinated by terpyridine $[C_{15}H_{10}N_3Ru]^+$ (m/z 334). The assignments are made also on the basis of the isotopic distribution (see for example the inset in Figure 32 showing the expected isotopic distribution of Ru^+.

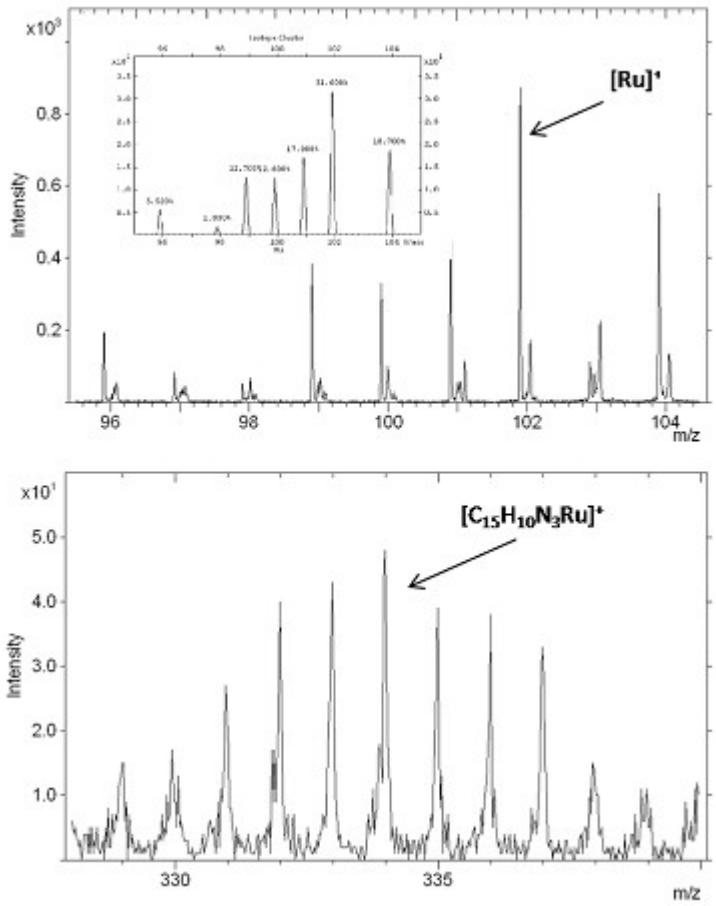

Figure 32. Partial ToF-SIMS spectra of a sample containing PPTP-Ru-Terpy (the expected isotopic distribuition of Ru is reported in the inset)

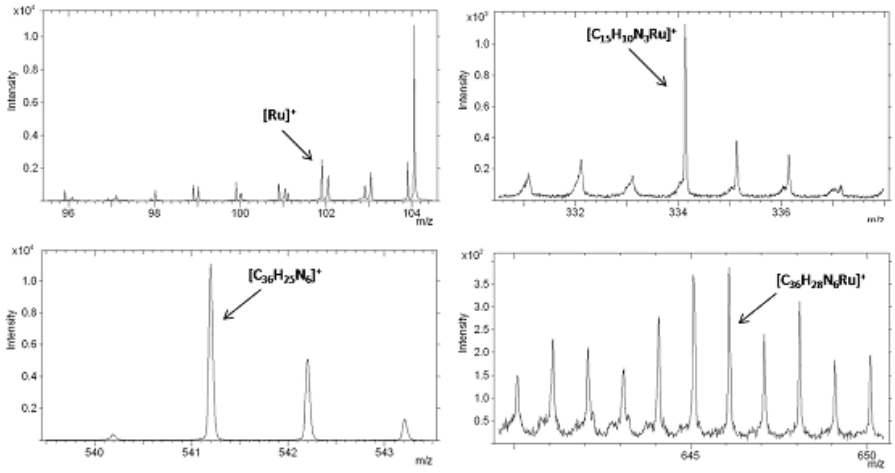

Figure 33. ToF-SIMS spectra of sample containing PPTP-Ru-DT complex, obtained by reaction of the Ru-containing PPTP platform with a monolayer of DT deposited by LB method.

Figure 33 shows the ToF-SIMS spectrum of a sample containing a monolayer of the complex PPTP-Ru-DT, obtained from Ru(II) precursor and Langmuir-Blodgett ligand deposition. It is possible to observe peaks related to the metal ion $[Ru]^+$ (m/z 102), to the lingand $[C_{36}H_{25}N_6]^+$ (m/z 541), to a fragment containing a terpyridine group plus a ruthenium ion $[C_{15}H_{10}N_3Ru]^+$ (m/z 334) and to the Ru-DT $[C_{36}H_{28}N_6Ru]^+$ (m/z 646).

The preparation of ruthenium complexes at surface, although demonstrated, was limited to the formation of a single layer. The attempts of preparing multilayers were unsuccessful, due the presence of competing reactions that caused the redissolution of the first layer of ligand and the formation of complexes in solution. By contrast, it was possible to prepare iron-based multilayers. In Figure 34 we report some regions of the spectrum of a sample obtained by iterating 15 times the iron/DT deposition on a ZP functionalised quartz substrate. Peaks assigned to the metal ion coordinated by DT are observed, namely $[C_{36}H_{24}N_6Fe]^+$ (m/z 596) and $[C_{36}H_{25}N_6FeO]^+$ (m/z 613).

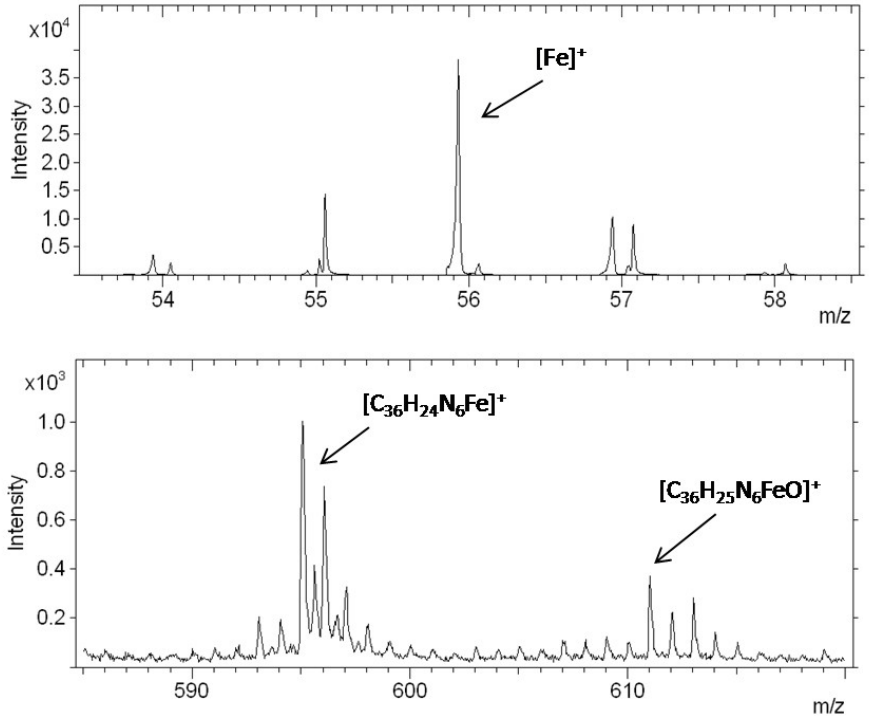

Figure 34. ToF-SIMS spectra of sample containing 15 Fe/DT layers deposited on quartz.

Figure 35 reports part of a spectrum of a similar sample (15 iron/DT layers) but prepared on a ITO substrate. The spectrum basically gives the same information as that of figure 35 (obtained from a quartz substrate sample), but with a much better quality of the information, most likely due to the conductive nature of the substrate that does not require the use of electron flooding for charge compensation, with the associated problems of sample damage. As matter of fact, in addition to the peaks observed in the spectrum of figure 35, $[C_{36}H_{24}N_6Fe]^+$ (m/z 596) and $[C_{36}H_{24}N_6FeO]^+$ (m/z 613), higher mass species are observed, related to the emission of a "complete" $Fe(DT)_2$ unit, namely $[(C_{36}H_{24}N_6)_2Fe]^+$ (m/z 1136)and the oxidised species $[(C_{36}H_{24}N_6)_2FeO]^+$ (m/z 1152).

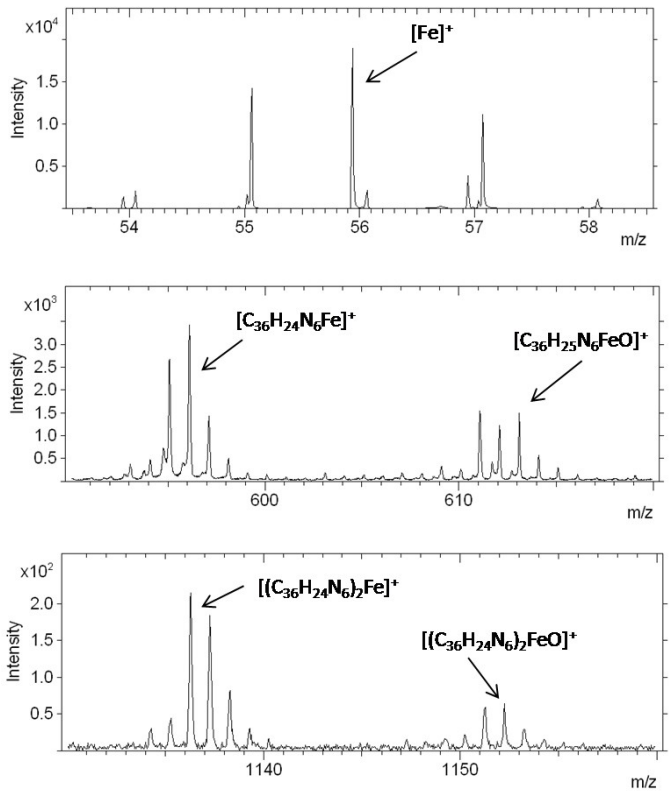

Figure 35. ToF-SIMS spectra of sample containing 15 Fe/DT layers deposited on ITO.

As mentioned in the previous sections, perilene bisimide-containing terpyridine ligands have been used as well for the preparation of both mono- and multi-layer of iron complexes on quartz and on ITO. In particular, Figure 36 reports the spectrum of a monolayer obtained on ITO in the same way above described, but using, as ligand to react with the iron-containing platform, the terpyridine-terminated perilene bisimide 1. Here it is possible to notice quasi-molecular peaks of the chromophore, alone $[C_{83}H_{75}N_5O_8]^+$ (1269,56m/z), cationised with iron $[C_{83}H_{75}N_5O_8Fe]^+$ (m/z 1325,48) also in oxidised form $[C_{83}H_{75}N_5O_8FeO]^+$ (m/z 1341,54).

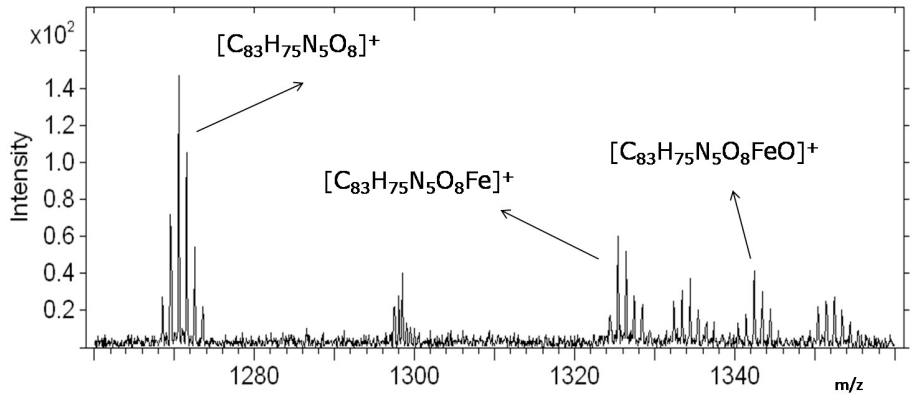

Figure 36. ToF-SIMS spectrum for the sample containing Fe/1 monolayer deposited on ITO.

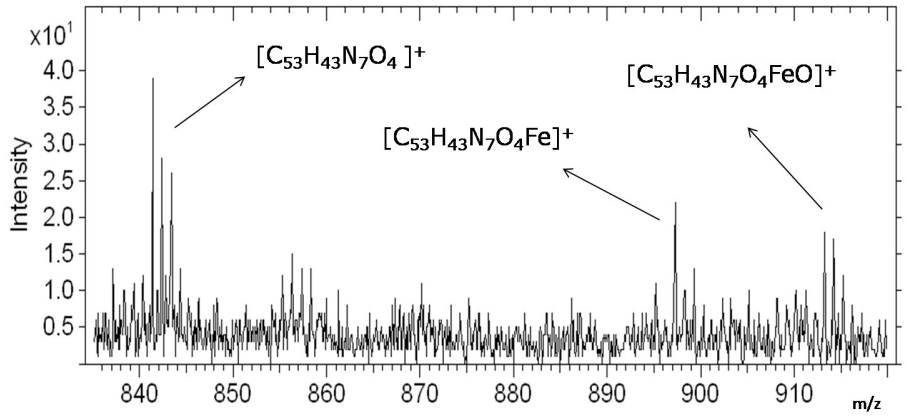

Figure 37. ToF-SIMS spectrum for the sample containing Fe/2 monolayer deposited on ITO.

Similar spectral patterns are observed by using chromophore 2, as shown in Figure 37 where one can observe the molecular peak of the ligand $[C_{53}H_{43}N_7O_4]^+$ (m/z 841,35), as wel as species containing both the chromophore and iron $[C_{53}H_{43}N_7O_4Fe]^+$ (m/z 897,29) and $[C_{53}H_{43}N_7O_4FeO]^+$ (m/z 913,28).

The use of iron allowed the preparation of multilayers with chromophores 1D and 2D, on both ZP functionalized quartz and ITO

substrates, applying the methodology already previously described in the case of DT. For the sake of conciseness, only the spectra related to ITO substrate are reported. The results on quartz substrates are very similar, although the quality of spectra is usually lower due to the aforementioned charge compensation problems. In Figure 38 we show the spectrum of a sample containing 6 iron/1D layers. The formation of the complex at the surface, also in this case, is confirmed by the presence of quasi-molecular ions and large fragments such as $[C_{94}H_{76}N_8O_8]^+$, (m/z 1445,59, M^+), $[C_{94}H_{76}N_8O_8Fe]^+$ (m/z 1501,51, MFe^+) and $[C_{94}H_{76}N_8O_8FeO]^+$ (m/z 1517,51).

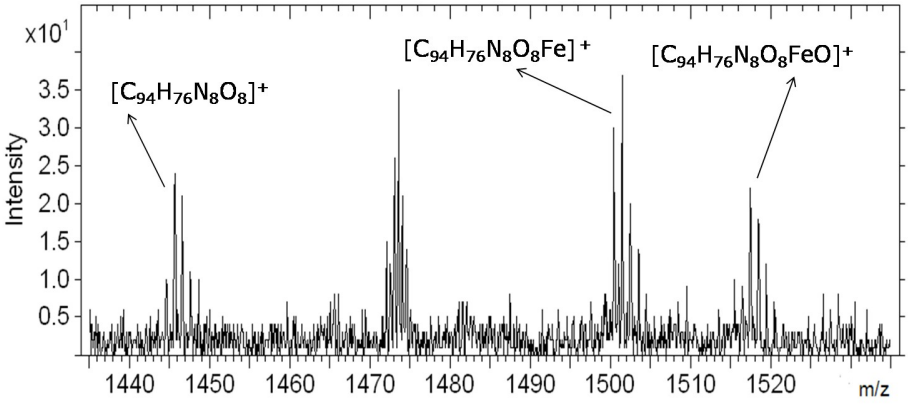

Figure 38. ToF-SIMS spectrum for the sample containing 6 Fe/1D multilayers deposited on ITO.

In Figure 39 it is shown the spectrum of a sample containing 6 iron/2D layers. Similarly to the sample containing 1D-based multilayers, we note to the presence of high mass peaks $[C_{62}H_{42}N_{10}O_4]^+$ (m/z 841,35, the molecular ion M^+), $[C_{62}H_{42}N_{10}O_4Fe]^+$ (m/z 897,29 MFe^+) and $[C_{62}H_{42}N_{10}O_4FeO]^+$ (m/z 913,28), again diagnostic of the presence of the iron(bis-terpyridine) complex.

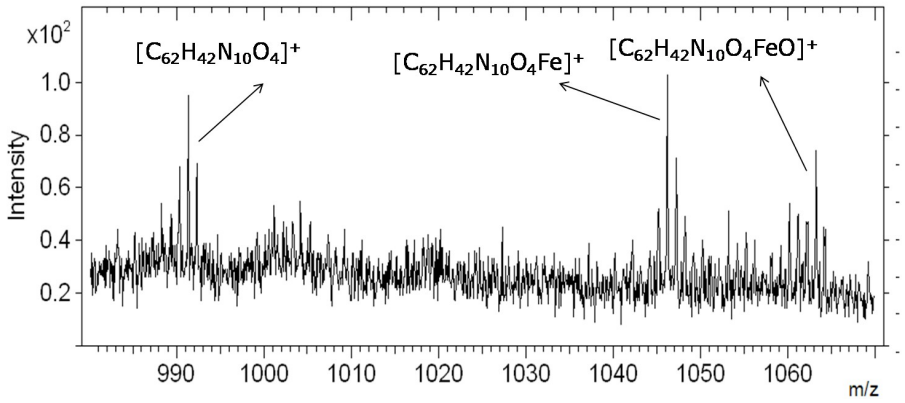

Figure 39. ToF-SIMS spectrum for the sample containing 6 Fe/2D multilayers deposited on ITO.

2.3.4 UV-Vis characterization

Although diagnostic of the formation of the desired complexes on the surface, ToF-SIMS data do not allow to obtain quantitative information on the growth of the multi-layers. Such information can be obtained from UV-Vis absorbtion spectra.
Measurements were acquired from multilayers obtained with each of the three available ditopic ligands (DT, 1D and 2D), in a Jasco V 650 UV-Vis-NIR spectrometer, with speed of 60 nm min^{-1} and step width of 0.1 nm.

The UV-Vis spectra of phenyl terpyridine (DT) based multilayers on quartz show the typical MLCT band of bis-terpyridine iron complex $[Fe(Tpy)_2]^{2+}$ at ≈ 585 nm (Figure 40 a). An increase of the MLCT band intensity is evident by increasing number of coordination steps. Moreover, the linear correlation between the optical density of such band with the nominal number of layers (Figure 40 b) indicates the formation of a constant number of iron complexes per step.

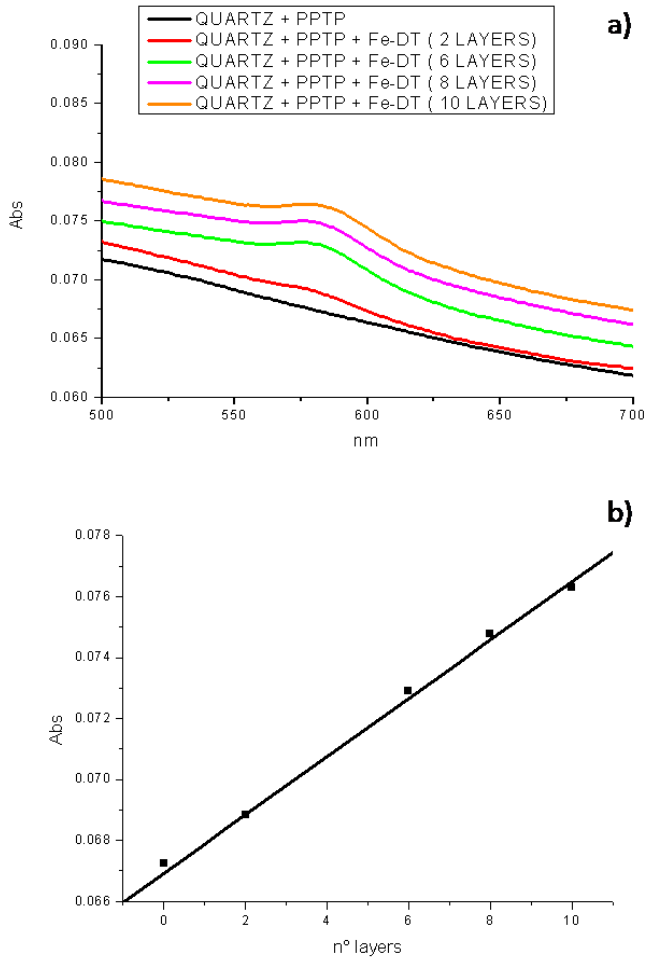

Figure 40. (a) UV-Vis spectrum acquired from an increasing number of layers for the sample Fe/DT on quartz substrate. (b) Optical density of the characteristic MLCT band as a function of the nominal number of layers.

Similar considerations hold for multlayers Fe/DT deposited on ITO. Also in this case, the success of the applied layer-by-layer methodology is evident, as demonstrated by the linear increase of the absorbance of the MLCT band with the number of layers (Figure 41).

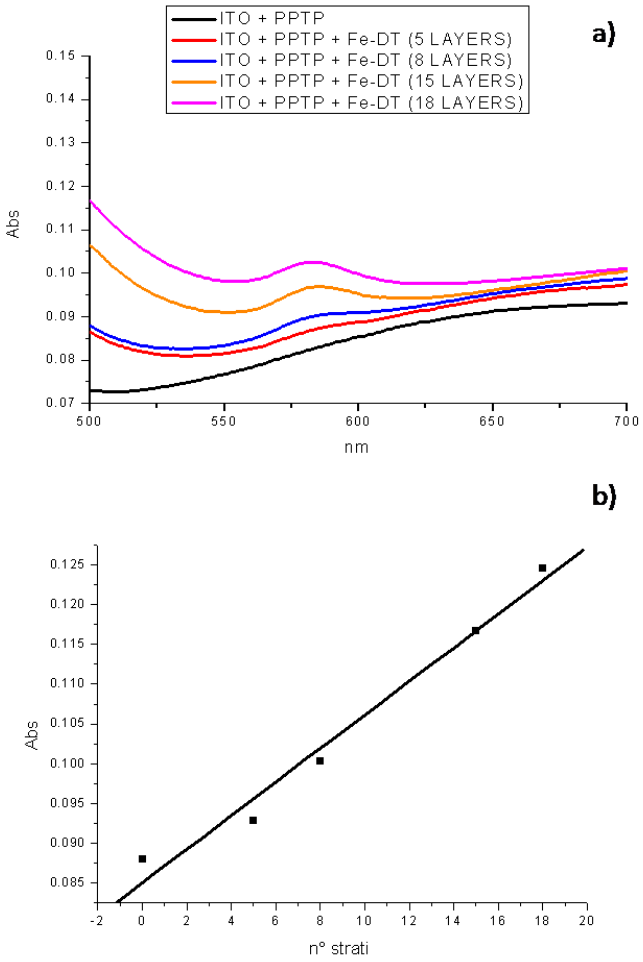

Figure 41. (a) UV-Vis spectrum acquired from an increasing number of layers for the sample Fe/DT on ITO substrate. (b) Optical density of the characteristic MLCT band as a function of the nominal number of layers.

A similar study has been carried out in order to monitor the growth of the multilayers obtained with the perilene bisimide-containing ligands. Such compounds display a strong absorbtion in the visible region, as shown by

the spectra, reported in Figure 42, obtained from diluted solutions of ligand 1D (red) and 2D (green) in dichloromethane.

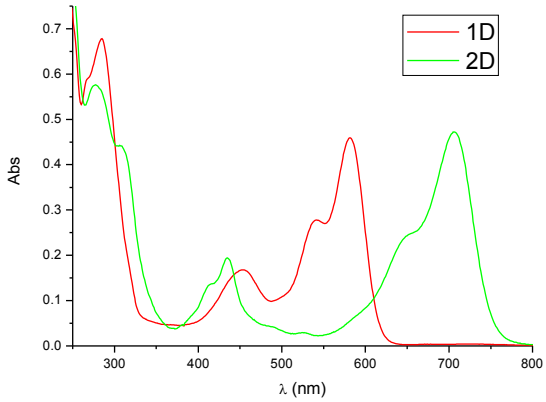

Figure 42. UV-Vis spectrum of 1D (red) and 2D (green) solutions in CH_2Cl_2.

Chromophore 1D (red) displays two large bands, at 582 nm and 451 nm, due to, respectively, the transitions $S_0 \rightarrow S_1$ and $S_1 \rightarrow S_2$. For chromophore 2D (green) the same bands are visible at 751 nm and 430 nm. It is known that molar extinction coefficient values ε for the two transitions are about 50.000 ($S_0 \rightarrow S_1$) and 20.000 ($S_1 \rightarrow S_2$).[89] In the range from 200 nm to 350 nm the bands due to the absorbtion of terpyridine are visible for both the chromophores.
Making a comparison between UV-Vis spectra of the two chromophores for the solution and the surface, respectively, it is clear that there are some differences, principally due to the formation of iron complex. For a 20 layer specimen of 1D/Fe it is possible to individuate a large band at ≈ 590 nm, resulting from the overlap between the MLCT (metal-to-ligand charge transfer) band of $[Fe(Tpy)_2]^{2+}$ and $S_0 \rightarrow S_1$ band of the ligand. There is no evidence about the band at 451 nm (Figure 43).

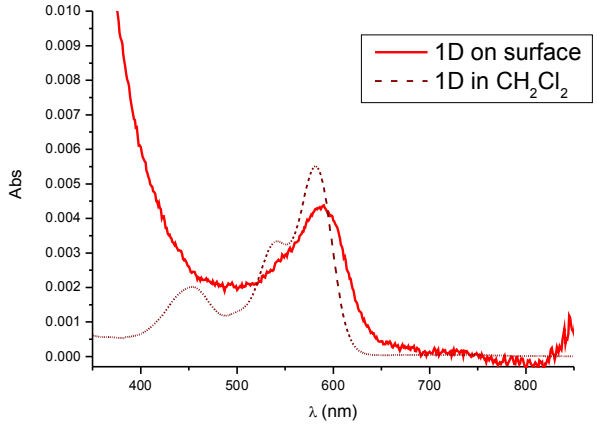

Figure 43. UV-Vis spectrum of 1D in solution and on surface (20 layers on quartz ZP).

For the 20 layers specimen of 2D/Fe it is possible to individuate a band at ≈ 720 nm (characterized by a red shift if compared with the spectrum of the solution), resulting from $S_0 \rightarrow S_1$ transition of the chromophore, and a band at ≈ 575 nm assigned to the MLCT transition of $[Fe(Tpy)_2]^{2+}$ (Figure 44).

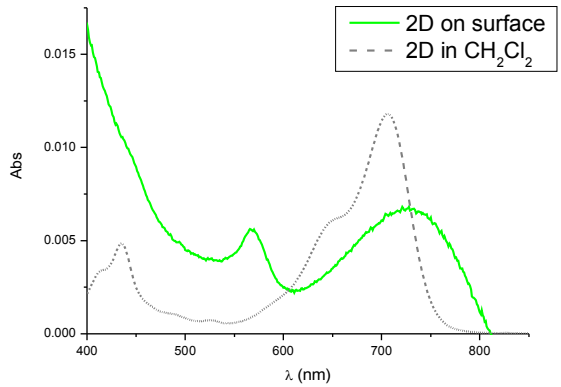

Figure 44. UV-Vis spectrum of 2D in solution and on surface (20 layers on quartz ZP).

By measuring UV-Vis spectra of the perylene bisimide films with a different number of layers one observes that the typical band of the perylene bisimide iron complex at 580 nm[90] grows with the number of coordination steps (Figure 45 a for 1D chromophore, Figure 46 a for 2D chromophore). Moreover, the linear correlation between the optical densities of the characteristic multilayer band at 589 nm as a function of the nominal number of layers (Figure 45 b and Figure 46 b) indicates the formation of a constant number of iron complexes per step.

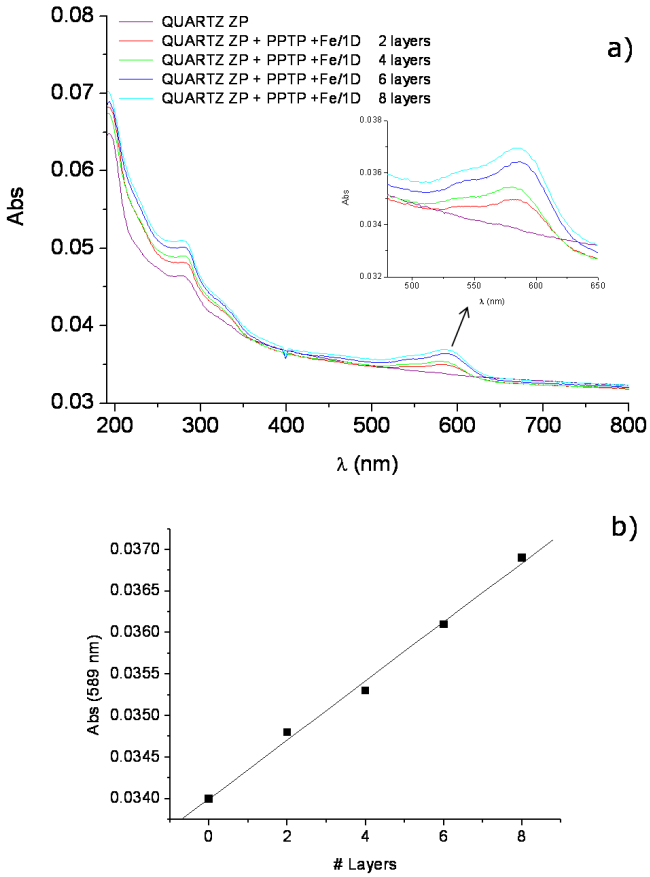

Figure 45. UV-Vis spectra acquired from an increasing number of layers for the sample Fe/1D (a) on quartz substrates. Optical densities of the characteristic MLCT band as a function of the nominal number of layers is reported (b).

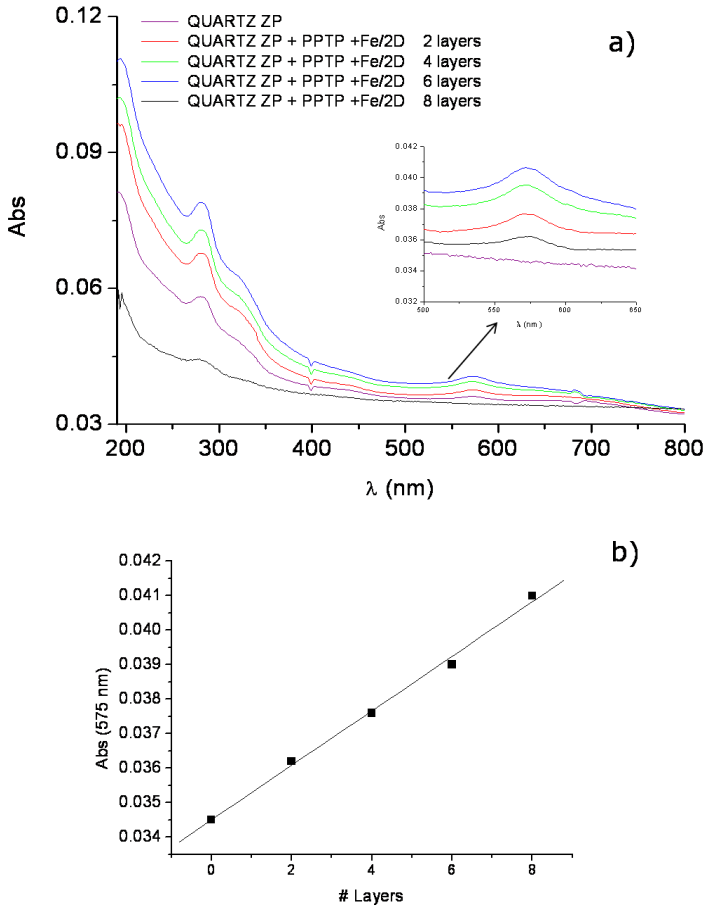

Figure 46. UV-Vis spectra acquired from an increasing number of layers for the sample Fe/2D (a) on quartz substrates. Optical densities of the characteristic band at 575 nm as a function of the nominal number of layers is reported (b).

Similar considerations apply for chromophore/Fe multilayers growing on ITO substrates (Figure 47 for 1D chromophore and Figure 48 for 2D chromophore). Again, a linear increase of absorbance with the number of deposition steps indicates that a constant number of iron complex is formed during each step.

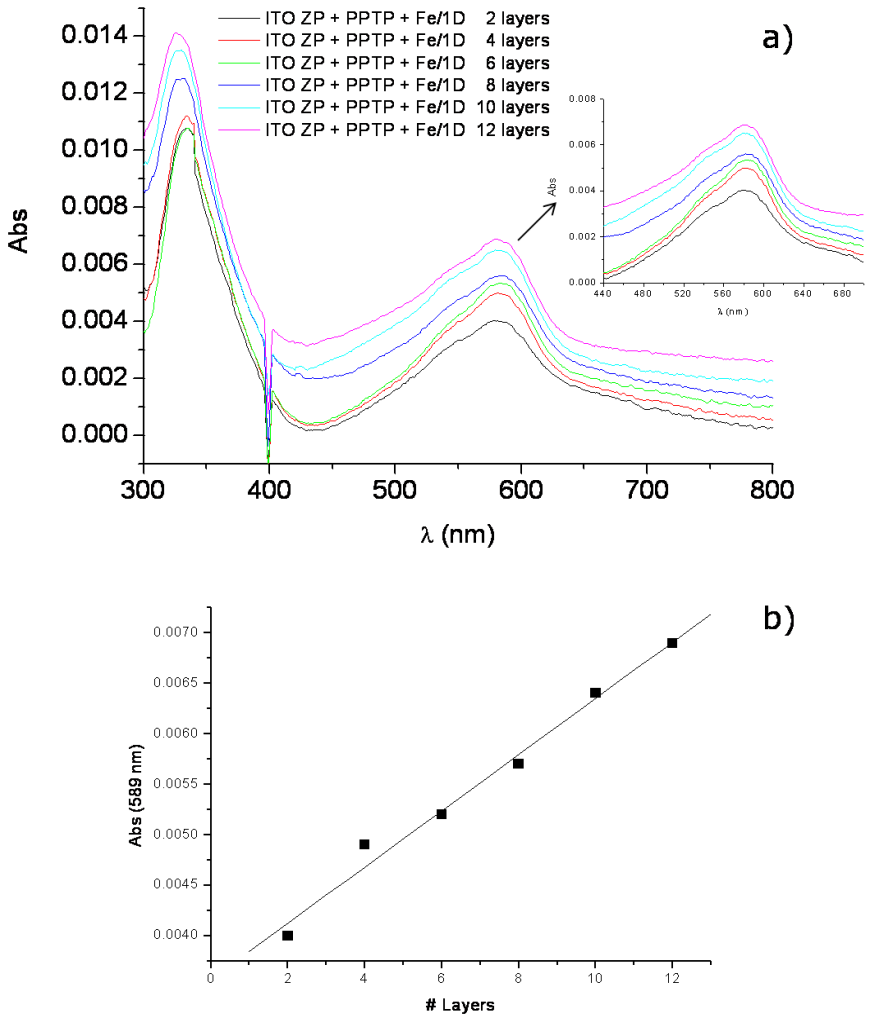

Figure 47. UV-Vis spectra acquired from an increasing number of layers for the sample Fe/1D (a) on ITO substrates. Optical densities of the characteristic band at 575 nm as a function of the nominal number of layers is reported (b).

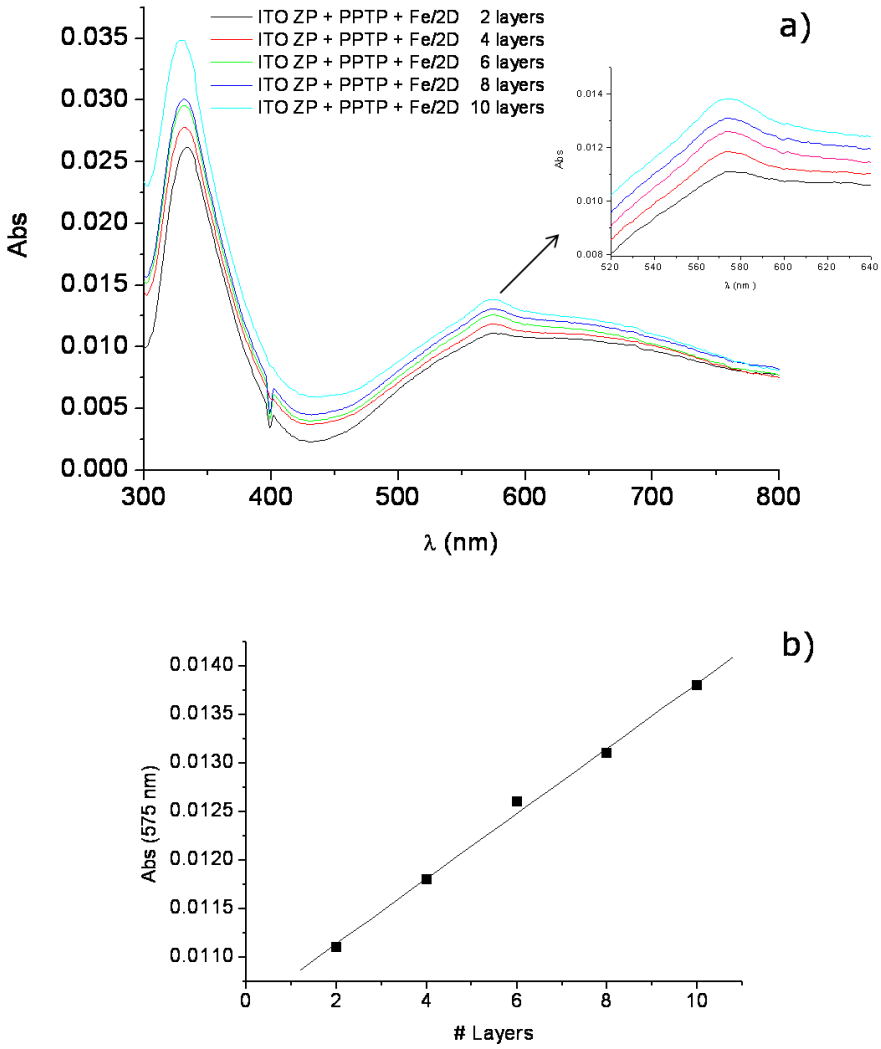

Figure 48. UV-Vis spectra acquired from an increasing number of layers for the sample Fe/2D (a) on ITO substrates. Optical densities of the characteristic MLCT band as a function of the nominal number of layers is reported (b).

2.3.5 Conclusions

In summary, metallosupramolecular mono- and multilayers of terpyridine-functionalized ligands with Fe ions have been prepared on oxide surfaces via a self-assembling stepwise method involving direct coordination reactions at the sample surface.
The formation and growth of the molecular films have been demonstrated by ToF-SIMS and UV-Vis spectroscopy. In particular ToF-SIMS allowed monitoring step by step every single reaction at the surface, demonstrating the presence of deposited molecular species.
UV-VIS spectroscopy gave informations about the multilayers growth, and allowed to observe the linear correlation between intensity of characteristic bands and the nominal number of deposited layers. Physico-chemical characterization, therefore, gave evidence that the stepwise methodology applied for growing terpyridine-based complexes is successful.
The possibility to create nanometre-scaled devices by means of anchoring molecular systems with interesting optical, electrical, and structural properties, as the molecules used in this work, on technologically interesting substrates, as Indium Tin Oxide, is a very attractive goal, for applications in the field of optoelectronics, sensor devices and molecular electronics. In particular, similar systems grown on gold have been already demontstrated to possess very interesting electron transport[82] or optical properties.

2.4 Anchoring of oligonucleotides on gold surfaces

2.4.1 Introduction and state-of-art

DNA microarrays, in which thousands of hybridization experiments are carried out in parallel, are nowadays widely used for addressing fundamental issues in biotechnology. Some important issues are fundamental in engineering of DNA-micro arrays using probes immobilized on the surface: optimal density, target and probe size, target concentration, hybridization[91] efficiency.
In these devices, the hybridization, i.e., the association of immobilized single-strand DNA "probes" with "target" sequences from solution, occurs at solid-liquid interface.[92]
Microarray fabrication involves the patterning of DNA on a proper substrate. Several methods have been developed for DNA patterning, including contact and noncontact printing of pre-synthesized DNA and in situ preparation of microarrays by using photolithography.[93]
Commercially available microarray slides are often obtained by robotic printing of drops of DNA solutions onto a reactively coated glass. One of the most serious drawbacks of this procedure is the formation of non-homogeneous DNA spots due to the evaporation of deposited liquid droplets,[94] leading to inconsistent interpretation of results. Accordingly, the development of uniform DNA surface patterning methods is currently one of the most challenging scientific tasks.
Until 1997,[95] [96] Tarlov and his research group have exploited the possibility to use alkanethiol self-assembly on gold in order to prepare DNA probe modified surfaces. In 2004, Arlinghaus and others[97] used particular kind of probes, called PNA (peptide nucleic acid),[98] in which phosphate and deoxyribose groups are replaced with a polypeptide. In this way it was possible to apply ToF-SIMS to microarray characterization, as label-free technique, considering the presence (or the absence) of PO_3^- peaks as the occurred (or not) hybridization.[99]
In 2006,[100] Castner and others reported a detailed study about the employ of alkanethiols as "thinners" of probes anchored on gold surface. With this study it was clear that surface densities greater than 1.4×10^{12}

probe/cm^2 decrease hybridization efficiency due to the increase of steric hindrance between neighbouring probes and target that have to interact with anchored probes.
Efficient anchoring of supramolecular architectures on gold surfaces can be achieved by exploiting the spontaneous formation of a bis-terpyridine metal complex directly at the solid-liquid interface. This involves the functionalization of the gold surface with a terpyridine-containing mixed component self-assembled monolayer (SAM),[101] that acts as a "platform" for the subsequent anchoring of a variety of suitably functionalized molecules on the surface via coordination chemistry. This approach for efficient surface anchoring of tolylterpyridine-tagged DNA single strands (ssDNA-ttpy) onto metal electrodes was applied during this thesis work.[102]
The strategy is based on the building up of supramolecular architectures via coordination chemistry,[103] and it is exploited for the surface anchoring of oligonucleotides.
According to previous achievements,[101b] the micro-patterned arrays of terpyridine-containing SAM platform are obtained by exploiting low current focused ion beam lithography (FIB). A simple exchange reaction between the (Fe(II) bis-terpyridine complexed) SAM platform and tolylterpyridine-tagged DNA single strands (ssDNA-ttpy) finally allowed us to obtain highly uniform ssDNA-ttpy spots. The surface adsorption kinetics of ssDNA-ttpy as well as its hybridization efficiency was monitored in situ by the quartz crystal microbalance with dissipation monitoring (QCM-D) technique[104] and time of flight secondary ion mass spectrometry (ToF-SIMS). The homogeneity of the patterned DNA regions has been monitored by means of ToF-SIMS chemical mapping.

2.4.2 Gold surface priming

As substrate, gold film (Au 99.99%) evaporated on silicon was used. It was treated in UV-O_3 for 15 minutes and rinsed with ethanol.
The "platform" used for anchoring of ssDNA-ttpy on gold substrates via formation of a Fe(II) complex consists of a mixed (1:1) component self-assembled monolayer of [4'-(4-mercaptophenyl)-2,2':6'2''-terpyridine] (MPTP) and mercaptobenzene (MB)[105] (see Figure 49). Mercaptobenzene

was used as lateral spacer in order to minimize steric hindrance between the molecules and to obtain a compact, stable and oriented SAM. Thiols solutions were prepared in ethanol (≈ $5 \cdot 10^{-5}$ M); gold samples were dipped in 1:1 mixed solution for 24 hours, then rinsed with ethanol.

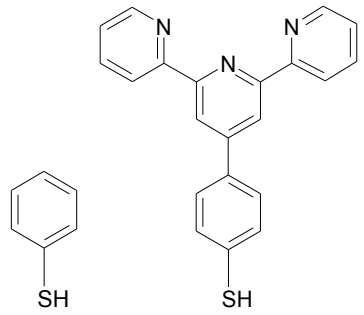

Figure 49. Molecular structure of MB (on the left side) and MPTP (on the right side).

2.4.3 Molecular building blocks

As probe was used a terpyridine-functionalized 17-mer single strand oligonucleotide sequence, henceforth ssDNA-probe-TPY (4'(4-$CONC_2HPO_4$-3'AT.TTA.AAT.TAT.TTT.TTT5'-phenyl)-2,2':6'2''-terpyridine), showed in Figure 50. As target were used two molecules, one complementary to the probe (3'AA.AAA.AAT.AAT.TTA.AAT5', henceforth C-ssDNA-target), the other non complementary (3'TG.CAC.TCA.ACT.CTG.CA5', henceforth NC-ssDNA-target).

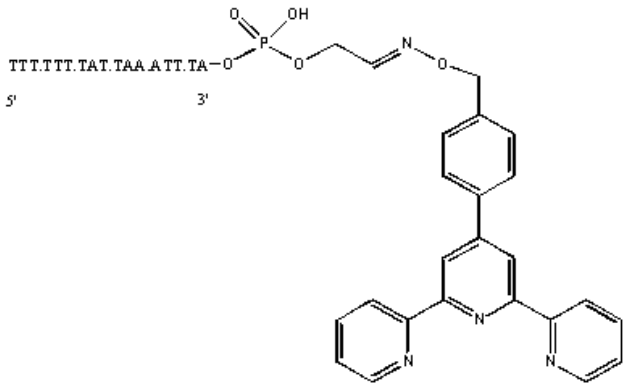

Figure 50. Molecular structure of ssDNA-probe-TPY.

2.4.4 QCM-D surface coverage studies

In principle, we could use the MPTP/MB SAM, after reaction with iron, for a one-step reaction with ssDNA-probe-TPY, obtaining a bis-terpyridine Fe(II) complex. However, preliminary experiments (not reported) showed that such a procedure leads to a high surface concentration of the ssDNA probe and to a poor control of the surface coverage, crucial for optimizing the hybridization efficiency.[106]
The method we adopted in this study, outlined in Figure 51, exploits the exchange reactions peculiar of terpyridine metal complexes and allows better control of the surface density of ssDNA molecules.

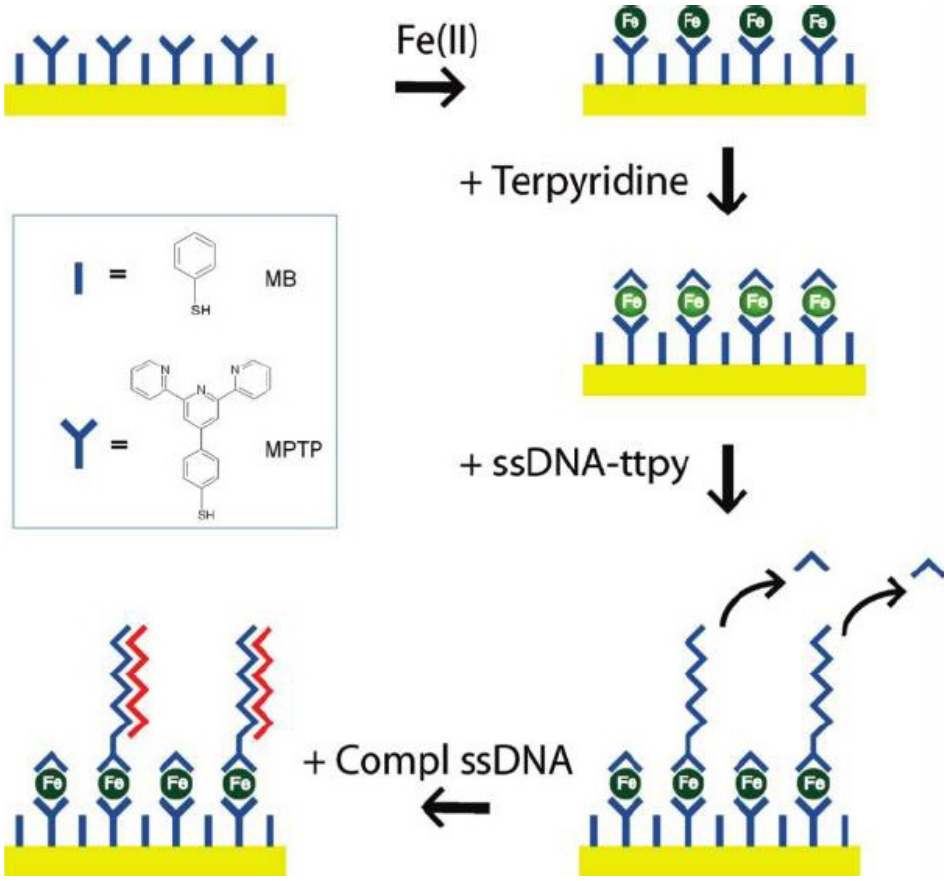

Figure 51. Scheme of exchange reaction for anchor ssDNA-probe-TPY.

In particular, first the bis-terpyridine Fe(II) complex SAM is prepared on the surface via the reaction between the Fe(II)terpyridine-based SAM and a terpyridine solution. Afterward, the specimens are immersed in ssDNA-probe-TPY solution in order to anchor ssDNA-probe-TPY by exchange with the upper terpyridine ligands of the anchored iron(II) complex.
In situ QCM-D measurements were performed in order to determine the adsorption behavior of ssDNA-probe-TPY onto a model unpatterned monolayer of Fe(II) bis-terpyridine based SAM.

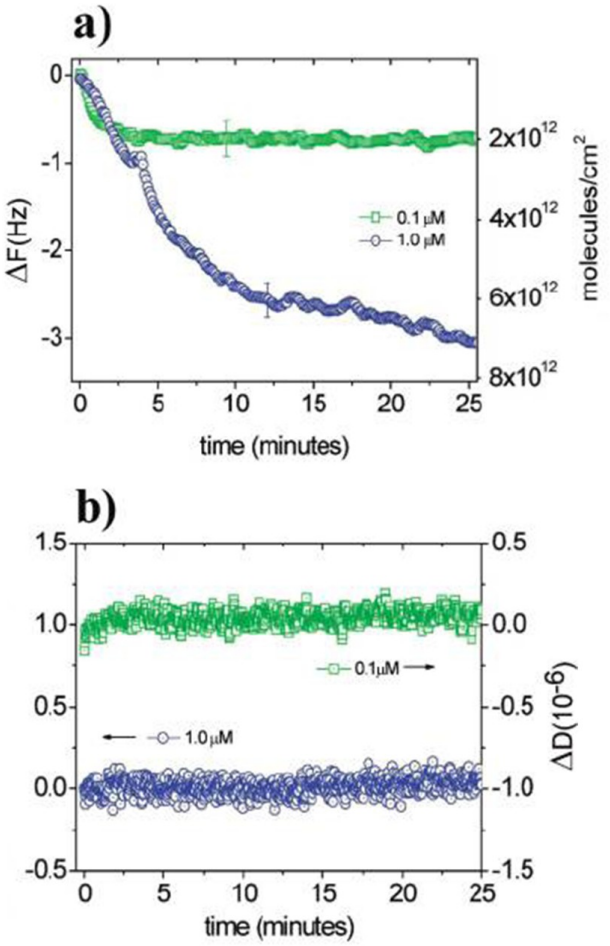

Figure 52. QCM-D monitoring of ssDNA-ttpy adsorption onto an unpatterned Fe(II)bis-terpyridine based SAM: (a) frequency shift; (b) dissipation behaviour.

Figure 52 shows the time-dependent behaviour of frequency (proportional to the adsorbed mass) and dissipation (depending on the viscoelastic properties), respectively, for 1 μM and 0.1 μM solutions (see Figure 52a). It can be seen that, while at relatively high concentration (i.e., 1 μM) the ssDNA-probe-TPY adsorption slowly approached saturation (not reached after 25 minutes), for the lower concentration saturation occurred very quickly (after a few minutes).

In both cases, the measured null dissipation (Figure 52b) indicated the formation of rigid elastic films, enabling the use of Sauerbrey equation[107] to obtain a quantitative estimate of the mass uptake on the surface from the frequency shift. Thus, while in the case of the higher concentration (1.0 μM), the mass uptake, still increasing after 25 minutes, corresponds to about $\approx 7 \cdot 10^{12}$ ssDNA-probe-TPY molecules/cm^2, in the case of the lower concentration (0.1 μM), mass uptake at the steady state corresponded to a surface coverage of $\approx 2 \cdot 10^{12}$ molecules/cm^2. It is worth it to stress that this coverage value, which is considered the most appropriate for achieving an optimal DNA hybridization,[108] was reproducibly obtained in the low concentration regime and, for this reason, it was chosen as the optimal working condition in our experiments to achieve a constant surface density of anchored ssDNA-probe-TPY.

2.4.5 Patterning by means of a focused ion beam

For pattern preparation, SAMs of (1-mercapto-11-undecyl)hexa-(ethylene glycol) were prepared on gold and then ion-beam etched with a 10 keV Bi^+ focused beam, obtaining square patterns of uncovered gold, on which the MPTP/MB SAM was assembled.
Finally, in order to prepare ssDNA patterns the following step-by-step procedure was employed. First, the gold substrates were functionalized with a SAM of (1-mercapto-11-undecyl)hexa- (ethylene glycol) in order to obtain a surface resistant to nonspecific DNA adsorption. Afterward, it was used a focused ion beam for etching such a SAM from selected areas, obtaining an array of rectangular ($\approx 75 \times 75$ μm^2) bare gold regions. Finally, the procedure of Figure 51 was followed for anchoring ssDNA-probe-TPY on these regions.
Each step of the protocol (vide supra) was monitored by ToFSIMS. In particular, Figure 53 shows the ToF-SIMS chemical maps obtained from a patterned specimen after adsorption of ssDNA-probe-TPY.

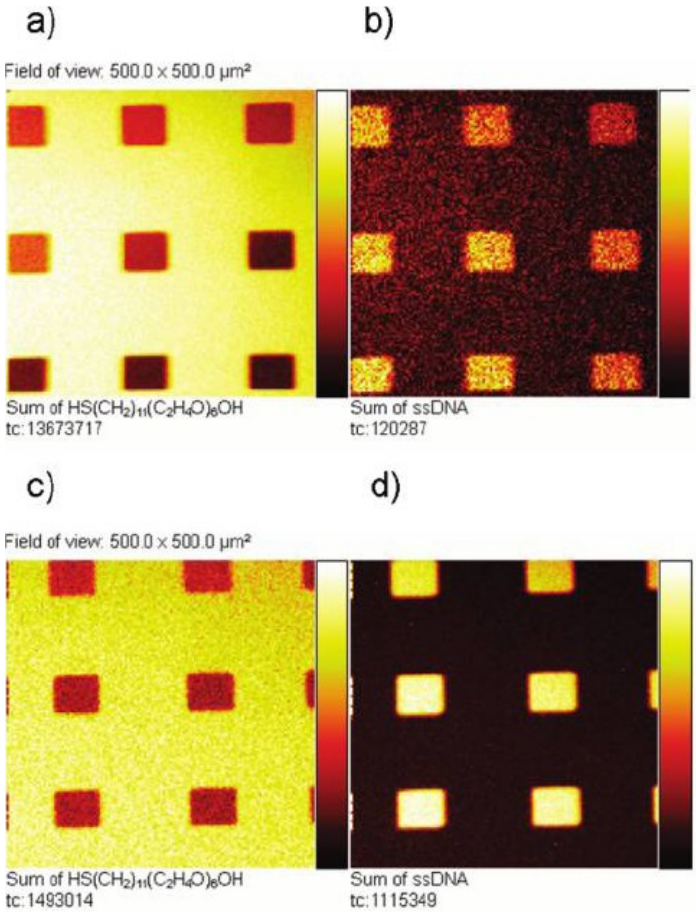

Figure 53. ToF-SIMS imaging of the patterned surface after ssDNA-probe-TPY anchoring: (a) positive ions from masking SAM, (b) positive ions from ssDNA-probe-TPY, (c) negative ions from masking SAM, and (d) negative ions from ssDNA-probe-TPY.

Both positive-ion (Figure 53 a, b) and negative-ion (Figure 53 c, d) chemical maps were obtained by adding the intensity of the peaks characteristics of the ethylene glycol-based SAM (Figure 53 a, c) and of the adsorbed ssDNA-probe-TPY (Figure 53 b, d), respectively. In each map, the color of each pixel is related to the intensity of the species considered, a brighter color from a certain region indicating that a higher

signal of the considered species is obtained from that region. The maps of Figure 53 (especially those obtained in negative ion mode, showing higher intensity and better signal-to-noise ratio) clearly indicate that ssDNA-related signals are present only inside the patterned rectangular regions, whereas the signals related to ethylene glycol based SAM are present outside those regions. Note that the weak DNA-related signal present outside the squares, as well as the signal of the masking SAM inside the squares, is at the same level of noise in the respective mass regions, as demonstrated by mass spectra (not shown) reconstructed from the areas of interest. Moreover, DNA-related signal intensity inside each individual rectangular region appears to be quite homogeneous, indicating the absence (within the lateral resolution of the technique, of the order of 1 μm) of inhomogeneities that often are observed in microarrays obtained with other techniques.[109]

2.4.6 Hybridization studies by ToF-SIMS and QCM-D analysis

Quartz crystal microbalance with dissipation monitoring studies were performed in a QCM-D (Q-Sense AB, Sweden) apparatus. ToF-SIMS high mass resolution spectra and images were obtained with a TOFSIMS IV (ION-TOF,Germany) spectrometer.
The samples prepared by means of the above methodology were further examined in several DNA hybridization experiments on the surface. For this purpose, a solution of the C-ssDNA-target strand was allowed to interact with the DNA strands immobilized on the surface. A first indication of the success of the hybridization was obtained by ToF-SIMS measurements. Indeed, ToF-SIMS is able to give indication of the relative abundance of the DNA bases on the sample surface (as well as on their spatial distribution), based on the identification of distinctive ion fragments.
Since immobilized ssDNA-probe-TPY is constituted by 12 thymine and 4 adenine bases, an increase of the A/T ratio in ToF-SIMS signal intensity indicates hybridization.

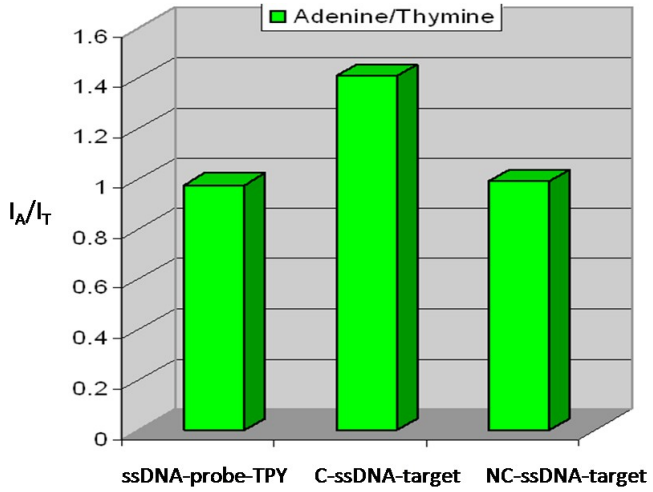

Figure 54. ToF-SIMS intensity ratio of adenine (I_A) and thymine (I_T) related signals before and after adding a complementary or a noncomplementary ssDNA-target onto a ssDNA-probe-TPY based SAM.

As shown in Figure 54, such an increase is observed only in the case of incubation with the complementary ssDNA target, while the A/T intensity ratio remains unchanged (after proper washing) in the case of interaction with the non-C-ssDNA-target strand. This is a clear indication that the surface anchored ssDNA-probe-TPY is able to hybridize with the related target and rules out the hypothesis of unspecific adsorption.
QCM-D experiments yielded a quantitative estimate of the hybridization efficiency. Figure 55 shows the frequency shift for complementary and non-cDNA targets onto a ssDNA-probe-TPY monolayer.

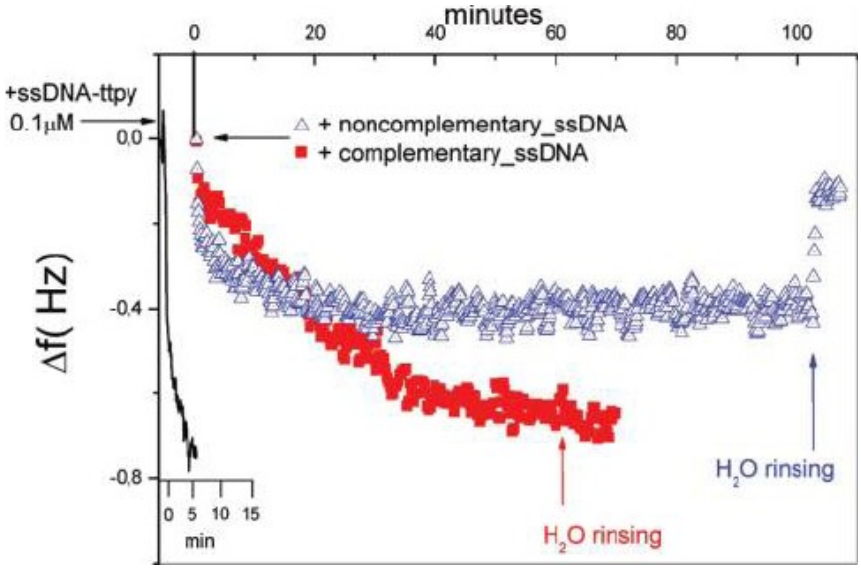

Figure 55. QCM-D monitoring of the mass adsorption of the complementary (■) and noncomplementary (Δ) DNA targets on a surface functionalized with a 0.1 μMsolution of ssDNA-probe-TPY. The black curve on the left side refers to the formation of the initial layer of ssDNA-probe-TPY.

Again, in both experiments a null dissipation was observed (not reported), so the frequency shift could be converted to mass uptake by means of the Sauerbrey equation. As shown in Figure 55, the non-complementary ssDNA target gives rise to a relatively small frequency shift, corresponding to a very small non-specific adsorption, as indicated by the fact that water rinsing restores the initial frequency, i.e., the non specifically adsorbed molecules are easily desorbed. By contrast, the mass uptake of the complementary strands is slightly higher and is not affected by water rinsing, indicating that a specific interaction occurred, producing a stable hybrid. Furthermore, the number of adsorbed complementary ssDNA molecules ($\approx 1.5 \cdot 10^{12}$ molecules/cm^2) provided comparable results to the ssDNA-probe-TPY strands of the anchored layer, indicating remarkably good hybridization efficiency.

2.4.7 Conclusions

A stepwise methodology for surface anchoring of single-stranded oligonucleotides has been developed. The surface coverage is controlled by exploiting an exchange reaction between Fe(II)bis-terpyridine complexed SAMs and ssDNA-probe-TPY. Our results show that, by using the proper concentration of ssDNA-probe-TPY, it is possible to prepare ssDNA layers, having reproducible and controlled surface density, and that these layers show very good hybridization efficiency.
Also, the proposed method, joined with FIB patterning, allows the preparation of patterns characterized by homogeneous distribution of ssDNA in each spot. The reported results suggest a new possible approach to solving problems related to inhomogeneities observed in microarrays prepared with different techniques. Finally, the anchoring method used here could be exploited in conjunction with other patterning approaches, more common or less expensive than FIB, provided that they are able to form on bare gold regions with sharp contours.

2.5 Formation of pseudo-rotaxanes at gold surfaces

2.5.1 Introduction

A rotaxane is a mechanically-interlocked molecular architecture consisting of a "dumbbell shaped molecule" which is threaded through a "macrocycle" (see graphical representation in Figure 56). The name is derived from the Latin for wheel (rota) and axle (axis). The two components of a rotaxane are kinetically trapped since the ends of the dumbbell (often called stoppers) are larger than the internal diameter of the ring and prevent disassociation (unthreading) of the components since this would require significant distortion of the covalent bonds. A pseudo-rotaxane is a rotaxane which has one or no bulky stoppers on the thread.

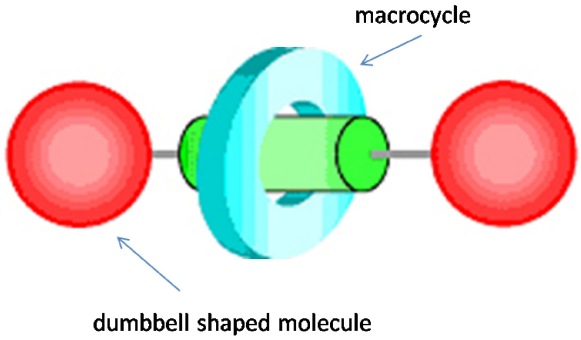

Figure 56. Graphical representation of a rotaxane.

If properly designed, a shuttlable rotaxane can be switched between different co-conformational states when external energy (*e.g.* chemical, electrochemical, photochemical, or entropical) is applied. The ability of these shuttlable rotaxanes to switch between alternative states has raised opportunities in the fabrication of molecular machines and molecular devices.
Rotaxane-based molecular machines have been of initial interest for their potential use in molecular electronics as logic molecular switching elements and as molecular shuttles.[110] These molecular machines are usually based on the movement of macrocycle on the dumbbell. The

macrocycle can rotate around the axis of the dumbbell like a wheel and axle or it can slide along its axis from one site to another. Controlling the position of the macrocycle allows the rotaxane to function as molecular switch with each possible location of the macrocycle corresponding to a different state. These rotaxane machines can be manipulated both by chemical[111] and photochemical inputs.[112]

If properly designed, two recognition sites for the macrocycle can be arranged within the dumbbell component. Moreover, the strengths of the non-covalent bonding interactions between two recognition sites with the ring component are quite different, and as a result, the ring component locates preferentially in the site that has stronger interactions with the ring (ground state in Figure 57). In such a system, when a suitable external stimulus—either chemical or physical—is applied, the binding activity sequence of the two recognition sites is altered, as a consequence, the ring component shuttles from the original recognition site to another (switched state in Figure 57). In the ideal case, the properties of the two recognition sites can be shifted reversibly back to the original ones by another stimulus. Such a molecule constitutes a molecular shuttle.[113]

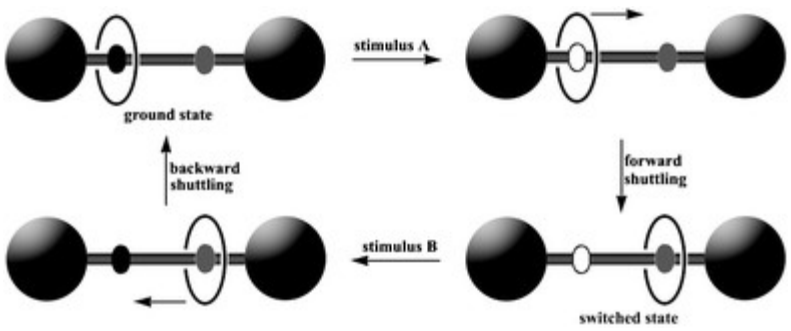

Figure 57. The stimuli-triggered reversible shuttling motions in a [2]rotaxane.

It can be seen that the external stimulus employed to affect the switching motion of a rotaxane must be able to weaken the relative binding forces which stabilize the initial state. Thus, the type of stimulus used depends on the nature of the binding forces. A chemical (acid/base), an entropic

stimulation, or a solvent change can drive a molecular machine based on hydrogen-bonding; Chemicals (oxidant/reducer), electrochemical (redox) processes, or photochemical (photoinduced redox) processes can power a molecular machine relying on donor/acceptor interactions. A photoisomerization process can also induce relative spacial changes among the components and thus can drive a molecular shuttle. Like a macroscopic machine displaying intercomponental relative position changes when applying power, a switchable rotaxane performs shuttling motion in response to external stimuli. From this point of view, a molecular shuttle is also deemed as a molecular machine, and the external stimuli are the driving forces or energy supplies of the machine system.

2.5.2 Surface anchoring of axle and formation of the rotaxane directly at the surface

The purpose of this work is the anchor on surface of a SAM of guest molecule and the subsequent complexation, directly at the surface, with a solution of host molecule, following the scheme outlined in Errore: sorgente del riferimento non trovata.. Guest molecule is characterized by a thiol as head group and an amino group as tail. The head reacts with the gold surface, the tail will be used to interact with the host. Host molecule is a calix[6]arene characterized by tert-butylic groups at the upper rim, and hexylic groups (R = $CH_2(CH_2)_4CH_3$) at the lower rim. Both host and guest molecules were synthesised by the research group of Prof. P. Neri at University of Salerno, Italy, and their molecular structurs are reported in Figure .

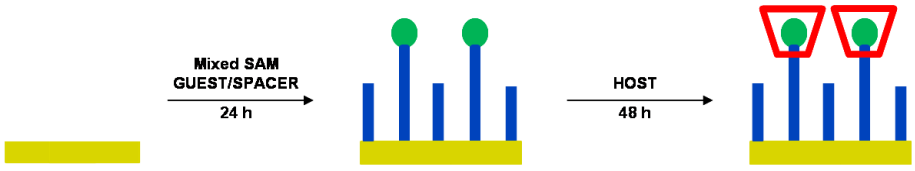

Figure 58. Schematic rappresentation of directly complexation on surface.

In order to avoid steric hindrance that can occur between the tails of the guest molecules and, more important, between the host molecules to be incorporated in the pseudorotaxane, 1-decanthiol was used as lateral spacer.
Typically, thiol-based SAMs are obtained from ethanolic solutions. In this case it is not possible to use ethanol as solvent because the molecules involved in the reaction are very sensible to the presence of protons. In fact, if pronotation of these molecules occurs, it is poissible to swich from a complexed mode to a non-complexed mode. So reagents were solubilised in anhydrous chloroform in order to obtain $5x10^{-4}$ M concentrations, and the same solvent was used for rinsing. These solution were kept at low temperature and out of light.
As substrate, gold film (Au 99.99%) evaporated on silicon was used. It was treated in UV-O_3 for 15 minutes, rinsed with ethanol, and then dried under N_2 flux.

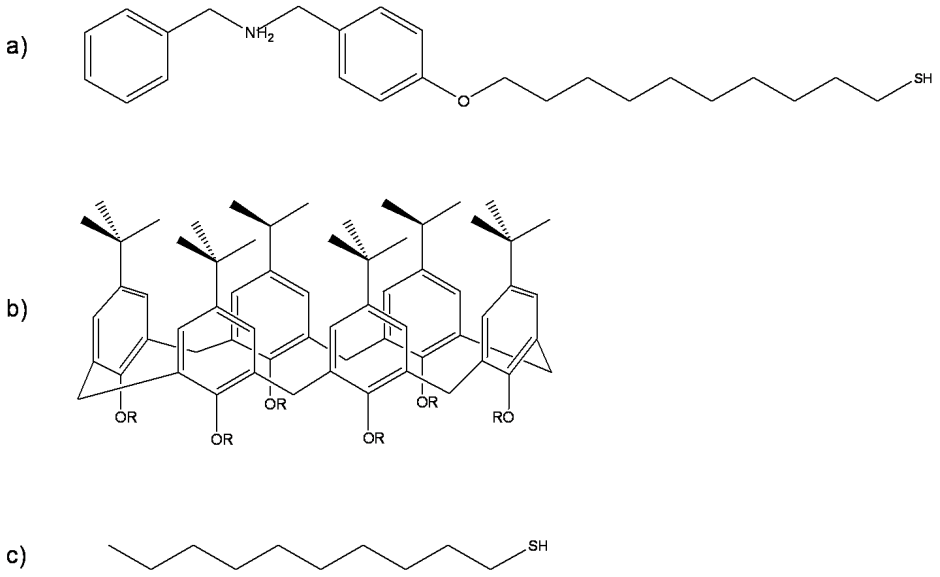

Figure 59. Molecular structure of a) guest, b) host and c) lateral spacer.

In order to prepare the guest-containing SAM, gold substrates were dipped in the mixed thiol solution for 24 hours. Different guest-spacer ratios were used: a) 100% guest, b) 1:1 guest-spacer, c) 1:3 guest-spacer, and d) 1:5 guest-spacer. Incubation reaction were allowed to occur in the dark. After 24 hours, samples were rinsed with anhydrous chloroform, then dried under N_2 flux.
Samples functionalised with the guest-containing SAM were dipped in host solution for 48 hours, rinsed with anhydrous chloroform, and then dried under N_2 flow. At this step it is important to understand which is the role of spacer, if its presence is really useful for leading to the complexation reaction, and which is the right concentration to use in order to have a successful interaction between host and guest directly on the surface. To this aim, ToF-SIMS measurements were extremely useful.

2.5.3 ToF-SIMS characterization

ToF-SIMS spectra were acquired with a TOFSIMS IV spectrometer (ION-TOF GmbH, Muenster, Germany) using 25 keV Bismuth primary ions (≈ 1 pA, 200·200 μm^2 area). Spectra were acquired in static mode (Bi^+ primary ion fluence < 10^{12} ions·cm^{-2}) in order to preserve the molecular information.
In order to obtain preliminary information on the fragmentation patterns of each individual molecules involved, ToF-SIMS measurements were carried out on samples prepared by depositing on gold substrates a small drop of the solution.
Figure 60 shows ToF-SIMS spectrum of the drop-cast guest on gold surface; it is possible to observe the presence of the molecular ion $[C_{24}H_{36}NOS]^+$ (m/z 386) and of a gold-cationised species $[C_{24}H_{35}NOSAu]^+$ m/z 582).
Figure 61 reports the relevant part of the ToF-SIMS spectrum of the drop-cast host on gold; three molecular structure-related peaks are visible, namely the molecular ion at m/z 1478 $[C_{102}H_{156}O_6]^+$ and other two peaks where the host is cationized with copper (m/z 1541 $[C_{102}H_{156}O_6Cu]^+$) and gold (m/z 1675, $[C_{102}H_{156}O_6Au]^+$). The presence of copper is not much surprising, considering the high tendency of calixarenes to include

cations, so that low level of copper impurities present in some phase of the purification or in the gold substrate can be easily trapped.

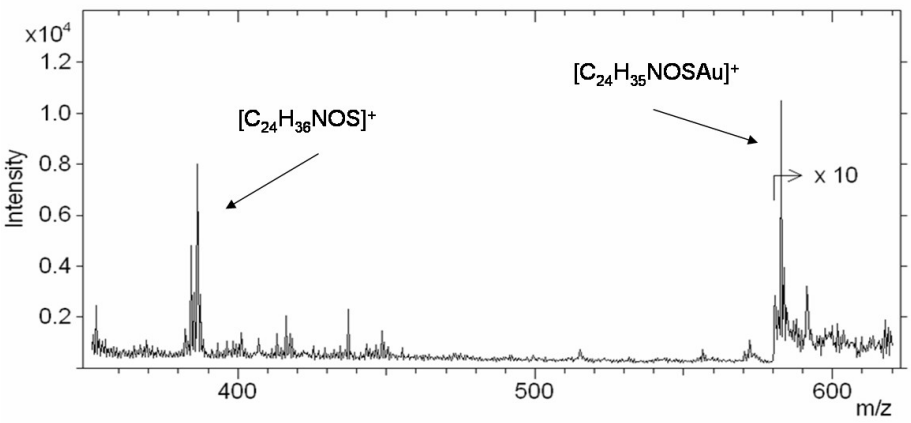

Figure 60. ToF-SIMS spectrum of physisorbed guest on gold.

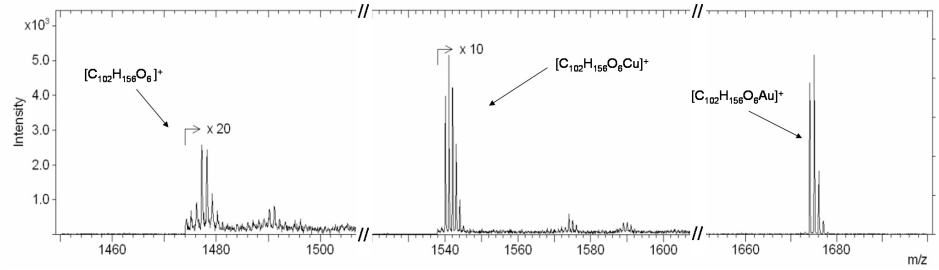

Figure 61. ToF-SIMS spectrum of physisorbed host on gold.

ToF-SIMS analysis of SAMs on gold was also performed for samples containing 100% guest, and 1:1, 1:3, 1:5 ratios of guest and spacer (see Figure 62). For all the samples, it is possible to detect the molecular ion of the guest (m/z 384 $[C_{24}H_{34}NOS]^+$) and, for the mixed SAMs, the quasi-molecular ion of the spacer linked to gold (m/z 369 $[C_{10}H_{20}SAu]^+$). In all the samples we detect also species containing the guest molecule linked with gold, although in some cases (100% guest sample, 1:3 mixture) such species contains only one gold, while in the 1:1, and 1:5 samples the observed peak contains two gold atoms.

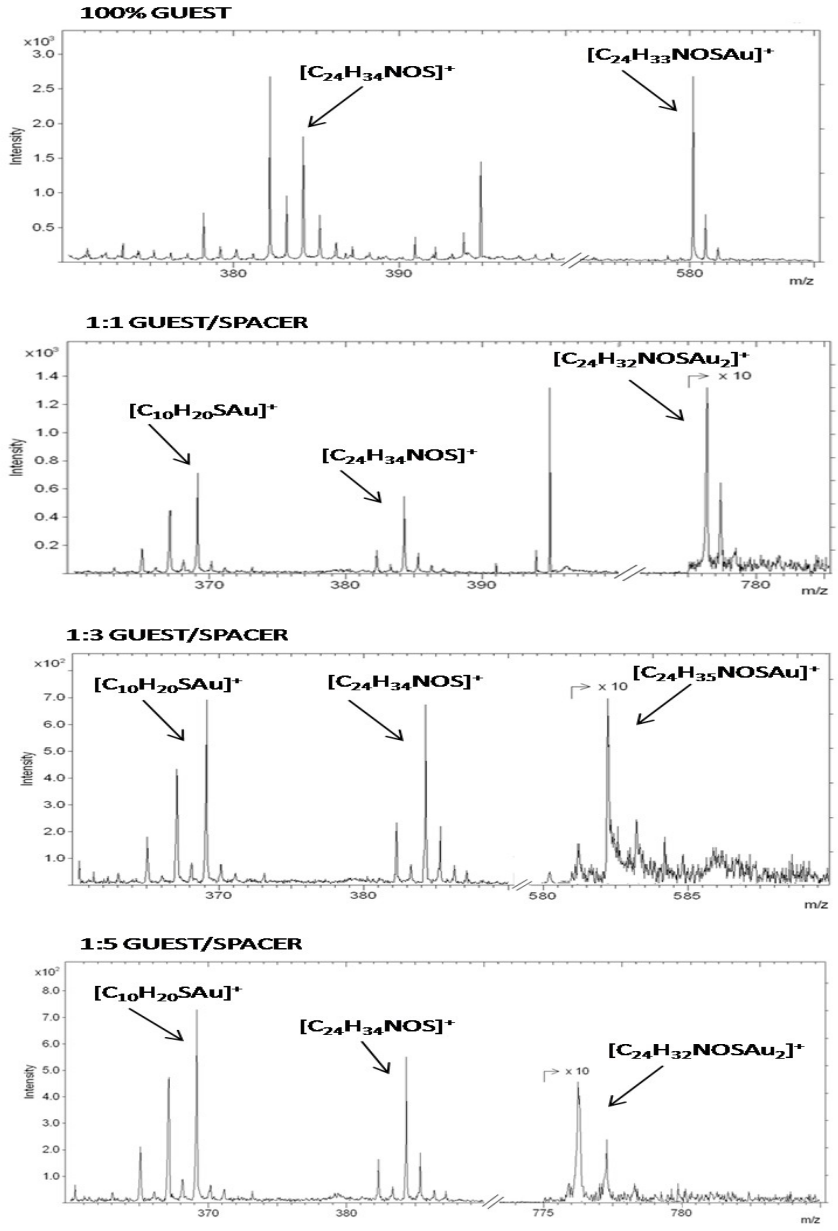

Figure 62. ToF-SIMS spectra of samples containing guest and laterarl spacer.

ToF-SIMS analysis of SAMs was of course performed for samples after the incubation with the host, in order to verify if the host-guest interaction occurred. For the four guest-spacer ratios studied, peaks related to guest and spacer are still present (not showed), but the evidence of complexation was observed only in the case of 1:5 guest-spacer ratio (after incubation with host for 48 hours). In fact, for this sample, as shown in Figure 63 we observe the presence of a peak at m/z 1675 $[C_{102}H_{156}O_6C_{14}H_{16}N]^+$ that is assigned to the entire the host molecule plus the guest molecule missing of the alkyl chain.

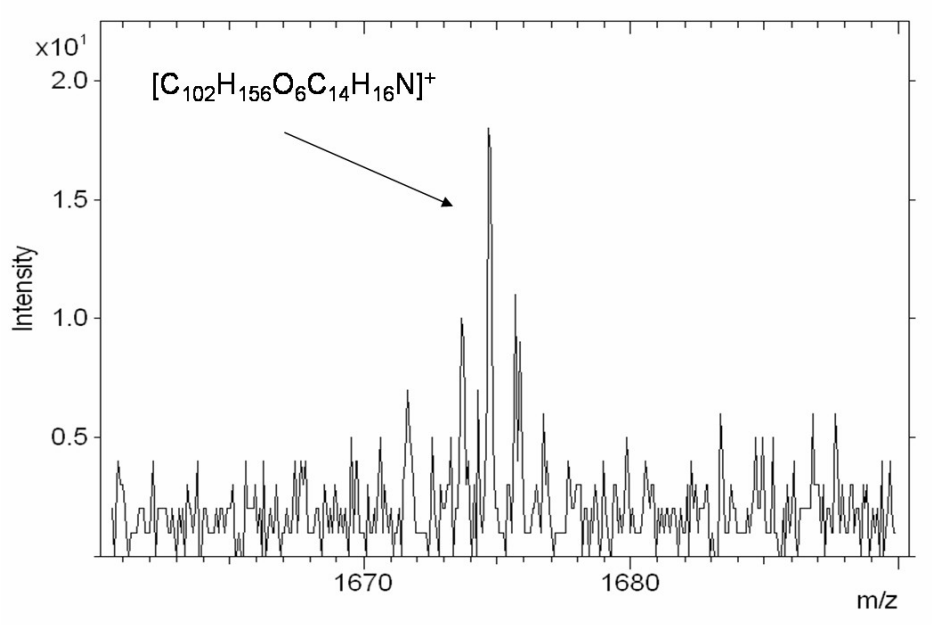

Figure 63. ToF-SIMS spectrum of sample 1:5 guest/spacer ratio after incubation with host.

2.5.4 Conclusions

The purpose of this part of the work was to explore the possibility of obtaining, directly at the sample surface, the formation of a pseudo-rotaxane by exploiting self-assembly between the guest immobilisef on the gold surface and the host contained in the solution. As guest we used

a molecule characterized by a thiol group necessary for chemisorption on gold surface, and a secondary ammine as a group that is able to react with the host, a calix[6]arene. A great issue was related to find a way to decrease the steric hindrance between such bulky molecules in order to promote SAM formation. The key was found in using a lateral spacer in different ratios with the guest. ToF-SIMS characterization was useful to understand which was the best guest-spacer ratio to use, as well as for monitoring the surfaces after each manipulation step. It turned out that guest-to-spacer ratios higher than 1:5 were not sufficient for decreasing the steric hindrance and to allow the formation of the host/guest complex. So, the unique evidence of complexation directly at the surface was obtained for guest-spacer 1:5 ratio sample.

.
.

3 Conclusions

3.1 Conclusions

This thesis focused on the preparation and on the characterization of functional organic and metalorganic thin films on oxides and metal surfaces. The approach adopted was a bottom-up one, based on the formation of self assembled layers. In particular our general aim was that of obtaining mono- and multi- layers of functional molecular systems by exploiting non covalent interactions that in many cases are able to lead to the formation of the desired system *directly at the surface*, by using the proper building blocks. This was obtained by anchoring, on the selected surface, a self assembled monolayer exposing upwards suitable functional groups that are capable of non covalent interations that in turn are exploited for the formation of the final system. In the present work we used a terpyridine group for anchoring layers via formation of a metal complex or an amino group for obtaining a pseudorotaxane. In other words, such functional monolayer is used as a "platform" on which the final system is "constructed". This approach provides a large degree of flexibility and can be adapted to different kinds of surfaces by a proper choice of the functional group (head group) that assures the anchoring of the platform to the substrate. In fact, we used phosphonic groups for obtaining the anchoring on properly primed oxide surfaces and thiol groups for anchoring on gold.
The approach above outlined was used for developing a methodology for functionalizing oxide substrates. The deposition of the "platform" monolayer involves the formation of a zirconium-phosphate-phosphonate (ZP) layer, and takes advantage from the high affinity of phosphate and phosphonate groups for zirconium ions. Both ToF-SIMS and XPS were used to gain information on the anchoring geometry of the SAM and to obtain quantitative information about ZP layer. The terpyridine-ended self-assembled monolayer was then used for binding various metal complexes, through a stepwise procedure involving the coordination reactions directly at the surface. This approach allowed layer-by-layer synthesis of complex systems. The assembled mono- and multilayers were tailored in terms of type of metal or ligand, number of layers, and thickness.

In particular, ruthenium based self-assembled monolayers and iron based multilayers have been prepared by such stepwise layer-by-layer method, using - as ligands - various terpyridine-based molecules characterized by interesting electronic, photonic, and redox properties. ToF-SIMS characterization allowed us to verify the formation of the terpyridine-based complex by direct reaction at the surface. Moreover, ToF-SIMS gave preliminary information about the growth of multilayers. UV-Vis spectroscopy confirmed the formation of the complex and proved that the multilayers grow linearly by iterating the layer-by-layer procedure. We also demonstrated, as confirmed by AFM results, that the ZP "platform" can be prepared in a patterned way by means of micro-contact printing.

A similar terpyridine-based "platform", anchored on gold *via* thiol groups, was exploited for developing a method for the preparation of surface patterns of DNA-microarrays by the formation of an heteroleptic iron-terpyridine complex between the terpyridine groups of the platform and a terpyrydine conjugated oligonucleotide sequence. Then, this system was allowed to interact with both a complementary and non-complementary oligonucleotide sequence, in order to demonstrate its ability to hybridize. This was accomplished by QCM-D measurements that gave also information about the surface coverage. An OH-terminated alkanethiol SAM was used as "mask" in order to cover part of the available gold surface and create a pattern of SAM on the substrate as a DNA-array. ToF-SIMS imaging showed that the patterning process was successful and also demonstrated the selective growth of the DNA SAM on the "mask-free" areas of the surface as well as the selective adsorbtion of the complementary strands on the areas functionalised with the DNA SAM.

Finally, self-assembly was also employed for preparing, a SAM containing a guest that, by interaction with a calixarene host can form, directly at the surface, a pseudorotaxane. Considering the hindrance (both electronic and steric) of the host, a lateral spacer was used in order to facilitate its interaction with the SAM. ToF-SIMS measurements allowed to verify the anchoring of the molecules at the surface, and to demonstrate that the formation of the pseudo-rotaxane can take place at the surface, provided that a proper dilution of the guest molecule in the SAM in obtained by using a suitable amount of lateral spacer molecule.

In conclusion, all the examples described above demonstrate the powerful capabilities and the flexibility of the stepwise approach followed and appear to be themselves interesting systems for possible applications in devices for molecular electronics, photonics, and for molecular recognition purposes.

.

4 Appendix: Techniques

4.1 ToF-SIMS

Secondary ion mass spectrometry, SIMS, is one of the major techniques for the surface characterisation of solids. This section discusses the theoretical fundamentals of the technique and some basic information about instrumentation.

4.1.1 Static SIMS

During SIMS analysis, ionised particles (secondary ions) are emitted when a surface is bombarded by energetic (primary) ions. From the sample will be emitted "secondary" particles, neutral species atoms or molecules, atomic and clusters ions. The main part of species emitted is neutral but it is the secondary ions that are detected and analysed by a mass spectrometer. In ToF-SIMS, ions are analysed by means of time of flight analyzer.
The chemical information in SIMS, are carried out by atomic and molecular secondary ions which are emitted from any surface under primary ion bombardment.[114] Mass analysis of these so-called secondary ions supplies direct information on their nature and thereby on the chemical composition of the uppermost monolayer of the bombarded surface area. In addition to these ions, neutral atoms and molecular species during sputtering are emitted from the surface. In general, these neutral species represent the majority of the emitted secondary particle flux. As result of primary ion bombardment the sample surface is heavily modified not only by the loss of secondary particles, but also by a variety of further radiation effects such us amorphisation, primary ion implantation, fragmentation of surface molecules or molecular structures etc. Originally, SIMS was considered as a new technique for elemental analysis of solid materials, and sputtering as another efficient and universal means for ion formation from any solid sample. Because of their limited sensitivity at that time, SIMS instruments had to operate with high primary ion current densities corresponding to erosion rates typically equivalent to the removal of up to several hundred monolayers in one second. This "dynamic" mode of SIMS could be applied only for

bulk characterisation of solid. The uppermost monolayer disappeared completely within a fraction of a second and any kind of surface analysis is impossible in such short period. However, surface analysis should become feasible if the erosion process could be decelerated to such a degree that a complete analytically useful mass spectrum could be acquired without considerably sputtering or damaging this uppermost monolayer. In principle this should be possible by reducing the primary ion current density by several order of magnitude, provided a sufficient signal intensity remains in the spectrum. With pulsed primary ion beams and ToF analyser now it is possible, therefore, a "static" SIMS (SSIMS) can be performed to obtain chemical information about the surface of solids. A more extensive introduction to the phenomenology of sputtering and secondary ion emission can be found elsewhere.[115]

The distinction between dynamic and static SIMS can be understood by computing the lifetime, tm, of the topmost atomic layer as a function of the primary beam flux at the sample surface:

$$t_m = \frac{10^{15}}{I_p} \times \frac{A}{Y}$$

where A cm^2 of surface (surface layer atom density of 10^{15} atoms cm^{-2}) is bombarded by a primary beam of flux density I_p particles and the sputter yield is Y. Usually the primary beam flux is measured in Amps cm^{-2}. Using this equation, assuming a sputter yield of 1, if an analysis require say 20 minutes than static condition can only be safely attained for beam current of about 1nA cm^{-2} or less. An alternative approach take account of the fact that each impact physically influences an area of $10nm^2$ wich implies 10^{13} impacts cm^{-2} to influence all the atoms in the surface. This is generally accepted as the static primary particles dose limit. However, it is known that a static limit of this value is probably too high for most organic materials. Studies by a number of primary ion beam induced effects on polymers demonstrated that damaged can be detected even before 10^{12} impact cm^{-2}.[116]

SSIMS is concerned with the analysis of secondary ions. Ionisation occurs at, or close to, emission of particles from the surface with the consequence that the matrix participates in the electronic processes involved. This means that the yield of secondary ions is strongly influences by the electronic state of the material being analysed with

consequent complications for quantitative analysis. The basic SIMS equation is:

$$I_m = I_p Y_m \alpha^+ \theta_m \eta$$

where I_m is the secondary ion current of species m, I_p is the primary particles flux, Y_m is the sputter yield, α^+ is the ionisation propability to positive ions, θ_m is the fractional concentration of the chemistry m in the surface layer and η is the transmission of the analysis system.

4.1.2 Collision cascade and surface damaging

When an energetic ion impinges on a surface, it starts a collision cascade: the projectile dissipates its energy by collisions with the target atoms. If these are energetic enough, they collide with other atoms etc. Via these collisions, energy is transferred to the surrounding medium. A fraction of the primary ions energy may gradually be reflected towards the surface and causes sputtering.
The basic concept comes from the classic collision cascade theory that has been initially developed for elemental and inorganic solids.[117] In this thesis, the mainly part of ToF-SSIMS spectra were obtained on organic materials. Therefore, in this section will be show the fundamental aspects of damage and energy transfer in the surface region of organic materials.

4.1.3 Organic molecules overlayers

Organic overlayers on metal substrates were investigated by Benninghoven and co-workers in the seventies and eighties.[118] In their experiments with amino acid monolayers, they measured the rate of degradation of several parent-like ions as a fincion of the primary ion dose and introduced the definition of damage cross-section σ. For a secondary ion i, with intensity I_i, and a flux of primary ions φ, the damage cross-section σ_i, is expressed by

$$I_i(\phi) = I_{i0} \exp(-\sigma_i \phi)$$

Various meanings have been attributed to the damage cross-section σ, including the average surface area damaged by a single ion and the average ejection area of the sputtered species. A basic definition of σ would be: the average area per incident particle from where ejection of the corresponding fragment is excluded. The order of magnitude of damage cross-sections measured for small organic molecules under KeV ion bombardment indicates an upper dose limit for SSIMS measurements. Indeed, for a damaged cross-section equal to 10^{-14} cm^2, equation shows that the value of the intensity is reduced by 1-10% for a dose in the range of 10^{12}-10^{13} ions cm^{-2}. Therefore, this dose range certainly must not be exceeded in SSIMS experiments.

4.1.4 Emission process

SIMS is an extremely surface-sensible technique. The information depth is of the order of a monolayer. In the context of the SIMS interaction, two factors influence the information depth related to a secondary particle:

1. Penetration depth – it is the volume of collision cascade
2. Attenuation length – it is the attenuation of the flux of upward moving of secondary particles

In contrast to XPS, both factors have similar order of magnitude, therefore the penetration depth of the primary ion must be a relevant physical parameter in the explanation of the information depth. It has been claimed often in literature that the information depth of SIMS of the order of 10 Å. This value is somewhat arbitrary and must depend on the sample nature and properties.

Qualitative models have been developed to describe the sputtering process of molecular and organic solids. Michl assumes a two-step mechanism involving the prompt knocking out of small energetic fragments followed by the late and lower energy emission of larger pieces of material.[119] The co-existence of direct emission and recombination process has been proposed by Cooks and Rabalais et al. as the only way to explain the observed peaks in the mass spectra.[120] For

large molecules, the concept of violent ejection leading to fragmentation, as opposed to the emission of intact molecules by softer mechanisms, has been proposed by Benninghoven in the precursor model.[121]

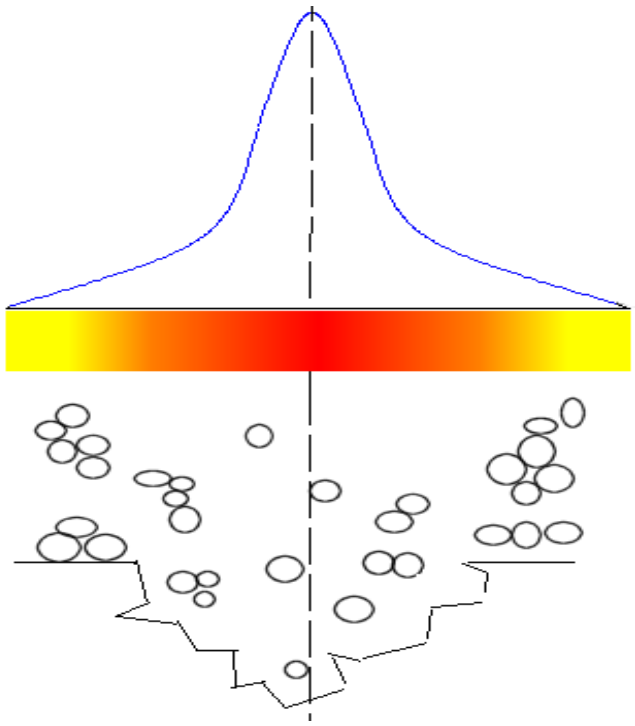

Figure 64. Schematic representation of intact molecules emission process.

These processes are correlated to the distribution of the primary particle energy at the surface. Molecules on the surface are fragmentized near the impact point, where the energy density is high, whereas intact molecular ejection should happen farther away, where the energy density is too low to break covalent bonds.
In a quantitative way, classic molecular dynamics has been successfully applied to describe the sputtering of various compounds.[122]

4.1.5 Instrumental parts

The most important parts of a ToF-SIMS instrument are the ToF analyzer and the primary ion beams. This section shows a brief introduction about these important instrumental parts.

- ToF analyzer

During the ToF-SIMS analysis, a very short-pulsed keV primary ion beam strikes the sample and cause the almost instantaneous emission of secondary ions. The pulsing of the primary ion beam provides the start signal for the time measurement. Secondary ions are then accelerated by a short electrostatic extraction section and they enter the section of length L_d.

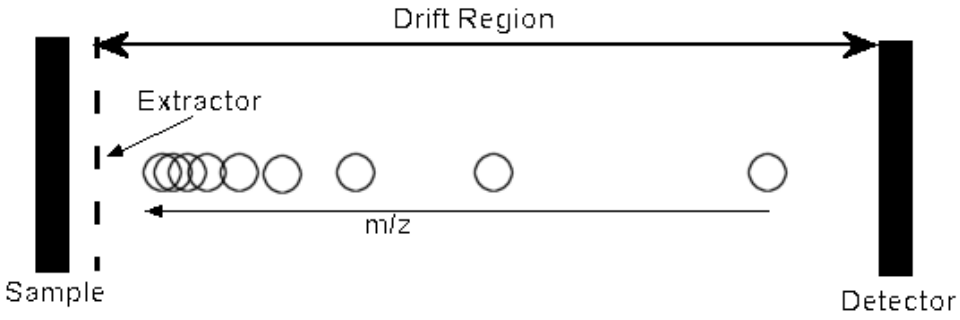

Figure 65. Schematic representation of linear ToF-SIMS.

An electrostatic extraction section of length *d* accelerates all ions of a given polarity to the same kinetic energy *eUa*.
Since,

$$E_{kin} = mv^2 / 2 = eUa$$

The flight time through the drift region to the detector is:

$$T = L_d (m / 2eUa)^{1/2}$$

The mass calibration reduces to the simple form:

$$T = A + B \cdot \sqrt{m}$$

Where A and B are extracted from a least square fit using known calibration peaks in the ToF spectrum. A takes into account the electronic delay during the time measurement.
One of the most important features of ToF analyzer is the parallel ion detection. By contrast to other mass spectrometers, it is possible to detect all ion masses of a given polarity which are emitted from the sample.
The most important factor determining the quality of a mass analyzer is the mass resolution $m/\Delta m$. Adjacent masses can only be separated in the mass spectrum if the time difference of the arrival at the detector is sufficient. The smaller possible time width of a mass signal is obviously set by length of the primary ion pulse. The most significant limitation to the mass resolution in a linear ToF analyser is the well-known fact that secondary ions are not all emitted with the same energy but with a more or less broad energy distribution. The initial energy spread is some eV for organic molecular and tens of eV for atomic secondary ions. To minimize the effect of energy spreading no linear ToF analyzer are used. A reflectron consist of a combination of drift region with an ion mirror. In the single-state reflectron, a combination of drift region with a single mirror provides energy focus.

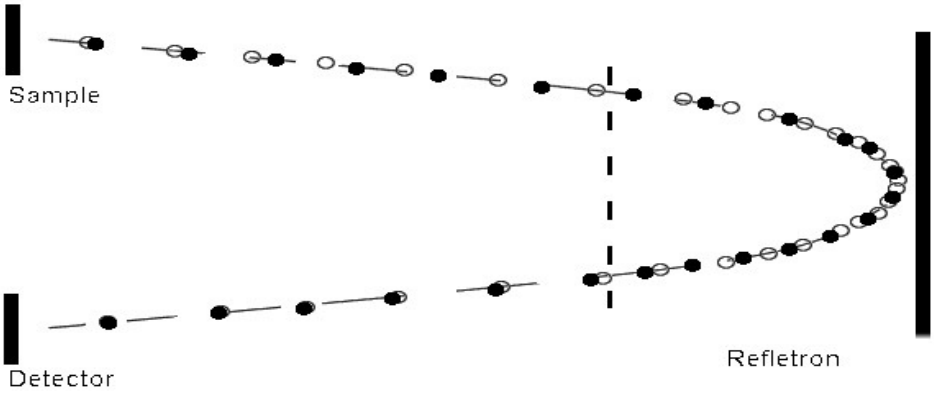

Figure 66. Schematic representation of energy compensation in ToF system with reflectron. Secondary ions with low energy are represented with opened symbols, high energy with closed one.

The flight path for ions having different initial kinetic energy through a single-stage ion mirror system is illustrated Figure 66. When starting from the sample, the higher energy ions will, at a given time, be further along the drift region than the lower energy ions. After entering the mirror field, the secondary ions are slowed down, come to a stop and turn around to exit the mirror. Up to the point inside the mirror where the ions reverse direction, low-energy ions are trailing behind the high-energy ions. Ions of higher kinetic energy will penetrate the mirror deeper than low-energy ions. At the point of reversing direction towards the detector, the high-energy ions are trailing behind the low-energy ions. The ions are then accelerated out of the ion mirror and they enter the drift region towards the detector. High-energy ions will then close on low-energy ions until they arrive at the detector simultaneously. With this geometry it is possible obtain mass resolution of the order of magnitude of 10.000.

- Primary ion beams

The most common used ion source in ToF system are the liquid metal ion source type. Gallium liquid metal ion is most frequently used, but in the last years new instruments uses indium, gold and bismuth too.

Typically, in a gallium source the reservoir and needle containing metal are welded to a filament that in turn is held on two support legs. These legs also serve as electrical contacts and they are set in an insulating disc. When an extractor plate has a potential typically in the range of -5 to -10kV relative to the source, an intense electric field is set up around the tip of the needle. Responding to the electrostatic force, Ga^+ ions near the tip move forward, while electrons travel back down the needle. This results in the liquid metal extending to form a cone and the emission can starts from the apex. Gallium liquid metal ion source offer good stability and consistency in operation. Other metals with higher mass or reactivity can offer better secondary ion yields. Liquid metal ion sources using indium, bismuth and gold are used to this end.
Some ToF-SIMS instruments are equipped with caesium guns because of the substantially enhanced yield of negative secondary ion under caesium bombardment. Beams of noble gas ions, oxygen ions or, recently, fullerene ions can be produced using a variety of electron bombardment source or plasma source.
In a ToF-SIMS system, the high-intensity of the beam reduces the static limit but it increases the secondary ion emission, the dimension of the spot of the beam affects the lateral resolution, the pulse durations influence the mass resolution. All of these parameters have to be optimized in order to obtain that the analysis requires.
The duty cycle is defined by the duration of the ion beam pulse, and the repetition rate of pulsing. For analysis area A cm^2, current of singly-carged ions I nA, pulse length t ns and repetition rate f Hz, the time, in seconds, to the static limit is given by:

$$T = \frac{A \times e \times 10^{30}}{I \times f \times t}$$

where e is the electron charge 1.602×10^{-19} C.
A 25 KeV ^{69}Ga pulse occupies 2.6mm of ion gun space per 10ns pulse duration. To obtain high-mass resolution without reducing the number of primary ions per second it is possible shorten the pulse in time by compressing it in space using two plates with concentric central aperture: bunched mode. Commercial ion beam bunchers typically compress a 20ns raw pulse in to less than 1ns at the sample.

In modern ToF instruments, spatial resolution of less than 0,1 μm is a routine expectation. To achieve this, ions can only be accepted from a limited area of the source and with limited angular acceptance. Therefore, a source of high brightness and low-energy spread is required. The main determinants of the spatial resolution in the ion-optical column are the lenses, the aperture, the pulsing unit and electrical supply to the column. The extractor potential produces a divergent beam. It is possible to focus a beam of ion extracted from a source using a single lens. However, the introduction of more lenses allows the production of a family of beams of different magnification. In a typical ion column, the ions from the source are accelerated and they enter into the first lens of optical column. This can produce an intermediate focus. The ions pass trough a second lens that focuses them onto the sample. Normally, the beam rastering occurs after the final lens. However, there are exceptions to this general layout.

4.1.6 Image analysis

The high transmission and parallel detection of ToF analyzer joined to the high focused of ion beams allows ToF-SIMS technique to made static imaging analysis of the surfaces. Commercially available ToF-SIMS instrumentation is capable of rapidly collecting and storing images which contain the full mass spectrum at every image pixel. Without initial hypothesis about the nature of the sample and the peaks of interest, it is possible made one mass resolved image for each peak in the spectrum: chemical maps. Otherwise can be reconstructs retrospective spectra from areas of interest.

4.2 X-ray Photoelectron Spectroscopy (XPS)

X-ray photoelectron spectroscopy is a surface sensitive analytical technique. The material under analysis is bombarded with soft X-ray capable of penetrating many micrometers into the bulk. X-ray adsorption by an atom in solid leads to ejection of an electron. A fraction of these electrons, generated close to the surface, escape out far from the material. The photoelectron emission is energy analysed.
For a conducting sample, the kinetic energy of the emitted electron E_k is given by:

$$E_k = hv - Eb - \phi$$

where *hv* is the energy of the exciting X-ray photon, *Eb* is the electron binding energy (BE) relative to the Fermi level of the sample and φ is the work function of the spectrometer.

4.2.1 XP signals

In a typical XP spectrum is present a primary structure due to the elastic photoemission of electron ejected from an atom in the solid and escaped from the surface.A scheme of the principal process of photoelectron emission is shown in figure. Moreover, in a XP spectrum is present a secondary structure related to other kind of physical processes. In the next sections will be shown the principal “kinds” of photoelectron.

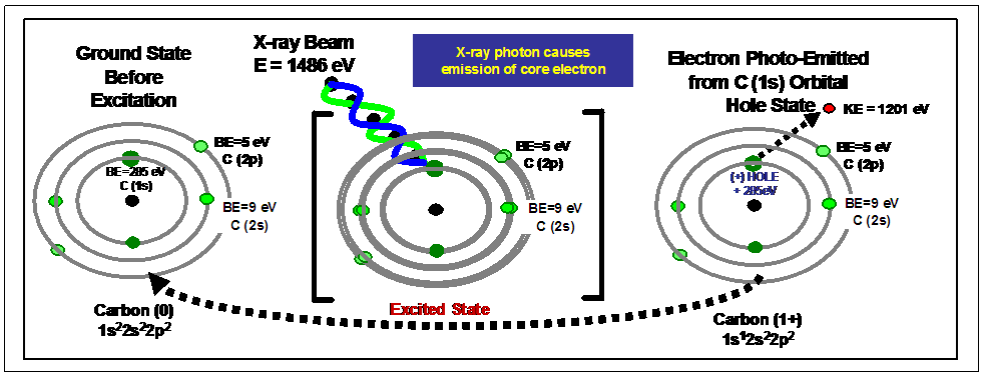

Figure 67. Schematic representation of photoemission process during XPS analysis.

- Core electrons

X-ray used in XPS analysis has enough energy to produce photoemission of electrons lying on the core energy levels of the atoms. The nomenclature for core levels is nlj where n is the principal quantum number, l is the orbital momentum quantum number and j is the total angular momentum quantum number, j=(l+s) where s is the spin angular momentum number (±1/2). The difference in energy between the doublet components is proportional to the spin-orbit coupling constant. The separation can be many electron volts. The relative intensities of the components are given by the ratio of their degenerancies (2j+1).
The relative intensity of a core-level peak is depending from the atomic photoemission cross-section, σ.[123] The intensities are also function of the spectrometer and mode operation which define the transmission function.[124] The peak width in XPS has several contributes: natural line width, width of the excitation source and analyzer resolution.

- Valence level

Valence level are those occupied by electrons with low BE which are involved in delocalised or bonding orbitals. The spectrum in this region consists of many closely-spaced energy levels, producing a band structure.

- Auger

Auger electrons arising from the de-excitation of core holes resulting from photoemission can lead to dominant peaks in the photoelectron spectrum. The energy of an Auger electron is given approximately by

$$E_{ABC} = E_A - E_B - E_C$$

where E_A is the BE of the photoionised level (A), E_B the BE of the level (B) from which an electron moves to fill the hole created and E_C the BE of the level (C) from which the Auger electron is emitted.

- Secondary structure

Several secondary structure peaks are present in a XP spectrum.
Multiplet splitting of core level peaks can occur when the system has unpaired electron in the valence levels.
Shake-up satellites, can be present when after the photoemission of a core electron there is a reorganisation of valence electrons because the photoemission is equivalent to an increasing in the nuclear charge. The energy required for this transistion is not available to the primary photoelectron and thus the two-electron process leads to discrete structure on the low KE side of the peak (shake-up satellites).
Vibrational fine structure is observed as form of asymmetry in the C1s XP peak of polymers that contain saturated hydrocarbon component.
Plasmon loss features ore of most importance for clea metal surface. Electrons passing trough a solid may excite modes of collective oscillation of the conduction electrons, and in so-doing suffer a characteristic energy loss (plasmon loss).

4.2.2 Elemental information

A single survey scan acquired under appropriate condition allows a complete elemental analysis because the peak position on BE scale in the XP spectrum are sufficiently for element identification. There are only a small number of overlaps such as C1s/Ru3d, O1s/Sb3d and Al2p/Cu3p.

The intensity of a peak is directly proportional to the density of the atom within the sampled volume. In sample case of a homogeneous solid, the relative atomic concentration of any chosen element (A) is given by:

$$C_A = \frac{\frac{I_A}{S_A}}{\sum_n \left(\frac{I_n}{S_n}\right)}$$

where C_A is usually expressed as atomic % of all elements determined, hydrogen excluded. The intensity (I) are divided for the relative sensitivity factors.

4.2.3 Chemical information

In the XP spectrum the same atom in different chemical environments can give rise to discrete core level components. The relative BE differences, called "chemical shifts", are correlated in a simple model by:

$$Ei = Ei^\circ + kq_i + e\sum_{i \neq j} \frac{q_i}{r_{ij}}$$

where Ej is the BE of particular core level on atom i, Ei° is a reference energy, k is a constant, qi is the charge on atom i and r id the average valence orbital radius.
The chemical shift range for any element is quite small, typically less than 10eV, and, since peak widths are of the order of 1 eV there are three consequences for data analysis. First, often occurs an overlapping of the component that requires curve fitting; second, the background subtraction can have significant effects on results and third, for insulating samples, the BE and chemical shift have to be established relative to a reference value.

4.2.4 Surface sensitivity and thickness

The surface sensitivity of XPS is due to the low probability that electrons are generated below the surface leave of the solid with their original energy and contribute to the XP peaks.
The quantification of overlayer thicknesses is commonly made by XPS. The intensities of a pure layer of A of thickness d on a substrate B are given by

$$I_A = I_A^{\infty}\left\{1 - e^{\frac{-d}{[L_A(E_A)\cos\theta]}}\right\} \quad \text{and} \quad I_B = I_B^{\infty} e^{\frac{-d}{[L_A(E_B)\cos\theta]}}$$

where θ is the angle of emission of the detected electrons from the surface normal, E is the kinetic energy of the emitted photoelectron. In the approximation of no elastic scattering, the L_A value would be the IMPFs. These equations are not easy to solve for d from values of intensities. For metals and their oxides as overlayers, equations can be used for the oxygen peak and the substrate in the metallic form. However, a better method is touse the substrate intensities in the oxide (o) and elemental (e) state using XPS. In these conditions E_A=E_B, thus:

$$d = L_o \cos\theta \ln(1 + R_{expt} / R_o)$$

where $R_{expt} = I_o / I_e$ and $R_o = I_o^{\infty} / I_e^{\infty}$. The value of Ro for common materials (such us silicon/silicon oxide) is calculated,[125] but anyway can be measured experimentally.
In the specific case of Self-Assembled Monolayer on gold is possible measure the thickness of the organic monolayer on metal substrate using the method proposed by Dannenberger et al.[126] The proposed method uses a comparison approach with similar sample with known thickness. The thickness of the organic overlayer was computed from the Cls to and Au4f intensity.

$$\frac{I_{C1s}}{I_{Au4f}} = K\frac{1-\exp(-d_c/\lambda_c)}{\exp(-d_{cs}/\lambda_{Au})}$$

where d_{cs} is the thickness of the thiol layers, dc is the thickness of the carbon layer only, λ_c is the length of the mean free path (MFP) of the Cls photoelectrons through the carbon layer and λ_{Au} is the MFP of the Au photoelectrons through the thiol layer. K is a system and apparatus specific constant which was obtained from measurements for long-chain thiols having known thickness obtained from independent measurements. The case of two elements having photoelectrons of very different kinetic energy is a little more complex. A computer spreadsheet is easily capable of finding the solution to transcendent equations.

4.2.5 Instrumental parts

The most important parts of a XPS "laboratory instrument" are the X-ray source and the energy analysers. This section shows a brief introduction about these important instrumental parts.

- X-ray source

X-ray source used in the common XPS instruments, uses the bombardment of metallic target with high-energy electrons to produce X-ray. A small portion of the bombarding electrons cause vacancies in inner electron shells of the target atoms and electrons from higher level fall to fill the vacancies with the simultaneous emission of X-ray photons. If the electron falls the L shell to the K shell, then the X-ray is designated a Kα X-ray.
In a typical dual anode source, the anode is fabricated from cooper and the faces of the tube are coated with materials from which it is desired to excite X-rays. The aluminium/magnesium combination is a popular one because both lines give relatively intense photoelectron spectra and both have relatively narrow Kα lines. Al Kα = 1486.6 eV with FWHM ~ 0.85 eV, Mg Kα = 1253.6 eV, FWHM ~ 0.70 eV. The dual anode source is pseudo monochromatic because produces a strong Kα line on a continuous background, the Bremsstrahlung. Often, high-energy

resolution instruments are fitted with monochromatic X-ray source. A single anode source with aluminium target is combined with a focusing monochromator using a crystal. The monochromator scheme is based upon Bragg diffraction. The monochromator action produce a focused spot (< 10 μm) of radiation of ~0.26 eV and eliminates the Bremsstrahlung as well other unwanted lines.

- Energy analysers

All commercial XPS instruments use electrostatic analysers.
Using the electrostatic hemispherical analyser (HAS) the electrons entering in the hemispherical are repelled by a negative potential V2 applied by an hemispherical plate having radius r_2 and attracted by positive one V1 (radius r_1) and travel along, or near to, the mean radius ro to refocus at the exit slit.
The voltage between the plates is:

$$V2 - V1 = Vo\left(\frac{r_2}{r_1} - \frac{r_1}{r_2}\right)$$

If the central radius ro is 127.0 mm, the outer 152.4 mm and the inner 101.6 mm and the energy is 10eV (E_o), the voltage on outer hemisphere is -13.33 V and that on the inner hemisphere -5.00V. The central energy (10eV in this case) is known as pass-energy.

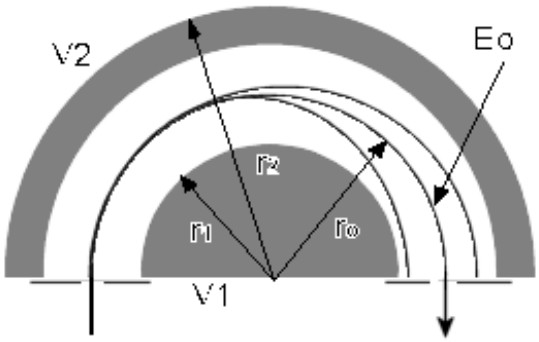

Figure 68. Scheme of electrostatic hemispheric analyzer.

The spherical mirror analyser (SMA) consists of an inner mesh hemispherical electrode and an outer hemisphere. The energy scan is similar to the HAS but with this geometry it is possible obtain imaging information.

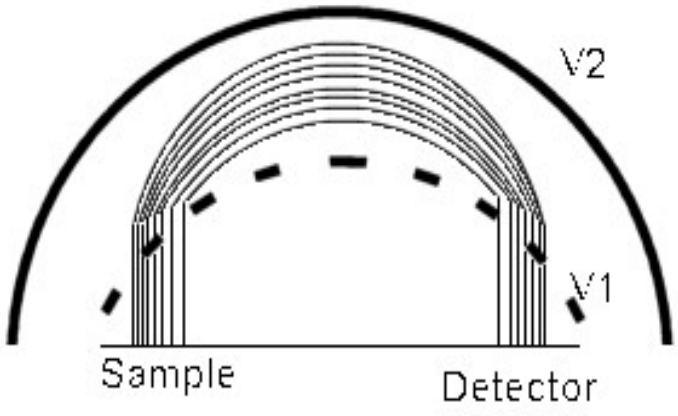

Figure 69. Scheme of electrostatic spherical mirror analyzer.

4.3 Atomic Force Microscopy (AFM)

Atomic force microscopy (AFM) is one of several types of scanned-proximity probe microscopes. All of these microscopes work by measuring a local property with a probe or "tip" placed very close to the sample.

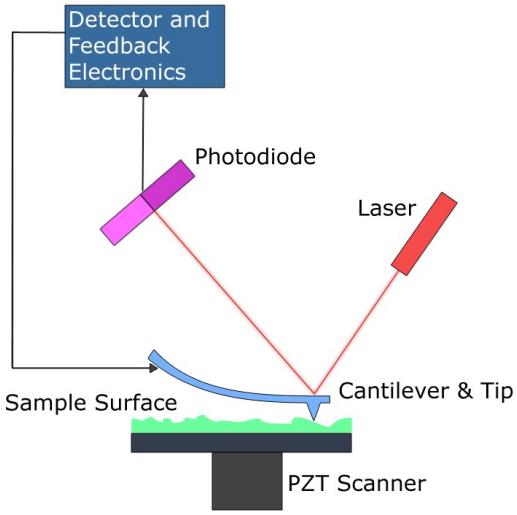

Figure 70. Scheme of AFM instrument.

AFM consists of a microscale cantilever with a sharp tip (probe) at its end that is used to scan the specimen surface. The cantilever is typically silicon or silicon nitride with a tip radius of curvature on the order of nanometres. When the tip is brought into proximity of a sample surface, forces between the tip and the sample lead to a deflection of the cantilever according to Hooke's law. Depending on the situation, forces that are measured in AFM include mechanical contact force, Van der Waals forces, capillary forces, chemical bonding, electrostatic forces, magnetic forces, solvation forces etc. Typically, the deflection is measured using a laser spot reflected from the top of the cantilever into an array of photodiodes.

If the tip was scanned at a constant height, there would be a risk that the tip would collide with the surface, causing damage. Hence, in most cases a feedback mechanism is employed to adjust the tip-to-sample distance to maintain a constant force between the tip and the sample. Traditionally, the sample is mounted on a piezoelectric scanner, that can move the sample in the z direction for maintaining a constant force, and the x and y directions for scanning the sample. The resulting map of s(x,y) represents the topography of the sample.
The AFM can be operated in a number of modes, depending on the application. In general, possible imaging modes are divided into contact modes and a variety of different modes depending of kind of tips are used.

4.3.1 Imaging modes

In the contact mode operation, the static tip deflection is used as a feedback signal. The force between the tip and the surface is kept constant during scanning by maintaining a constant deflection. In this mode it is possible obtain other information from the lateral deflection of the tip during the scan. In particular, form friction images it is possible discriminate different “chemical” features of the surface.
In the tapping mode, the cantilever is externally oscillated at or close to its resonance frequency. The oscillation amplitude, phase and the resonance frequency are modified by the tip-sample interaction forces. These changes in oscillation with respect to the external reference oscillation provide information about the sample's characteristics. Changes in the oscillation amplitude or phase provide the feedback signal for imaging. Changes in the phase of oscillation can be used to discriminate between different types of materials on the surface.
Using tip made by different materials it is possible obtain other physical-chemical information. By using magnetic or conductive tip, it is possible to study magnetic domains eventually presents on the surface or to measure the electric properties of the sample. By functionalizing the tip with suitable chemical moiety, it is possible to study specific interaction between the functional groups present on the tip and the surface.

4.4 Quartz Crystal Microbilance with Dissipation Monitoring (QCM-D)

The QCM-D technique allows the simultaneous measurement of resonance frequency (Δf) and energy dissipation (ΔD) changes.

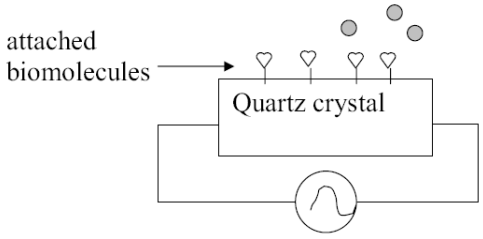

When an alternating electric field is applied across the quartz crystal through upper and lower metal electrodes covering the quartz surface, a mechanical oscillation of characteristic frequency is produced in the crystal. When same substance attaches to the surface sensor, the oscillation frequency decreases due to mass increase. When a thin film is attached to the sensor crystal the frequency shift is proportional to the adsorbed or desorbed mass, and in such case the mass can be calculated by using the Sauerbrey relation:[127]

$$\Delta m = -\frac{C \cdot \Delta f}{n}$$

where C is a constant, which value is 17.7 ng Hz-1 cm-2 for a 5 MHz quartz crystal, and n (1,3,5,7) is the overtone number. It is also possible to get an estimation of the thickness (df) of the adhering layer:

$$d_f = \frac{\Delta m}{\rho_f}$$

where ρf is the effective density of the adsorbed film. The other parameter is the dissipation factor (D), it is the reciprocal of the Q factor:[128]

$$D = \frac{1}{Q} = \frac{E_{dissipated}}{2\pi E_{stored}}$$

where $E_{dissipated}$ is the energy dissipated during one period of oscillation, and E_{stored} is the energy stored in the oscillation system. The method used by Spencer and Smith in 1966 to measure the dissipation factor was based on monitoring the amplitude of oscillation, A, as a function of time when the driving power to a simple oscillator is switched off at t=0 and fitting the recordered curve described by equation of exponential damped sinusoid:

$$A(t) = A_0 e^{-t/\tau} \sin(\omega t + \varphi) + const \tan t$$

$t \geq 0$

where ι is the decay time constant, φ is the phase and the constant is the dc offset. The dissipation of the crystal's oscillation is a measure of the dissipative behaviour of the adsorbed film, in fact the dissipation shift is not noticeable (D~0x10-6) for rigid film. Otherwise, for non rigid layer the QCM-D response varies for the different overtones due to the viscoelastic properties of the film.[129] In other words, the effectively coupled mass depends on the nature of the oscillatory motion of the crystal through a viscoelastic film. One additional important factor in this context is that water (including solvent molecules) may couple as an additional mass via direct hydration, viscous drag and/or entrapment in cavities in the adlayer or as hydrodinamically layer coupled to sensor surface and contributes to damp the crystal's oscillation. So changes in the dissipation factor are related to the shear viscous losses induced by the adsorbed layers, and thus provide information that has the potential to identify structural differences between different adsorbed systems, or structural changes in the same type of molecule during the adsorption process.

5 References

5.1 References

[1] D. W. Schubert, Polym. Bull., 1997, 38, 177.

[2] G. L. Gaines Jr., Insoluble Monolayers at Liquid-Gas Interfaces, Interscience, New York, 1966.

[3] a) Ulman, A. Chem. Rev. 1996, 96, 1533. b) Bishop, A.R.; Nuzzo, R.G. Current Opinion in Colloid and Interface Science 1996, 1, 127. c) Dubois, L.H.; Nuzzo, R.G. Annu. Rev. Phys. Chem. 1992, 43, 437.

[4] a) Poirier, G. E.; Pylant, E. D. Science (Washington, D.C.) 1996, 272, 1145. b) Nuzzo, R. G.; Allara, D. L. J. Am. Chem. Soc. 1983, 105, 4481. c) Porter, M. D.; Bright, T. B.; Allara, D. L.; Chidsey, C. E. D. J. Am. Chem. Soc. 1987, 109, 3559. d) Dubois, L. H.; Nuzzo, R. G. Annu. Rev. Phys. Chem. 1992, 43, 437. e) Bain, C. D.; Evall, J.; Whitesides, G. M. J. Am. Chem. Soc. 1989, 111, 7155. f) Bain, C. D.; Whitesides, G. M. Science (Washington, D.C.) 1988, 240, 62. g) Biebuyck, H. A.; Bain, C. D.; Whitesides, G. M. Langmuir 1994, 10, 1825. h) Laibinis, P. E.; Whitesides, G. M.; Allara, D. L.; Tao, Y. T.; Parikh, A. N.; Nuzzo, R. G. J. Am. Chem. Soc. 1991, 113, 7152. i) Dubois, L. H.; Zegarski, B. R.; Nuzzo, R. G. J. Chem. Phys. 1993, 98, 678.

[5] Laibinis, P. E.; Whitesides, G. M. J. Am. Chem. Soc. 1992, 114, 1990.

[6] Bain, C. D.; Biebuyck, H. A.; Whitesides, G. M. Langmuir 1989, 5, 723. Stranick, S. J.; Weiss, P. S.; Parikh, A. N.; Allara, D. L. J. Vac. Sci. Technol., A 1993, 11, 739.

[7] Nuzzo, R. G.; Allara, D. L. J. Am. Chem. Soc. 1983, 105, 4481.

[8] Bain, C. D.; Troughton, E. B.; Tao, Y. T.; Evall, J.; Whitesides, G. M.; Nuzzo, R. G. J. Am. Chem. Soc. 1989, 111, 321.

[9] Self-Assembled Monolayers of Thiolates Chemical Reviews, 2005, Vol. 105, No. 4 1111

[10] Nuzzo, R.G.; Allara, D.L. J. Am. Chem. Soc. 1983, 105, 4481.

[11] Bareman, J. P.; Klein, M. L. J. Phys. Chem. 1990, 94, 5202.

[12] Valiokas, R.; Oestblom, M.; Svedhem, S.; Svensson, S. C. T.; Liedberg, B. J. Phys. Chem. B 2002, 106, 10401.

[13] a) Camillone, N., III; Chidsey, C. E. D.; Eisenberger, P.; Fenter, P.; Li, J.; Liang, K. S.; Liu, G. Y.; Scoles, G. J. Chem. Phys. 1993, 99, 744. b) Fenter, P.; Eisenberger, P.; Liang, K. S. Phys. Rev. Lett. 1993, 70, 2447.

[14] Xia, Y.; Whitesides, G. M. Angew. Chem., Int. Ed. Engl. 1998, 37, 550.

[15] Liu, G.-Y.; Xu, S.; Qian, Y. Acc. Chem. Res. 2000, 33, 457.

[16] Sun, S.; Chong, K. S. L.; Leggett, G. J. J. Am. Chem. Soc. 2002, 124, 2414.

[17] a) Geyer, W.; Stadler, V.; Eck, W.; Golzhauser, A.; Grunze, M.; Sauer, M.; Weimann, T.; Hinze, P. J. Vac. Sci. Technol., B 2001, 19, 2732. b) Weimann, T.; Geyer, W.; Hinze, P.; Stadler, V.; Eck, W.; Golzhauser, A. Microelectron. Eng. 2001, 57-58, 903. c) Golzhauser, A.; Eck, W.; Geyer, W.; Stadler, V.; Weimann, T.; Hinze, P.; Grunze, M. Adv. Mater. 2001, 13, 806.

[18]

Chabinyc, M. L.; Love, J. C.; Thywissen, J. H.; Cervelli, F.; Prentiss, M. G.; Whitesides, G. M. Langmuir 2003, 19, 2201.
[19]
Xia, Y.; Whitesides, G. M. Angew. Chem., Int. Ed. Engl. 1998, 37, 550.

[20] a) K. B. Blodgett, J. Am. Chem. Soc., 1934, 55, 495. b) K. B. Blodgett, J. Am. Chem. Soc., 1935, 57, 1007. c) I. Langmuir, J. Franklin Inst., 1934, 218, 153.

[21] A.Ulman, An Introduction to Ultrathin Films: From Langmuir-Blodgett to Self Assembly, Academic Press, New York, 1991.

[22] Maskus, M.; Abruna, H., Langmuir 1996, 12, 4455.

[23] Lehn J-M (1978) Cryptates: inclusion complexes of macropolycyclic receptor molecules. Pure Appl Chem 50:871–892.

[24] Mitchell P (1961) Coupling of phosphorylation to electron and hydrogen transfer by a chemiosmotic type of mechanism. Nature 191:144–148.

[25] Fischer E (1894) Einfluss der configuration auf die wirkung der enzyme Ber Dtsch. Chem Ges 27:2985–2993.

[26] Leininger, S., Olenyuk, B. & Stang, P. J. (2000) Chem. Rev. 100, 853–907.

[27] a) Maskus, M.; Abruna, H. D. Langmuir 1996, 12, 4455–4462; b) Figgemeier, E.; Merz, L.; Hermann, B. A.; Zimmermann, Y. C.; Housecroft, C. E.; Gu1ntherodt, H.-J.; Constable, E. C. J. Phys. Chem. B 2003, 107, 1157–1162; c) Miyachi, M.; Yamanoi, Y.; Yonezawa, T.; Nishihara, H.; Iwai, M.; Konno, M.; Inoue, Y. J. Nanosci. Nanotechnol. 2009, 9, 1722–1726.

[28] a) O'Regan, B.; Gr€atzel, M. Nature 1991, 335, 737–740 ; b) Grätzel, M. Nature 2001, 414, 338–344. c) Grätzel, M. J. Photochem. Photobiol. C: Photochem. Rev. 2003, 4, 145–153.

[29] a) Li, Chao; Lei, Bo; Fan, Wendy; Zhang, Daihua; Meyyappan, M.; Zhou, Chongwu J. Nanosci. Nanotechnol. 2007, 7, 138–150. b) Ju, S.; Lee, K.; Janes, D. B.; Yoon, M.-H.; Facchetti, A.; Mark, Tobin J. Nano Lett. 2005, 5, 2281–2286. c) Holman, M. W.; Liu, R.; Adam, D. M. J. Am. Chem. Soc. 2003, 125, 12649–12654.

[30] a) Rotzinger, F. P.; Kesselman-Truttmann, J. M.; Hug, S. J.; Shklover, V.; Grätzel, M. J. Phys. Chem. B 2004, 108, 5004–5017. b) Vittadini, A.; Selloni, A.; Rotzinger, F. P.; Grätzel, M. J. Phys. Chem. B 2000, 104, 1300–1306. c) Huga, S. J.; Bahnemann, D. J. Electron Spectrosc. Relat. Phenom. 2006, 150 (2-3), 208–219.

[31] a) Terada, K.; Kobayashi, K.; Haga, M. Dalton Trans. 2008, 36, 4846–4854. b) Bae, E.; Choi, W. J. Phys. Chem. B 2006, 110, 14792–14799. c) Morisue, M.; Kalita, D.; Haruta, N.; Kobuke, Y. Chem. Commun. 2007, 2348–2350. d) Trammell, S. A.; Moss, J. A.; Yang, J C.; Nakhle, B. M.; Slate, C.l A.; Odobel, F.; Sykora, M.; Erickson, B. W.; Meyer, T. J. Inorg. Chem. 1999, 38, 3665–3669.

[32] Taylor, C. E.; Schwartz, D. K., Octadecanoic acid self-assembled monolayer growth at sapphire surfaces. Langmuir 2003, 19, (7), 2665-2672.

[33] Pawsey, S.; Yach, K.; Halla, J.; Reven, L., Self-assembled monolayers of alkanoic acids: A solid-state NMR study. Langmuir 2000, 16, (7), 3294-3303.

[34] Aswal, D. K.; Lenfant, S.; Guerin, D.; Yakhmi, J. V.; Vuillaume, D., Self-assembled monolayers on silicon for molecular electronics. Analytica Chimica Acta 2006, 568, (1-2), 84-108.

[35] Abraham Ulman, Chem. Rev., 1996, 96 (4), 1533-1554.

[36] Stephen R. Wasserman, Yu Tai Tao, and George M. Whitesides, Langmuir, 1989, 5 (4), 1074-1087.

[37] Janos H. Fendler; Chem. Mater. 2001, 13, 3196-3210.

[38] a) Brzoska, J. B.; Ben Azouz, I.; Rondelez, F. Langmuir 1994, 10, 4367–4373. b) Silberzan, P.; Leger, L.; Ausserre, D.; Benattar, J. J. Langmuir 1991, 7, 1647–1651.

[39] a) Le Grange, J. D.; Markham, J. L.; Kurkjian, C. R. Langmuir 1993, 9, 1749–1753. b) Brzoska, J. B.; Shahidzadeh, N.; Rondelez, F. Nature 1992, 360, 719-721.

[40] Ashkenasy, G.; Cahen, D.; Cohen, R.; Shanzer, A.; Vilan, A., Molecular engineering of semiconductor surfaces and devices. Accounts of Chemical Research 2002, 35, (2), 121-128.

[41] Mutin, P. H.; Guerrero, G.; Vioux, A., Hybrid materials from organophosphorus coupling molecules. Journal of Materials Chemistry 2005, 15, (35-36), 3761-3768.

[42] a) Kohli, P.; Blanchard, G. J. Langmuir 2000, 16, 695–701. b) Kohli, P.; Blanchard, G. J. Langmuir 1999, 15, 1418–1422. c) Bakiamoh, S. B.; Blanchard, G. J. Langmuir 1999, 15, 6379–6385.

[43] a) Morotti, T.; Calabrese, V.; Cavazzini, M.; Pedron, D.; Cozzuol, M.; Licciardello, A.; Tuccitto, N.; Quici, S. Dalton Trans. 2008, 2974–2982.

[44] a) Ulman, A. Chem. ReV. 1996, 96, 1533. b) Dubois, L. H.; Nuzzo, R. G. Annu. ReV. Phys. Chem. 1992, 43, 437. c) Xia, Y.; Whitesides, G. M. Angew. Chem., Int. Ed. 1998, 37, 551.

[45] a) Karpovich, D. S.; Blanchard, G. J. Langmuir 1994, 10, 3315. b) Schessler, H. M.; Karpovich, D. S.; Blanchard, G. J. J. Am. Chem. Soc. 1996, 118, 9645.

[46] Hong, H.-G.; Sackett, D. D.; Mallouk, T. E. Chem. Mater. 1991, 3, 521.

[47] a) Katz, H. E.; Wilson, W. L.; Scheller, G. J. Am. Chem. Soc. 1994, 116, 6636. b) Yonemoto, E. H.; Saupe, G. B.; Schmehl, R. H.; Hubig, S. M.; Riley, R. L.; Iverson, B. L.; Mallouk, T. E. J. Am. Chem. Soc. 1994, 116, 4786. c) Katz, H. E.; Bent, S. F.; Wilson, W. L.; Schilling, M. L.; Ungashe,

S. B. J. Am. Chem. Soc. 1994, 116, 6631. d) Frey, B. L.; Hanken, D. G.; Corn, R. M. Langmuir 1993, 9, 1815. e) Yang, H. C.; Aoki, K.; Hong, H.-G.; Sackett, D. D.; Arendt, M. F.; Yau, S.-L.; Bell, C. M.; Mallouk, T. E. J. Am. Chem. Soc. 1993, 115, 11855. f) Vermeulen, L.; Thompson, M. E. Nature 1992, 358, 656. g) Ungashe, S. B.; Wilson, W. L.; Katz, H. E.; Scheller, G. R.; Putvinski, T. M. J. Am. Chem. Soc. 1992, 114, 8717. h) Cao, G.; Rabenberg, L. K.; Nunn, C. M.; Mallouk, T. M. Chem. Mater. 1991, 3, 149. i) Katz, H. E.; Schilling, M. L.; Chidsey, C. E. D.; Putvinski, T. M.; Hutton, R. S. Chem. Mater. 1991, 3, 699.

[48] a) Lee, H.; Kepley, L. J.; Hong, H.; Mallouk, T. E. J. Am. Chem. Soc. 1988, 110, 618–620. b) Cao, G.; Hong, H. G.; Mallouk, T. E. Acc. Chem. Res. 1992, 25, 420–427.

[49] Katz, H. E.; Wilson, W. L.; Scheller, G. J. Am. Chem. Soc. 1994, 116, 6636–6640.

[50] Putvinski, T. M.; Schilling, M. L.; Katz, H. E.; Chidsey, C. E. D.; Mujsce, A. M.; Emerson, A. B. Langmuir 1990, 6, 1567–1571.

[51] T. M. Putvinski, Marcia L. Schilling, Howard E. Katz, Christopher E. D. Chidsey, A. M. Mujsce, and A. B. Emerson,Langmuir, 1990, 6,1567-1571.

[52] a) P. Kohli and G. J. Blanchard, Probing Interfaces and Surface Reactions of Zirconium Phosphate/Phosphonate Multilayers Using 31P NMR Spectrometry, Langmuir 2000, 16, 695-701. b) P. Kohli and G. J. Blanchard, ; Design and Growth of Robust Layered Polymer Assemblies with Molecular Thickness Control; Langmuir 1999, 15, 1418-1422. c) S.B. Bakiamoh and G.J.Blanchard, Demonstration of oriented multilayers through asymmetric metal coordination chemistry; Langmuir 1999, 15, 6379-6385.

[53] a) Cao, G.; Hong, H. G.; Mallouk, T. E. Acc. Chem. Res. 1992, 25, 420–427. b) Katz, H. E.; Wilson, W. L.; Scheller, G. J. Am. Chem. Soc. 1994, 116, 6636–6640.

[54] Benninghoven, A. Angew. Chem. Int. Engl. Ed. 1994, 33, 1023–1043.

[55] Leggett, G.J. In ToF-SIMS:Surface Analisys by Mass Spectrometry; Vickerman, J. C., Briggs, D., Eds.; SurfaceSpectra Ltd., Manchester & IMPublications: Chichester, U.K., 2001.

[56] Tuccitto, N.; Torrisi, V.; Cavazzini, M.; Morotti, T.; Puntoriero, F.; Quici, S.; Campagna, S.; Licciardello, A. ChemPhysChem 2007, 8, 227–230.

[57] Torrisi, A. Appl. Surf. Sci. 2008, 254, 2650–2658.

[58] Scofield, J. H. J. Electron Spectrosc. Relat. Phenom. 1976, 8, 129–137.

[59] Seah, M. P.; Dench, W. A. Surf. Interface Anal. 1979, 1, 2–11.

[60] Moulder, J. F., Stickle, W. F., Sobol, P. E., Bomben, K. D. Eds. Handbook of X-ray Photoelectron Spectroscopy; Perkin Elmer Corp.: Eden Prairie, MN, 1992, and references therein.

[61] Keane, M. P.; Naves de Brito, A.; Correja, N.; Svensson, S. Chem. Phys. 1991, 155, 379–387.

[62] J. L. Wilbur, A. Kumar, H. A. Biebuyck, E. Kim and G. M. Whitesides, Nanotechnology, 1996, 7, 452.

[63] G. N. Fontes, A. Malachias, R. Magalhães-Paniago, and B. R. A. Neves, Langmuir 2003, 19, 3345-3349.

[64] a) J.-M. Lehn, in Supramolecular Chemistry: Concept and Perspectives, VCH,Weinheim, 1995; b) J. V. Barth, J.Weckesser, C. Cai, P. Günter, L. Bürgi, O. Jeandupeux and K. Kern, Angew. Chem., Int. Ed., 2000, 7, 1230; c) N. Lin, S. Stepanow, F. Vidal, K. Kern, M. S. Alam, S. Stromsdorfer, V. Dremov, P. Muller, A. Landa and M. Ruben, Dalton Trans., 2006, 2794; d) M. Haga, K. Kobayashi and K. Terada, Coord. Chem. Rev., 2007, 251, 2688.

[65] H. Langhals, Heterocycles, 1995, 40, 477; A. Facchetti, Mater. Today, 2007, 10, 28.

[66] F. Würthner, Chem. Commun., 2004, 1564; F. Wu¨ rthner, Pure Appl. Chem., 2006, 78, 2341.

[67] a) R. Dobrawa, D. G. Kurth and F. Wu¨ rthner, Polym. Prepr. (Am. Chem. Soc., Div. Polym. Chem.), 2004, 45, 378; b) T. J. Tang, A. Herrmann, K. Peneva, K. Müllen and S. E. Webber, Langmuir, 2007, 23, 4623.

[68] H. Zollinger, Color Chemistry, 3rd edn., VCH, Weinheim, 2003.

[69] W. Herbst, K. Hunger, Industrial Organic Pigments: Production, Properties, Applications, 2nd edn., WILEY-VCH, Weinheim, 1997.

[70] C. W. Struijk, A. B. Sieval, J. E. J. Dakhorst, M. Van Dijk, P. Kimkes, R. B. M. Koehorst, H. Donker, T. J. Schaafsma, S. J. Picken, A. M. van de Craats, J. M. Warman, H. Zuilhof, E. J. R. Sudhölter, J. Am. Chem. Soc., 2000, 122, 11 057.

[71] S. K. Lee, Y. Zu, A. Herrmann, Y. Geerts, K. Müllen, A. J. Bard, J. Am. Chem. Soc., 1999, 121, 3513.

[72] F. Würthner, Angew. Chem., Int. Ed, 2001, 40, 1037.

[73] L. Schmidt-Mende, A. Fechtenkötter, K. Müllen, E. Moons, R. H. Friend, J. D. MacKenzie, Science, 2001, 293, 1119.

[74] H. Langhals, Heterocycles, 1995, 40, 477.

[75] H. Langhals, S. Demmig, H. Huber, Spectrochim. Acta, 1988, 44A,1189.

[76] E. Hädicke, F. Graser, Acta Crystallogr., Sect. C, 1986, 42, 189.

[77] R. H. Friend, R. W. Gymer, A. B. Holmes, J. H. Burroughes, R. N. Marks, C. Taliani, D. D. C. Bradley, D. A. Dos Santos, J. L. Brédas, M. Lögdlund and W. R. Salaneck, Nature, 1999, 397, 121.

[78] C. J. Brabec, N. S. Sariciftci and J. C. Hummelen, Adv. Funct. Mater., 2001, 11, 15.

[79] J. S. Wilson, A. S. Dhoot, A. J. A. B. Seeley, M. S. Khan, A. Köhler and R. H. Friend, Nature, 2001, 413, 828.

[80] L. Brunsveld, B. J. B. Folmer, E. W. Meijer, R. P. Sijbesma, Chem. Rev., 2001, 101, 4071; M. Rehahn, Acta Polym., 1998, 49, 201.

[81] N. Tuccitto, I. Delfanti, V. Torrisi, F. Scandola, C. Chiorboli, V. Stepanenko, F. Würthner, A. Licciardello, "Supramolecular self-assembled multilayers of terpyridine-functionalized perylene bisimide metal complexes", Phys. Chem. Chem. Phys., 2009, 11, 4033–4038.

[82] Tuccitto, N.; Ferri, V.; Cavazzini, M.; Quici, S.; Zhavnerko, G.; Licciardello, A.; Rampi, M.A., Nat. Mater. 2009, 8, 41..

[83] (a) Balzani, V.; Scandola, F. Supramolecular Chemistry; Harwood: Chichester, U.K., 1991. (b) Balzani, V.; Juris, A.; Venturi, M.; Campagna, S.; Serroni, S. Chem. ReV. 1996, 96, 759. (c) Bignozzi, C. A.; Schoonover, J. R.; Scandola, F. Prog. Inorg. Chem. 1997, 44, 1. (d) De Cola, L.; Belser, P. Coord. Chem. ReV. 1998, 177, 301. (e) Barigelletti, F.; Flamigni, L. Chem. Soc. ReV. 2000, 29, 1. f) Harriman, A.; Ziessel, R. Chem. Commun. 1996, 925. g) Barigelletti, F.; Flamigni, L.; Collin, J.-P.; Sauvage, J.-P. Chem. Commun. 1997, 333.

[84] Calvert, I. M.; Meyer, T. J. Inorg. Chem. 1980, 19, 1404.

[85] (a) Young, R. C.; Nagle, J. K.; Meyer, T. J.; Whitten, G. G. J. Am. Chem. Soc. 1978, 100, 4773. (b) Segers, D.; DeArmond, M. J. Phys. Chem. 1982, 86, 3768. (c) Takeuchi, K. J.; Thompson, M. S.; Pipes, D. W.; Meyer, T. J. Inorg. Chem. 1984, 23, 1845.

[86] Tuccitto, N.; Torrisi, V.; Cavazzini, M.; Morotti, T.; Puntoriero, F.; Quici, S.; Campagna, S.; Licciardello, A. ChemPhysChem 2007, 8, 227–230.

[87] Norrby, T.; Börje, A.; A¡ kermark, B.; Hammarström, L.; Alsins, J.; Lashgari, K.; Norrestam, R.; Martenson, J.; Stenhagen, G. Inorg. Chem. 1997, 36, 5850.

[88] A. Benninghoven, Angew. Chem., Int. Ed. Engl., 1994, 33, 1023.

[89] Rainer Dobrawa, Marina Lysetska, Pablo Ballester, Matthias Grüne, Frank Würthner, Macromolecules 2005, 38, 1315-1325.

[90] a)R. Dobrawa, M. Lysetska, P. Ballester, M. Grüne and F. Würthner, Macromolecules, 2005, 38, 1315; b) R. Dobrawa and F. Würthner, Chem. Commun., 2002, 1878.

[91] Egholm, M., Buchardt, O., Christensen, L., Behrens, C., Frier, S. M., Driver, D. A., Berg, R. H., Kim, S. K, Norde´n, B., and Nielsen, P. E. (1993) Nature (London) 365, 566–568.

[92] Schena, M.; Shalon, D.; Davis, R. W.; Brown, P. O. Science 1995, 270, 467.

[93] Barbulovic-Nad, I.; Lucente, M.; Sun, Y.; Zhang, M. J.; Wheeler, A. R.; Bussmann, M. Crit. Rev. Biotechnol. 2006, 26, 237.

[94] Lee, C.; Harbers, G. M.; Grainger, D. W.; Gamble, L. J.; Castner, D. G. J. Am. Chem. Soc. 2007, 129, 9429.

[95] Tonya M. Herne and Michael J. Tarlov J. Am. Chem. Soc. 1997, 119, 8916-8920.

[96] Tonya M. Herne and Michael J. Tarlov, Kevin A. Peterlinz and Rosina M. Georgiadis, J. Am. Chem. Soc. 1997, 119, 3401-3402.

[97] H.F. Arlinghausa, M. Schrödera, J.C. Feldnera, O. Brandtb, J.D. Hoheiselb, D. Lipinsky, Applied Surface Science 231–232 (2004) 392-396.

[98] Ray, Norde´n, The Faseb Journal (2000) Vol. 14, 1041-1060.

[99] J.C. Feldner, M. Ostrop, O. Friedrichs, S. Sohn, D. Lipinsky, U. Gunst, H.F. Arlinghaus, Appl. Surf. Sci. 203 (2003) 722.

[100] Chi-Ying Lee, Ping Gong, Gregory M. Harbers, David W. Grainger, David G. Castner, and Lara J. Gamble, Anal. Chem. 2006, 78, 3316-3325.

[101] a) Auditore, A.; Tuccitto, N.; Marzanni, G.; Quici, S.; Puntoriero, F.; Campagna, S.; Licciardello, A. Chem. Commun. 2003, 19, 2494. b) Tuccitto, N.; Giamblanco, N.; Licciardello, A.; Marletta, G. Chem. Commun. 2007, 25, 2621.

[102] Nunzio Tuccitto, Nicoletta Giamblanco, Sumana Ghosh, Valentina Spampinato, Pierre Labbè, Pascal Dumy, Silvio Quici, Giovanni Marletta, Eric Defrancq, and Antonino Licciardello, Langmuir 2011, 27, 8595–8599

[103] a) Maskus, M.; Abru~na, H. D. Langmuir 1996, 12, 4455–4462. b) Kosbar, L.; Srinivasan, C.; Afzali, A.; Graham, T.; Copel, M.; Krusin-Elbaum, L. Langmuir 2006, 22, 7631. c) Nishimori, Y.; Kanaizuka, K.; Murata, M.; Nishihara, H. Chem. Asian. J. 2007, 2, 367. d) Tuccitto, N.; Ferri, V.; Cavazzini, M.; Quici, S.; Zhavnerko, G.; Licciardello, A.; Rampi, M. A. Nat. Mater. 2009, 8, 41. e) Tuccitto, N.; Delfanti, I.; Torrisi, V.; Scandola, F.; Chiorboli, C.; Stepanenko, V.; Wurthner, F.; Licciardello, A. Phys. Chem. Chem. Phys. 2009, 11, 4033. f) Tuccitto, N.; Torrisi, V.; Cavazzini, M.; Morotti, T.; Puntoriero, F.; Quici, S.; Campagna, S.; Licciardello, A. Chem. Phys. Chem. 2007, 8, 227.

[104] Rodahl, M.; H€o€ok, F.; Krozer, A.; Brzezinski, P.; Kasemo, B. Rev. Sci. Instrum. 1995, 66, 3924.

[105] Auditore, A.; Tuccitto, N.; Marzanni, G.; Quici, S.; Puntoriero, F.; Campagna, S.; Licciardello, A. Chem. Commun. 2003, 19, 2494.

[106] Herne, T. M.; Tarlov, M. J. J. Am. Chem. Soc. 1997, 119, 8916.

[107] Sauerbrey, G. Z. Phys. 1959, 155, 206.

[108] a) Irving, D.; Gong, P.; Levicky, R. J. Phys. Chem. B 2010, 114, 7631. b) Peterlinz, K.; Georgiadis, R. J. Am. Chem. Soc. 1997, 119, 3401. c) Levicky, R.; Herne, T. H.; Tarlov, M. J.; Satija, S. K. J. Am. Chem. Soc. 1998, 120, 9787.

[109] Lee, C.; Harbers, G. M.; Grainger, D. W.; Gamble, L. J.; Castner, D. G. J. Am. Chem. Soc. 2007, 129, 9429.

[110] a) C. A. Schalley, K. Beizai, and F. Vögtle (2001). "On the Way to Rotaxane-Based Molecular Motors: Studies in Molecular Mobility and Topological Chirality". Acc. Chem. Res. 34 (6): 465–476. b) J. P. Sauvage (1998). "Transition Metal-Containing Rotaxanes and Catenanes in Motion: Toward Molecular Machines and Motors". Acc. Chem. Res. 31 (10): 611–619.

[111] F. Coutrot, E. Busseron (2008). "A New Glycorotaxane Molecular Machine Based on an Anilinium and a Triazolium Station". Chem. Eur. J. 14 (16): 4784–4787.

[112] V. Serreli, C.-F. Lee, E. R. Kay and D. A. Leigh (2007). "Exercising Demons: A Molecular Information Ratchet". Nature 445 (7127): 523–527.

[113] a) A. H. Flood, R. J. A. Ramirez, W.-Q. Deng, R. P. Muller, W. A. Goddard, III and J. F. Stoddart, Aust. J. Chem., 2004, 57, 301. b) Balzani, A. Credi and M. Venturi, Molecular Devices and Machines: A Journey into the Nano World, Wiley-VCH: Weinheim, Germany, (2003).

[114] Benninghoven, A.; Bertrand, P.; Migeon, H. N.; Werner, H. W., Secondary Ion Mass Spectrometry, SIMS X. Wiley: New York, 1997.

[115] a) Vickerman, J. C.; Brown, A.; Reed, N. M., Secondary Ion Mass Spectrometry, Principles And Applications. Oxford University Press: 1989. b) Briggs, D.; Brown, A.; Vickerman, J. C., Handbook of Static SIMS. Wiley: Chichester, UK, 1989. c) Benninghoven, A.; Ruedenauer, F.; Werner, H. W., Secondary Ion Mass Spectrometry. Wiley: Chichester, UK, 1987.

[116] a) Briggs, D.; Hearn, M. J., Vacuum 1986, 36, 1005. b) Leggett, G. J.; Vickerman, J. C., Anal. Chem. 1991, 63, 561. c) Leggett, G. J.; Vickerman, J. C., Appl.Surf.Sci. 1992, 55, 105.

[117] a) Sigmund, P., Phys.Rev. 1969, 184, 383. b) Sigmund, P.; Claussen, C., J.Appl.Phys. 1981, 52, 990. c) Urbassek, H. M., Status of Cascade Theory in ToF-SIMS: Surface Analysis by Mass Spectrometry. IMP Surface Science: 2001.

[118] a) Benninghoven, A.; Jaspers, D.; Sichtermann, W., Appl. Phys. 1976, 11, 35. b) Sichtermann, W.; Benninghoven, A., Int.J.Mass.Spectrom.Ion.Phys. 1981, 40, 177. c) Lange, W.; JiriKowsky, M.; Benninghoven, A., Surf.Sci. 1984, 136, 419.

[119] Michl, J., Int.J.Mass.Spectrom.Ion.Phys. 1983, 53, 255.

[120] a) Murray, P. T.; Rabalais, J. W., J.Am.Chem.Soc. 1981, 193, (1007). b) Cooks, R. G.; Busch, K. L., Int.J.Mass.Spectrom.Ion.Phys. 1983, 53, 111.

[121] Benninghoven, A., Secondary Ion Mass Specctrometry, SIMS III. Springer Verlag: Berlin, 1982.

[122] Garrison, B. J.; Delcorte, A.; Krantzman, K., Acc.Chem.Res. 2000, 33, 69.

[123] Schofield, J. H., J.Electron.Spectrosc.Relat.Phenom. 1976, 8, 129.

[124] Seah, M. P.; in, Surface Analysis by Auger and X-ray Photoelectron Spectroscopy. IMP SurfaceSpectra: 2003.

[125] Seah, M. P.; Spencer, S. J., Surf.Interface.Anal. 2002, 33, 640.

[126] Dannenberger, O.; Weiss, K.; Himmel, H.-J.; Jaeger, B.; Buck, M.; Woell, C., Thin Solid Films 1997, 307, 183.

[127] Sauerbrey, G.Z. Phys. 1959,155-206-222.

[128] K.L. Smith, Electron, Wireless World, July, 51 (1986).

[129] H.o.ok F, Kasemo B, Nylander T, Fant C, Cott K, Elwing H. Anal. Chem 2001;73:5796–804.